FUNCTIONALIZATION OF LOW MOLECULAR WEIGHT NATURAL RUBBER: PREPARATION AND APPLICATION

By
MR. Kraiwut WISETKHAMSAI

A Thesis Submitted in Partial Fulfillment of the Requirements
for Doctor of Engineering CHEMICAL ENGINEERING
Department of CHEMICAL ENGINEERING
Silpakorn University
Academic Year 2024

มหาวิทยาลัยศิลปากร

ฟังก์ชันของยางธรรมชาติน้ำหนักโมเลกุลต่ำ: การใช้งานและการประยุกต์

โดย
นายไกรวุฒิ วิเศษคำใส

วิทยานิพนธ์นี้เป็นส่วนหนึ่งของการศึกษาตามหลักสูตรวิศวกรรมศาสตรดุษฎีบัณฑิต
สาขาวิชาวิศวกรรมเคมี แบบ 2.2
ภาควิชาวิศวกรรมเคมี
มหาวิทยาลัยศิลปากร
ปีการศึกษา 2567

By
MR. Kraiwut WISETKHAMSAI

A Thesis Submitted in Partial Fulfillment of the Requirements
for Doctor of Engineering CHEMICAL ENGINEERING
Department of CHEMICAL ENGINEERING
Academic Year 2024

Title	Functionalization of Low Molecular Weight Natural Rubber: Preparation and Application
By	MR. Kraiwut WISETKHAMSAI
Field of Study	CHEMICAL ENGINEERING
Advisor	Assistant Professor Dr. Weerawat Patthaveekongka, Ph.D.
Co advisor	Associate Professor Dr. Wanvimon Arayapranee, Ph.D.

Faculty of Engineering and Industrial Technology, Silpakorn University in Partial Fulfillment of the Requirements for the Doctor of Engineering

.....
(Assistant Professor Dr. Arunsri Leejeerajumnean, Ph.D.)
Dean of Faculty of Engineering and Industrial Technology

Approved by

.....
(Dr. Siriporn Larpkiattaworn, Ph.D.)
Chair person

.....
(Assistant Professor Dr. Weerawat Patthaveekongka, Ph.D.)
Advisor

.....
(Associate Professor Dr. Wanvimon Arayapranee, Ph.D.)
Co advisor

.....
(Assistant Professor Dr. Chanchai Thongpin, Ph.D.)
Committee

.....
(Dr. Thitirat Rattanawongwiboon, Ph.D.)
External Examiner

59404801 : Major CHEMICAL ENGINEERING
Keyword : Liquid natural rubber; degradation; grafting; polymer blend; poly(lactic acid); polypropylene

MR. Kraiwut WISETKHAMSAI : Functionalization of Low Molecular Weight Natural Rubber: Preparation and Application Thesis advisor : Assistant Professor Dr. Weerawat Patthaveekongka, Ph.D.

Liquid natural rubber (LNR), derived from the depolymerization of natural rubber (NR) into shorter chains, was produced through oxidative degradation using $NaNO_2$ and H_2O_2 in the presence of formic acid (HCOOH). The study examined how reagent concentrations, temperature, and reaction duration influenced the number-average molecular weight (M_n) of the product. Findings indicated that higher concentrations of H_2O_2 and HCOOH accelerated the degradation rate, while increased $NaNO_2$ concentration slowed down the reduction of the M_n. Extended reaction times and elevated temperatures led to a lower M_n. FTIR analysis showed that the LNR had hydroxyl end groups, due to the breaking of NR chains in an acidic environment, while a carboxyl-terminated LNR formed in an alkaline environment. SEM images revealed that the latex particles in LNR were spherical and smaller than those in NR. The study also found that the reaction orders for [H_2O_2], [HCOOH], and [$NaNO_2$] were 1.58, 0.79, and -0.65, respectively. Additionally, the pre-exponential factor was $1.04´10^9$ $M^{-1.72}$ t^{-1} and the activation energy (E_a) was 78.66 kJ/mol. TGA analysis indicated that the thermal stability of the rubber depended on its M_n . LNR with functional end groups showed thermal instability, making it a suitable starting material for various applications. The graft emulsion copolymerization of methyl methacrylate (MMA) onto a liquid natural rubber (LNR) backbone was conducted using CHPO/TEPA as redox initiators. This study examines the influence of process variables such as reaction time, initiator concentration, monomer concentration, and reaction temperature on the grafting reaction, followed by a kinetic analysis of the graft copolymers. The kinetics of the graft copolymerization were analyzed over a temperature range of 55 - 70°C to understand the effects of these variables on the overall copolymerization and grafting rates, as well as on grafting efficiency. This research also derived rate equations for the copolymerization and grafting reactions in the form of power functions of the process factors. FTIR, SEM, and TEM analyses confirmed the formation of graft copolymers, where MMA create a fully closed shell layer on the LNR core particles, resulting in core/shell composites. It was concluded that a lower monomer concentration leads to the highest grafting efficiency (%GE) for MMA grafted onto LNR. The kinetic rate study of PMMA/LNR graft copolymerization provided the relationships for the polymerization rate (R_p) and grafting rate (R_g), with equations R_p (mol/L.min) = 9.75×10^2 ($mol^{-0.07}/L^{-0.07}\cdot min^{0.17}$)·exp[-19.68 (kJ/mol)/RT][CHPO]$^{0.19}$[MMA]$^{0.88}t^{-0.83}$ and R_g (mol/L· min) =1.45×10^{11} ($mol^{-0.17}/L^{-0.17}\cdot min^{1.13}$)·exp[-75.09 (kJ/mol) /RT] [CHPO]$^{0.55}$[MMA]$^{0.62}t^{0.13}$

Increasing the concentrations of CHPO and monomer, as well as the reaction temperature, enhances both R_p and R_g, while increasing the reaction time reduces these rates. For PMMA/LNR graft copolymerization, the activation energy for copolymerization (Ea_p) was 0.98 kJ/mol, and for grafting (Ea_g), it was 75.09 kJ/mol. The resulting graft product of MMA-g-LNR can be used as a compatibilizer to improve the miscibility of polylactide (PLA) and polypropylene (PP). Polymers of the

PLA, PP, and a PLA/PP blend (70:30 wt%) were prepared using an internal mixer and compression molding, with liquid natural rubber-graft-methyl methacrylate (LNR-g-MMA) added at 0.0, 2.5, 5.0, and 10.0 phr as compatibilizers. The impact of LNR-g-MMA content on the blend's morphology, mechanical properties, water absorption, thermal degradation, and lifetime was explored. Scanning electron microscopy (SEM) showed that the PLA/PP blend exhibited phase separation, while the inclusion of LNR-g-MMA led to a more homogenized and refined blend structure. Thus, LNR-g-MMA served as a compatibilizer to enhance miscibility in the PLA/PP blend. The tensile strength, elongation at break, and impact strength of the polymer blends improved, whereas water absorption decreased with higher LNR-g-MMA content. The thermal degradation kinetics were analyzed over a temperature range of 50-800°C with varying heating rates. Results indicated that blends without LNR-g-MMA had better thermal stability than those with LNR-g-MMA, and stability decreased with increasing LNR-g-MMA content. The E_a was determined using the Kissinger-Akahira-Sunose method. PLA had a much lower E_a compared to PP, and incorporating PP into the PLA matrix increased the E_a. Adding LNR-g-MMA to the PLA/PP blend reduced the Ea. The lifetime of the PLA/PP blends decreased with the inclusion of LNR-g-MMA.

ACKNOWLEDGEMENTS

First and foremost, I would like to express my gratitude to my advisors, assistant professor Dr. Weerawat Patthaveekongka and associate professor Dr. Wanvimon Arayapranee, for their constant guidance, encouragement,and patience. I deeply thank Professor Dr. Garry L. Rempel, my co-advisor, for providing an opportunity to expand my knowledge and experience. It has been an honor to learn from you.

I sincerely thank my family for their encouragement and understanding during these years. I am grateful to my friends and lab mates at the Department of Chemical Engineering, Silpakorn University, for the time we shared in our laboratories. I would also like to acknowledge the help of Mrs. Chirarak, and technicians of the Rubber Authority of Thailand (RAOT) for several years.

Finally, I also gratefully acknowledge the financial support of Thailand Research Fund (TRF) and Silpakorn University through the Royal Golden Jubilee Ph.D.Program grant.

Kraiwut WISETKHAMSAI

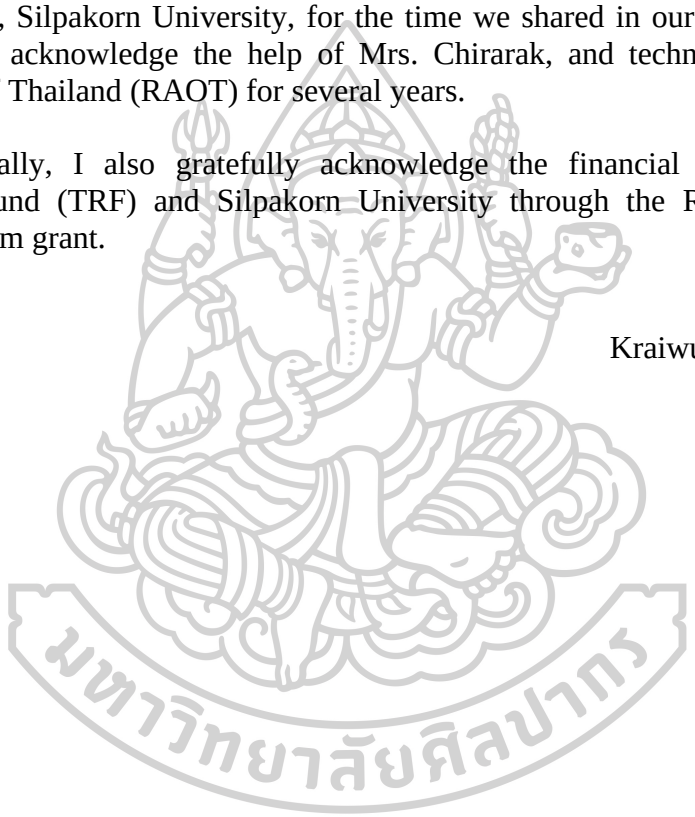

TABLE OF CONTENTS

Page

LIST OF TABLES

Page

LIST OF FIGURES

Page

CHAPTER 1

INTRODUCTION

1.1 Background and motivation

As the awareness of environmental problems has greatly increased in recent years, the utilization of renewable materials, such as natural polymers and their derivatives, has emerged as a new societal trend. A naturally biosynthetic polymer that is readily available in Thailand is natural rubber (NR), as Thailand is a leading producer and exporter of natural rubber in the world. Annually, natural rubber exports go to worldwide recipients located in the Asia Pacific and American regions, producing an income of approximately 2-3 hundred billion baht, which falls in the top five of all export values (Office of the Permanent Secretary Ministry of Commerce, 2023). Notably, about ninety percent of the rubber production was exported in the form of a ribbed smoked sheet (22 %), block rubber (38%), latex concentrate (19%), compound (19%), and a relatively small quantity of rubber air-dried sheet, crepe, and skim rubber (2%) (Rubber Research Institute of Thailand, 2023). Thus, only ten percent of all the rubber production is used for domestic consumption, which is relatively low. Of this portion, 88% is processed into value-added goods, such as tires, gloves, and elastic. Recently, the price of natural rubber has been falling for more than a year, which may be a result of fluctuations in world market demand, climate exchange rate, climate conditions, etc., resulting in a 31% decrease in the NR export value in Thailand (Cooperative Auditing Department, 2023). Therefore, an attempt has been made to enhance NR domestic consumption, as well as to increase the added value of NR. Due to the impact of the spread of the coronavirus, concentrated rubber latex is used as the main raw material for the production of rubber gloves, which is currently in demand around the world.

NR is harvested primarily in the form of latex, which is a tough, milky colloid. Natural latex can be obtained from nearly 2,000 tree species in tropical and temperate regions, but Hevea *brasiliensis* is the only commercial source of natural latex [1] . Hevea rubber contains more than 98% cis-1,4-polyisoprene by weight, which leads to a highly stereo uniform microstructure. Because of this remarkable uniformity, NR

chains can crystallize. Especially when stretched [2]. This results in NR's superior green strength and tear resistance, which are unavailable to synthetic rubber. NR also has abrasion resistance, flexibility and excellent dynamic properties. These beneficial properties of natural rubber are believed to be a result of the protein content in the latex [2],[3]. NR is commonly used in certain industries that require materials with high tensile strength. However, it can easily decomposes when exposed to sunlight, ozone, and heat. It is not resistant to oil-based materials or organic solvents such as petroleum and chemicals due to the presence of unsaturated carbon-carbon bonds in its structure. This has resulted in limitations in the use of NR for some industrial applications. Therefore, modifying NR to improve these poor properties is a way to expand its use and increase its value.

Liquid natural rubber (LNR) can be decomposed from NR with a structure similar to that of NR, consisting of shorter polymer chains and lower molecular weight [4]. LNRs resulting from the decomposition of NR latex involve the breaking of the NR chain, either by directly cleaving the C-C bonds or the C=C bonds of the NR backbone chain. The reduction of molecular weight of NR can be achieved by several methods, such as mechanism, photochemical, ozonolysis, chemical, and thermal hydrolysis in the dry state. Usually, mechanical methods for degradation of NR can be carried out by mastication with a high temperature in the air, which usually occurs before processing. To make it easier to process or combine other chemicals [5]. Silpasuwan et al. [6] proposed the synthesis of LNRs deproteinized with hydroxyl groups through a photochemical reaction. The photodegradation was operated by using H_2O_2 and TiO_2 film attached to the quartz surface. Ibrahim et al. [7] reported the degradation of NR via UV light using the H_2O_2 and nano TiO_2, prepared using the sol-gel method. The radicals attack the C-C bond of the NR backbone chain and breaking of the C=C bond by oxidation, LNR oxygen species with hydroxyl and carbonyl terminal groups was studied, which is the result of a break in the NR chain. LNR is used to improve compatibility in the NR/LLDPE [8-10]. Dahlan et al. [8] studied the effect of LNR content as a compatibilizer to improve the physical properties of NR/LLDPE blends, preparing LNR using an ultraviolet irradiation technique. LNR content was added to improve the compatibility of NR/LLDPE blends, and it can be summarized that adding LNR content into the NR/LLDPE blends slightly affected the

physical properties. Additionally, the molecular weights of LNR below 20,000 g/mol are attractive materials for further application. LNR are applied based on their terminal end groups, which are used as precursors for new materials. The researchers [11-13] reported the preparation of flexible foam from hydroxyl telechelic NR (HTNR) and poly(ε-caprolactone) diol (PCL). Initially, LNR with a carbonyl group (CTNR) was converted into LNR with a hydroxyl group (HTNR) using sodium borohydride. After that, carbonyl telechelic NR (CTNR) was produced by periodic acid and tetrahydrofuran in an oxidative chain cleavage reaction. According to their assertion, polyurethane foams based on HTNR exhibited enhanced elasticity and greater flexibility at low temperatures in comparison to foams made from commercial polyol. Dileep et al. [14] described the LNR with a carboxyl group used as a reactive polymeric plasticizer in NBR compounds. They reported that the NR component with the carboxyl-terminal of LNR attacked the NBR during sulfur vulcanization. As a result, a plasticizer exhibited neither volatility nor extractability. Nor and Ebdon [15] proposed the instrument to determine the kinetic of chain breaking and significant alterations in functional terminal groups of NR latex during ozonolysis reaction in chloroform at 0°C by gel permeation chromatography and Fourier transform infrared spectroscopy. During ozonolysis, the researchers observed that the high molecular weight of NR was reduced, along with the introduction of various oxygenated functional groups. Several studies have focused on LNR [16-18] and deproteinized LNR (LDNR) [19] by subjecting them to oxidative degradation using H_2O_2 and $NaNO_2$ reagents. The breaking chains of NR provide different terminal groups, which depend on the pH of the reaction. Isa et al. [16] investigated the degradation of NR using peroxide acid and $NaNO_2$ as reagents. The result indicates the degradation of NR into LNR with hydroxyl and epoxyl groups. The rate of decomposition is greatly affected by the reaction time and reaction temperature of the decomposition. Bac et al. [17] reported the chain scission of NR latex by situ epoxidation. Epoxide ring undergoes a ring-opening process for a longer time at low pH, forming carbonyl, hydroxyl, and ether groups. Ibrahim et al. [18] studied the mechanisms of degradation that were different by using H_2O_2 and $NaNO_2$ to conduct different ways in acidic and alkaline conditions. This result was that the LNR in the presence of hydroxyl and carbonyl were performed in acidic and alkaline, respectively. Fadhillah et al. [20]

proposed the effect of process variables, such as $CoCl_2$ catalyst and $NaNO_2$, on the average molecular weight of the LNR preparation. They found that the average molecular weight of the LNR depended on reaction time, $CoCl_2$ concentration, and $NaNO_2$ concentration. Phetphaisit and Phinyocheep [21] reported the kinetics degradation of NR was carried out in latex form by using potassium persulfate ($K_2S_2O_8$) and propanol as initiators. They conclude that both intrinsic viscosity and the molecular weight of the LNR depended on the reaction time, $K_2S_2O_8$ concentration, propanol concentration, reaction temperature, and dry rubber content.

Graft copolymers show branched molecular structures, and usually, the side chains distribute randomly. High-impact modified resistance polymers are based on two-phase polymer systems [22, 23]. The LNR-based products are made either directly from concentrated latex or coagulated latex and dry rubber is used as the raw material. The rubber particles may be modified by the graft copolymerization in latex form because the LNR, an unsaturated elastomer with carbon-carbon double bonds in its chains, can be readily grafted with a variety of monomers with the well-established technique of seeded emulsion polymerization [24]. In order to develop LNR-based raw materials and to extend its use, many chemical modifications of LNR have been tried, both in latex and in solution [25]. Chemical modification of LNR via graft copolymerization is a powerful means of improving LNR properties. Graft copolymerization is a technique for modifying the physical and chemical properties of natural and synthetic polymers. The modified NR provides a core-shell composite material in which the NR particles have a size in the range of 100 nm to 2 μmare encapsulated by a layer of the vinyl polymer of nano thickness [26]. This soft core/hard shell composite material enhances the functional properties obtained from vinyl monomers, such as oil resistance, high strength, etc., which are compatible with elastic core materials [27],[28]. With the addition of numerous vinyl monomers of methyl methacrylate (MMA) and styrene (ST) results in efficient grafting onto NR backbone chains, leading to high grafting level [29]. The grafting of vinyl polymer and NR have a high potential as new materials with an expansion in industrial applications, including the adhesive field [30]. The composite poly(MMA)/NR with various grafting levels, in the way of the commercial of adhesive raw material, which can be used for the production of furniture and shoes. For the composite

polystyrene/NR, the addition of this graft copolymer composite can improve the blend compatibility of NR and polystyrene, which is incompatible and immiscible [31]. The NR core for the graft composite is used as a toughening agent, whereas the polystyrene shell layer acts as a compatibilizer with the polymer matrix, thus reducing the interfacial tension between phases. Consequently, the compatibility between two immiscible polymers is enhanced. Additionally, such composite materials have been reported for use as impact modifiers for improving the toughness of plastics [22, 23], which is profitable for the production of automobile parts, transparent roofs, packaging materials, etc. The variation in the type and amount of monomer and initiator, including reaction temperature, the design of graft copolymers provides different properties, such as graft copolymer conversion, grafting efficiency, shell layer thickness, and size [24, 25, 28, 32, 33]. Hence, knowledge of the graft polymerization conditions and the product properties is optimized. For all these reasons, there is interest in studying the kinetics of graft copolymer formation because it is an important step in the development of industrial processes. Although the production process of grafting MMA onto natural rubber has been expanded to pilot plants in southern Thailand [34], an open discussion on the kinetic rate of grafting NR has received little attention. Some reports [35, 36] have reported a kinetic expression of grafting a vinyl monomer onto a polymer chain in which it is written in the form of a relation between the initial polymerization rate and a grafting variable. It is of interest to note that such rate expressions were derived during a steady-state rate interval of graft copolymerization, commonly 10 to 240 minutes after the start of the reaction, depending on the polymerization system and type of backbone polymer and monomer used [37-39]. A literature search of grafting onto NR revealed that a graft copolymer of NR is primarily produced within 2 to 8 hours after the start of the reaction [40]; this interval is outside the range of its steady-state rate. Consequently, kinetic data obtained from a time-to-time analysis during the course of the graft copolymerization is required.

Lastly, the resulting graft product (MMA-g-LNR) can be used as a compatibilizer to improve the miscibility between polylactic acid (PLA) and polypropylene (PP). In general, the PLA is bioplastic, which refers to biodegradable plastics that contain at least one key ingredient as a biopolymer. Raw materials can be

produced or replanted (Renewable raw materials). Therefore, biopolymers produced from agricultural raw materials have received great attention. This is because these plastics biodegrade more easily than plastics derived from commodity fossil fuels. Most importantly, it is environmentally friendly, so the polymer blend is very important. Because blends can provide a method for improving the impact resistance of fragile polymers, PLA and PP are among the main engineering plastic categories. It has many unique properties which are suitable for a wide range of technical and industrial products. The purpose of rubber filling is to improve the brittle properties of the base polymer. And improve the mechanical properties of materials. Impact resistance modifiers are especially used to increase the toughness of the rigid vinyl matrix. It provides a finely dispersed rubber phase to absorb energy. And thereby reducing the breakage. However, the incorporation between the PLA and PP is immiscible because PLA has polarity and PP has non-polarity [41], resulting in poor mechanical properties. The role of the compatibilizer in order to reduce the interfacial tension and adhesion between the two phases. Hence, a compatibilizer was added to improve the compatibility of the polymer blend [41-46]. Choudhary et al. [43] reported that the blend of PLA/PP at different ratios with PP-g-MAH and glycidyl methacrylate (GMA) was used as reactive compatibilizers to induce the miscibility of two polymers. This found that the presence of PP-g-MAH content resulted in the domain size of PP in the PLA matrix decreasing while the mechanical properties increased. Bijarimi et al. [47] studied the blending of the PLA, PP, and LNR mixed with PLA/PP (90/10) and PLA/PP/LNR ratios (90/10/10). In a Haake Rheomix internal mixer, to study the mechanical properties of stress-strain and impact. It was found that elongation at break, bending, and notch impact were significantly increased. The significance for LNR-compatible PLA/PP blends can be seen as immiscibility due to phase separation between PLA and PP particles. LNR has a short-chain polymeric and low viscosity, so blending PLA/PP (70/10) with LNR as a compatibilizer is evident almost homogenized.

1.2 Objectives of the Research

This research was divided into three sections:

(1) to prepare LNR, a modified form of NR latex, which can be done via oxidative degradation by using hydrogen peroxide (H_2O_2), sodium nitrite ($NaNO_2$), and formic acid (HCOOH) as reagents. The average molecular weight of degraded NR was determined based on the intrinsic viscosity ([η]) by Mark-Houwink-Sakurada (MHS) Equation [48-52]. The performance of degradation of NR depends on the reduction in the average molecular weight ($\bar{M}_n$). The effects of reaction time, including H_2O_2, HCOOH, and $NaNO_2$, reaction temperature were studied. The study of degradation kinetics of the NR chains based on ($\bar{M}_n$) data has been evaluated.

(2) to synthesize the graft copolymer using cumene hydroperoxide/tetraethylenepentamine (CHPO/TEPA). The graft copolymerization was operated by preparing LNR as the core and methyl methacrylate (MMA) as the shell monomers in the emulsion process. The effect of reaction time, reaction temperature, and concentration of initiator and monomer on graft efficiency was studied. Furthermore, the rate equations describing the overall copolymerization and grafting reactions were established herein in terms of the power function of these process factors. The reaction orders and the Arrhenius parameters are evaluated by fitting the proposed rate equation with experimental data under various reaction conditions, combined with using a natural logarithm plot and a linear regression technique for graft copolymerization of MMA and LNR.

(3) finally, to improve the compatibility between the PLA and PP blends by using the resulting graft product methyl methacrylate grafted liquid natural rubber (MMA-g-LNR) as compatibilizers. The effect of the polymer blend on morphology, mechanical properties, and thermal stability. The determination of activation energy (E_a) was evaluated by the model-free kinetic method, which can used to predict the lifetime of polymer blends.

The aim of this research was divided into three sections: (1) the preparation of LNR was a modified form of NR latex, which can be done via oxidative degradation by using hydrogen peroxide (H_2O_2), sodium nitrite ($NaNO_2$), and formic acid (HCOOH) as reagents. The average molecular weight of degraded NR was determined based on the intrinsic viscosity ([η]) by Mark-Houwink-Sakurada (MHS) Equation [48-52]. The performance of degradation of NR depends on the reduction in

the average molecular weight ($\bar{M}_n$). The effects of reaction time, including H_2O_2, HCOOH, and $NaNO_2$, reaction temperature were studied. The study of degradation kinetics of the NR chains based on ($\bar{M}_n$) data has been evaluated. (2) to synthesize the graft copolymer using cumene hydroperoxide/tetraethylenepentamine (CHPO/TEPA). The graft copolymerization was operated by preparing LNR as the core and methyl methacrylate (MMA) as the shell monomers in the emulsion process. The effect of reaction time, reaction temperature, and concentration of initiator and monomer on graft efficiency was studied. Furthermore, the rate equations describing the overall copolymerization and grafting reactions were established herein in terms of the power function of these process factors. The reaction orders and the Arrhenius parameters are evaluated by fitting the proposed rate equation with experimental data under various reaction conditions, combined with using a natural logarithm plot and a linear regression technique for graft copolymerization of MMA and LNR, and (3) finally, to improve the compatibility between the PLA and PP blends by using the resulting graft product methyl methacrylate grafted liquid natural rubber (MMA-g-LNR) as compatibilizers. The effect of the polymer blend on morphology, mechanical properties, and thermal stability. The determination of activation energy (E_a) was evaluated by the model-free kinetic method, which can used to predict the lifetime of polymer blends.

1.3 Scope of the Research

1.3.1 Preparation of LNR from NR latex was carried out by oxidation degradation with H_2O_2, $NaNO_2$, and CHOOH as reagents.

1. 3.2 Characterization of the LNR sample was investigated by Gel Permeation Chromatography (GPC), Viscometer, Fourier Transform Infrared Spectrophotometer (FTIR), Scanning Electron Microscopy (SEM), and Gel content.

1.3.3 To study the effect of process parameters on molecular weight.

- Reaction time at 0 - 12 h.
- Amount of hydrogen peroxide at 0.1 - 0.4 mol
- Reaction temperature at 55 - 70°C

- The pH was adjusted using 5% formic acid to obtain the required pH (5 - 9)
- Amount of sodium nitrite at 0.02 - 0.2 mol

1.3.4 To study the graft copolymer of the monomer onto LNR with emulsion polymerization technique using CHPO and TEPA as redox initiation systems.

1.3.5 Characterization of the grafted LNR was investigated by graft efficiency (GE), Gel content, Fourier Transform Infrared Spectrophotometer (FTIR), Scanning Electron Microscopy (SEM), and Transmission Electron Microscopy (TEM).

1.3.6 To study the effect of process parameters on graft efficiency.

- Reaction time at 0 - 8 h for graft copolymers of MMA onto LNR.
- The amount of CHPO and TEPA at a ratio of 1:1 was used at 0.5, 1.0, 1.5, and 2.0 of monomer.

1.3.7 To improve the compatibility of PLA/PP (70/30 %wt) blend with and without LNR-g-MMA as compatibilizer was carried out by melt blending in an internal mixer and molded by compression molding.

1.3.8 Characterization of the PLA/PP (70/30 %wt) blends was investigated by Tensile Testing, Izod Impact Testing, Scanning Electron Microscopy (SEM) and Thermogravimetric Analysis (TGA).

1.3.9 To study the effect of compatibilizer on morphology, mechanical properties, and thermal stability of PLA/PP blends with the addition of LNR-g-MMA with a content of 0.0 - 10.0 phr as a compatibilizer.

1.4 Contribution of research

1.4.1 Knowing the condition for studying the reduction molecular weight of NR latex by oxidation degradation, a graft copolymer of MMA onto LNR with emulsion polymerization technique.

1.4.2 The product obtained performs many functions in a wide range of applications, such as reactive rubber processing aid for the tire Industry, polymer binder for grinding wheels and friction products, reactive

vehicle for rubber additives, polymer base for molding and tooling systems and polymer base for electrical encapsulants.

1.4.3 Raw natural rubber latex can add value. Currently, the demand for raw natural rubber for processing is rapidly increasing as the coronavirus outbreak is ramping up the demand for glove products.

CHAPTER 2

LITERATURE REVIEW

The term latex is often used to denote a stable colloidal dispersion of a polymer in an aqueous medium [53]. It has sometimes been extended to include stable colloidal dispersions. The stability of polymers in non-aqueous media, in which the polymer is insoluble in water Latex systems, can be classified into two types. Synthetic latex is usually obtained through the polymerization of emulsification and condensation polymerization. Natural latex is obtained from plants. Natural latex may be cut from plant parts such as bark, roots, leaves, stems, tubers, and fruits. Latex production is a characteristic of many plants. However, latex-containing high amounts of rubber occur only in species of the families Moraceae, Euphorbiaceae, Apocynaceae, and Compositae.

2.1 Natural rubber

Natural rubber (NR) is obtained in the form of latex, which is extracted from the *Hevea brasiliensis* tree. NR consists of the cis-1,4-polyisoprene structure, as shown in Figure 2.1. The molar masses of rubber molecules range from 50,000 to 3,000,000 g/mol [54]. Hevea latex has a pH of 6.5-7.0 and a density of 0.98 g/cm3. Rubber particles varied in size from 0.15 μm to 3 μm [55].

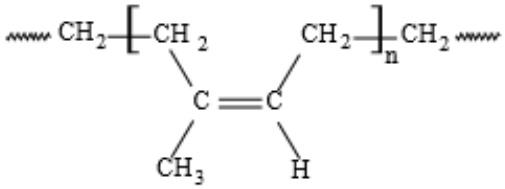

Cis-1,4- Polyisoprene

Figure 2.1 Structure of natural rubber

NR is one of the most valuable renewable resources. Latex is a polydispersed colloidal system of rubber particles in an aqueous phase [54]. The main components

in NR are rubber particles (30 - 40%), water (55 - 65%), protein (2 - 3%), sterol glycosides (0.1 - 0.5%), resin (1.5 - 3.5%), ash (0.5 - 1.0%), and carbohydrate (1.0 - 2.0%) [56] and stabilized with ammonia as showed the figure 2.2.

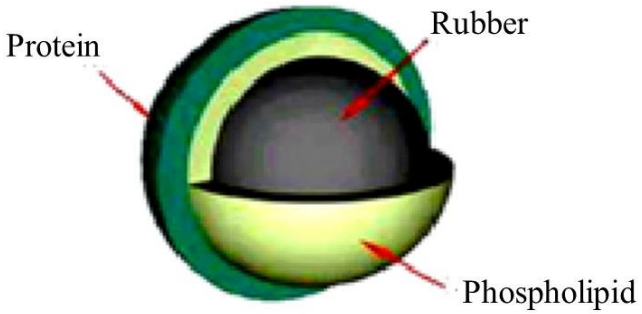

Figure 2.2 Natural rubber particle [57].

2.1.1 Properties of natural rubber

Rubber can be described as a material that is highly elastic, can be stretched without breaking, and will return quickly to its original length. Properties of vulcanized products made from NR are as follows:

2.1.1.1 High mechanical strength and excellent flexibility when can be compounded.

2.1.1.2 Excellent resistance to abrasion, relatively low cost, and significant options make it a preferred material for slurry pump liners, impellers, and tank linings.

2.1.1.3 Excellent dynamic properties are utilized in the manufacturing of tires, rubber springs, and vibration mounts.

2.1.1.4 Excellent low-temperature resistance, down into the range of -57°C.

2.1.1.5 The rubber material has a high-temperature heat aging resistance limit of approximately 75 °C.

2.1.1.6 The raw gum elastomer's inherent weather resistance (to UV radiation and ozone) is poor.

2.1.1.7 The rubber material can used for good electrical insulation.

2.1.1.8 The resistance to petroleum oils is poor, whereas the resistance to ketones and alcohols is significantly higher.

Some properties of NR are compared with those of other commonly used rubbers. NR has a very high structural regularity, providing it with unique and valuable characteristics. In particular, NR crystallizes under strain or at low temperatures and has very low hysteresis and high resilience. The strain-induced crystallization gives NR its very high tensile strength, even when gum vulcanizes, and it is resistant to tearing and abrasion. Because of this crystallization and also high molecular mobility, uncured NR has very high strength and building tack, which is particularly useful for building tires. NR has a very high elasticity. Coupled with low hysteresis, this leads, in dynamic applications, to low heat build-up and high fatigue resistance.

The potential disadvantages of NR are low resistance to heat, weather, and some chemical reagents due to its unsaturated C=C bonds. Applications of NR latex, NR is known for its excellent tensile strength and elongation properties and has become one of the most important materials for applications such as hoses, gloves, condoms, bridge bearings, dock fenders, and vehicle suspension systems.

2.1.2 Application of NR

NR is an important raw material that is widely used in industrial materials. NR can be used directly in the production of adhesive tapes and rubber solutions, but it is mainly vulcanized. With the increase in order to improve synthetic rubber grades, NR is replaced in several applications where heat resistance and swelling are required. However, natural rubber should be used on large tires. Due to its low thermal conductivity and heat accumulation. Which has always been extremely important to the production of truck tires. The introduction of passenger radial tires and heavy-duty radial truck tires has caused the use of NR to increase. The excellent flexibility of NR makes it ideal for sidewall compounds. And low heat build-up results in tires that run cooler [58]. Rubber can also attach to textile fibers and metals, including rayon, polyamide, glass, polyester, and steel cable. The tensile strength increases significantly when the reinforcing part possesses certain properties, while the

extendibility is increased. This use in most compounds makes rubbers much more useful in a lot of different situations.

2.2 Liquid Natural rubber

Liquid natural rubber (LNR) is defined as a modified natural rubber having a similar microstructure as NR but with shorter polymeric chains and lower molecular weights ($\bar{M}_w$ < 20000) [59]. The LNR with functionalization with specific functional groups is known as telechelic LNR [60]. LNR is used in various applications for binder [61], adhesive [62], coating [63], sealants, compatibilizer and grafting [53] as well as a precursor for new material [13]. Hence, the reduction of the molecular weight of NR has extended the potential and possible applications. The several methods to prepare LNR, such as mechanical, mastication, thermal, and chemical. Currently, The popular methods for LNR preparation, such as chemical and photochemical oxidation [58], ozonolysis [64], sonolysis, and metathesis. These methods are convenient and easier to control, and LNR was also normally carried out at a lower temperature than mechanical, thermal, and mastication methods.

2.2.1 Reaction of oxidation degradation

Chemical degradation was a popular method that involved a redox process in the presence of oxidizing agents using hydrogen peroxide and its derivatives. Among the reagents that had been used were metal nitrite or chlorite-air or oxygen or peroxide, phenylhydrazine-ferrous chloride [65], sodium chlorite/hydrogen peroxide [18], phenylhydrazine-O_2, ammonium persulfate-propanal [66], potassium persulfate-propanal [21, 67] and hydrogen peroxide/cobalt acetylacetonate [63]. It was a reducing agent such as p-methyl amino benzene sulfinic, sodium nitrite, fenylhydrazine, sodium hypochlorite, and sodium chlorite.

In this case, the degradation mechanisms of hydrogen peroxide and sodium nitrite in acidic and alkaline conditions. The reagents did not interact chemically in an alkaline condition but reacted spontaneously to produce peroxynitrite acid in an acidic medium [68], and the cleavage of NR chains took place through an oxidization reaction. As a result, LNR with carbonyl terminal groups is produced, as shown in

Figure 2.4. Peroxynitrite acid with pKa of 6.8 [69] decomposes by homolytic fission to produce hydroxyl radical and nitrogen dioxide [70], as shown in Figure 2.3. However, these reagents reacted to form peroxynitrous acid in acidic conditions, which then degraded to produce hydroxyl radicals, as shown in Figure 2.5.

$$H_2O_2 + NO_2^- \rightarrow ONOO^- + H_2O$$
$$ONOO^- + H^+ \rightleftarrows ONOOH$$
$$ONOOH \rightleftarrows {}^{\bullet}OH + NO_2$$

Figure 2.3 The proposed reactions of hydrogen peroxide and sodium nitrite in an acidic medium

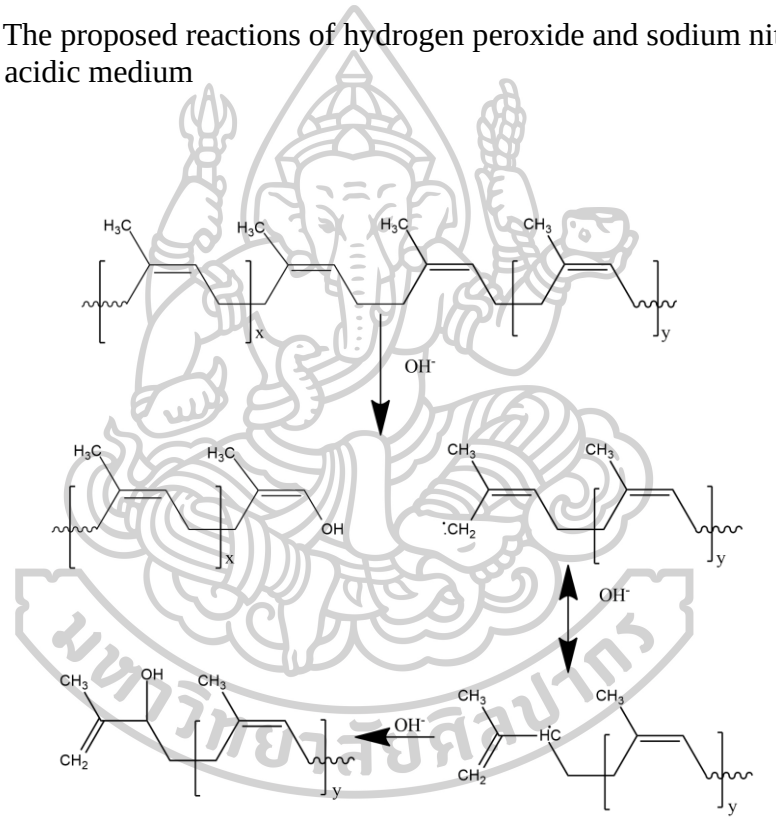

Figure 2.4 Proposed mechanism for degradation of NR chain in acidic condition.

2.2.2 Application of LNR

As mentioned above, LNR not only converts NR into a more useful material. But it has also been found useful as a plasticizer/processing aid, additive and precursor in advanced materials synthesis. LNR is used to increase the homogeneity and compatibility of in NR/LLDPE [71], LNR has improved the interaction between the polymer phases through the dissolution or incorporation of LNR into the amorphous portion of LLDPE to form a spherical honeycomb structure.

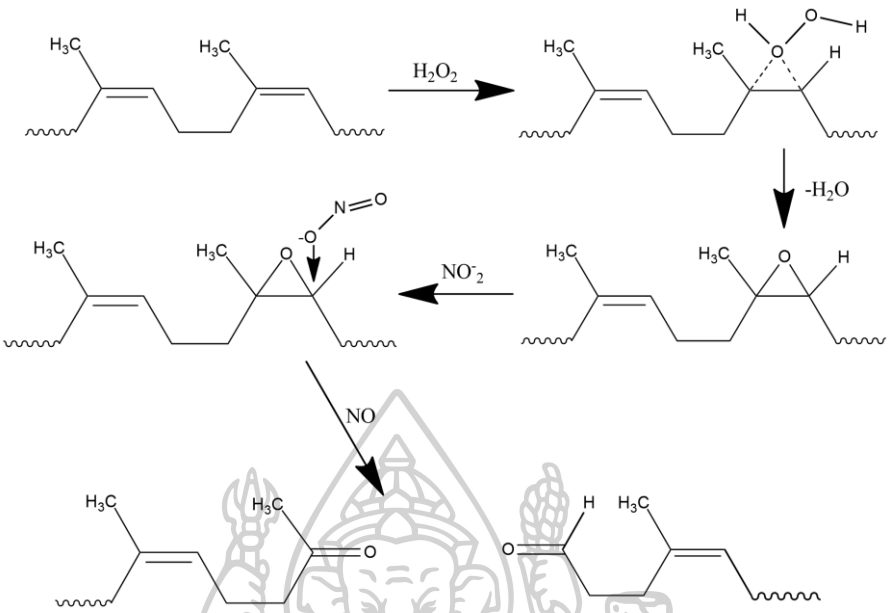

Figure 2.5 Proposed mechanism for degradation reaction of NR chain in alkaline and neutral conditions.

The morphology of the mixture with LNR allows it to be stabilized by exposure to electron beam radiation. It has been proven for composite applications where LNR has been shown to be a good hardener. When increasing impact strength and fracture toughness in polyester [72], epoxy resin [73], bitumen and nylon-6 [74]. These studies show that LNR has the potential to replace synthetic liquid rubber as a modifier. This increases the mechanical properties of the mixture. In another case, LNR and ENR are also used as polymer supports for slow release of fertilizers. These polymers are used to encapsulate free or cross-linked naphthyl acetic acid. which stimulates the production of latex from the Hevea tree.

2.3 Graft copolymerization

A polymer is a large molecule built up by the repetition of small simple chemical units known as monomers. These monomers react chemically to form long molecules, homopolymers composed of the same type of repeating monomers, and heteropolymers composed of several different types of repeating monomers. In some cases, the polymer chains are linear, while in other cases, the chains are branched or

interconnected to form three-dimensional networks. The polymer can be formed not only through linear addition but also through condensation of similar units as well. Copolymers are the most common forms of heteropolymers. Copolymers from three, four, and five species of monomers are accordingly called terpolymers, quaterpolymers, and quinter polymers. An older term for copolymer is interpolymer. Copolymers can be subdivided further into different categories depending upon the nature of the distribution of different monomers in the polymer chain.

(i) Random Copolymers

Random copolymers are formed by the random arrangement of monomer units in the chain, as shown below. Such copolymers are produced by bulk, aqueous suspension, or emulsion polymerizations using free radical initiators of the peroxide type of redox system.

----------A-A-B-B-B-A-B-B-B-B-B-A-A-A-A-B--------

(ii) Periodic Copolymers

In periodic copolymers, monomeric units are arranged in periodic sequences.

----------A-B-B-A-B-B-A-B-B-A-B-B-A-B-B----------

(iii) Alternating Copolymers

The monomeric units alternate in an alternating copolymer, which in turn is a special case of periodic copolymer. Alternating copolymers are produced during condensation polymerization when two different types of monomers, like diacids and diols.

----------A-B-A-B-A-B-A-B-A-B-A-B-A-B-A-------

(iv) Gradient Copolymers

Gradient copolymers exhibit a compositional gradient along the chain, one end of a biopolymer is enriched in ‘A’ units and the other end in ‘B’ units. Gradient copolymers are also called Tapered copolymers.

------- $(A)_nB$-A-A-A-A-A-B-B-A-A-A-B-B-A-A-B-B-B-A$(B)_m$-------

(v) Block copolymers

A block copolymer is a linear copolymer that contains a long chain of one monomer with another monomer in the polymer chain. The block copolymer modification of polymers using graft copolymerization has created increasing interest due to the variety of monomers and substrates participating in such a process. Graft copolymers are generally prepared by free radical, anionic, or cationic addition (or ring opening) polymerization of a monomer in the presence of a preformed reactive polymer. In addition to the genuine copolymer macromolecules, the rough copolymer product usually contains a grafted backbone, ungrafted backbone polymer, and homopolymer. The part of the graft copolymer that consists of macromolecules bearing grafts attached to the backbone will be referred to as “true copolymer”. The graft copolymer is usually separated from the homopolymer using the solvent extraction method. Of all the techniques available for synthesizing graft copolymers, the free radical technique has received the greatest amount of attention, although ionic graft copolymerizations are also gaining importance.

2.3.1 Method of graft copolymer

There are three methods available for synthesizing graft copolymer [75]. The first method is “grafting onto” in which the growing polymeric chain produced from the second monomer reacts with an active site on an existing polymer backbone [76]. The second method is known as “grafting from” involves the copolymerization of the second monomer from the active site on an existing polymer backbone. The third method called as “grafting through” polymerization (or copolymerization) of macropolymer, which is usually a vinyl macropolymer. The reaction for these various graft copolymerization methods is shown in Figure 2.6.

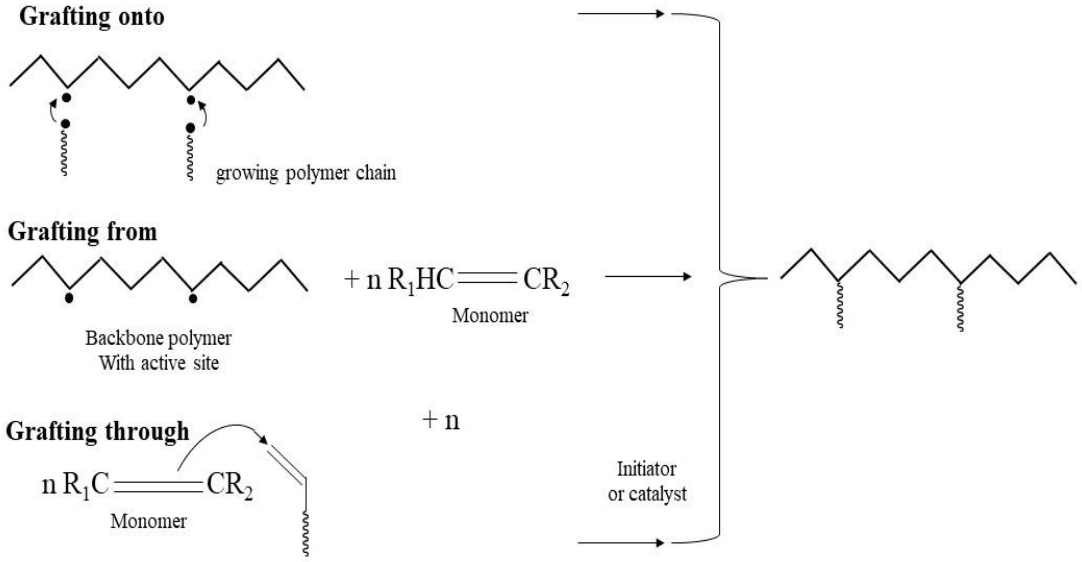

Figure 2.6 Reaction for the graft copolymer

2.3.2 Graft copolymer onto LNR

Both "grafting onto" and "grafting from" methods may be used to prepare graft copolymer-base NR. These methods are usually performed via radical polymerization in either solution or emulsion systems. However, requires a lot of organic solvents to dissolve LNR. Usually, these solvents are toluene or chlorobenzene, which are expensive and toxic. Hence, grafting in an emulsion system is more environmentally friendly and suitable for LNR latex. The main ingredients used for graft copolymerization are an initiator, monomer, emulsifier, rubber latex, and water. For example, the graft copolymer of NR and methyl methacrylate has been one of the main interests. It was found that this type of graft copolymer was useful as a shoe adhesive under the trade name of Heveaplus MG® or MG rubber [77]. This was carried out by dissolving graft copolymer, which contained little PMMA homopolymer and ungrafted natural rubber, in a solvent mixture of MEK/toluene. Furthermore, the MG rubber product could be used as a reinforcing agent [78].

Methyl methacrylate (MMA) is a clear liquid with a distinctive, sharp, fruity odor. It is an organic compound monomer used to produce poly(MMA). By free-radical polymerization, poly(MMA) can be produced via bulk, emulsion, or suspension polymerization systems. The chemical structure of MMA is shown in Figure 2.7.

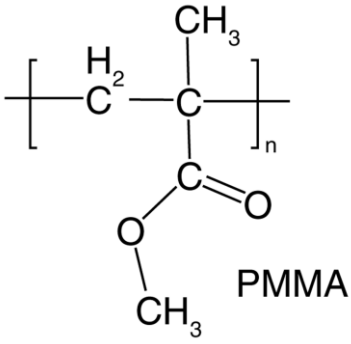

Figure 2.7 Chemical structure of MMA and its polymer.

2.4 Polymer blends

Polymer blend can be predicated as one of the most economical and convenient methods. The blending of polymers was a mixture of two or more polymers that manufacture new multiphase polymeric materials. Therefore, the blending is able to meet the complex demands for performance. Depending on the interactions between the ingredients, polymer blends can be classified into miscible, partially miscible, and immiscible blends [79]. Miscible polymer blends have appeared as homogeneous phases in that individual polymers are mutually soluble in one another. The polymer blend is a partially immiscible blend (partially miscible blend) that is observed by a wide interface with good interfacial adhesion, and the latter (immiscible blend) is observed by a coarse morphology and a sharp interface [80]. However, the physical properties of a polymer blend will depend on the morphology, miscibility, and phase behavior of polymer blends. Immiscible polymer blends can form various phase morphologies, such as sea-island, double emulsion, laminar, fibers, co-continuous, and ordered microphases, which have an important influence on the properties of the polymer blend [81], as shown in Figure. 2.8.

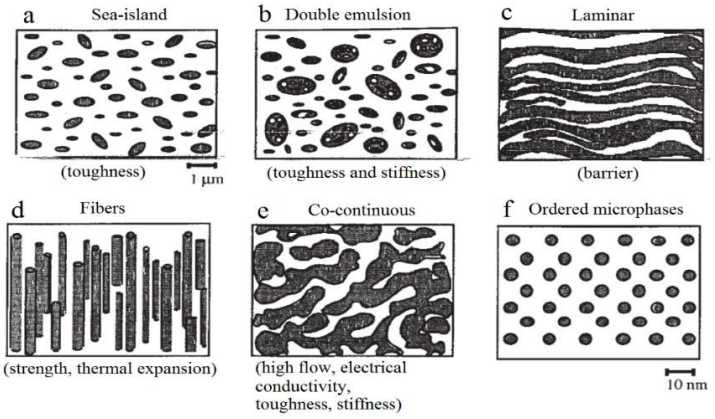

Figure 2.8 Schematic of useful morphologies of polymer blends: (a) sea-island, (b) double emulsion, (c) laminar, (d) fibers, (e) co-continuous and (f) ordered microphases.

Polylactic acid (PLA) is a linear aliphatic thermoplastic polyester derived from lactic acid, which is obtained from the fermentation of 100% renewable and biodegradable plant sources, such as corn or rice starches and sugar feedstocks. The density of both grades is 1.24 g/cm^3. As determined from differential scanning calorimetry (DSC) analysis, PLA exhibits a glass transition temperature (T_g) and a melting temperature (T_m) of 52.14°C and 146.68°C, respectively. It can be produced by chemical conversion of corn or other carbohydrate sources into dextrose. Dextrose is fermented to lactic acid, followed by polycondensation of lactic acid monomers or lactide. However, the most common way to produce PLA is the ring-opening polymerization of lactide monomer formed from lactic acid [82]. The chemical structure of PLA is shown in Figure 2.9.

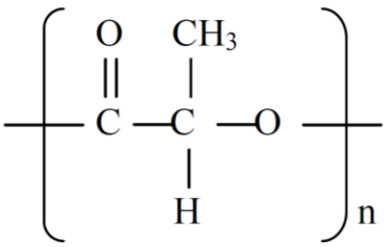

Figure 2.9 Chemical structure of polylactic acid.

Polypropylene (PP) is a very versatile plastic. The high melting point of PP makes it suitable for applications where thermal resistance is required. PP is chemically inert and resistant to most commonly found organic and inorganic chemicals. It has good water, oil, and fat resistance properties. It can produce an effective heat seal within a narrow temperature range and is an excellent medium on which to print. It is a difficult material to tear initially, but once torn, it can propagate the tear easily. PP films can be metalized and then heat-seal coated to produce a film with a high barrier to gas and water vapor. PP films coextruded with PS, EVOH, and PE are used to form reportable pouches. The chemical structure of PLA is shown in Figure 2.10.

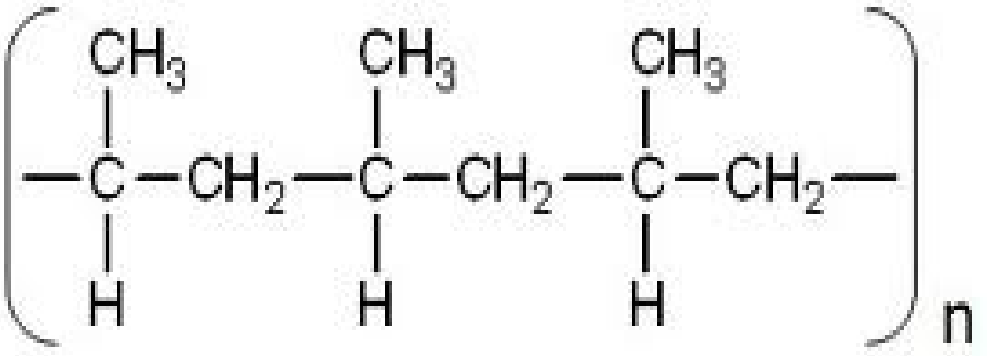

Figure 2.10 Chemical structure of polypropylene.

2.5 Characterization

2.5.1 Fourier transforms infrared spectroscopy (FTIR)

Infrared (IR) spectroscopy is the most crucial among vibrational spectroscopy techniques and is widely utilized for determining and identifying molecular structures. Typically, IR spectroscopy measures the asymmetric vibrations of polar groups. Figure 2.11 illustrates the optical layout of an IR spectrometer. In the active IR mode, an oscillating electric dipole moment must occur within polymeric molecules. Figure 2.12 depicts the vibrational modes of the bonds and IR activities, indicating the partial charges on atoms, with arrows showing the direction of movement.

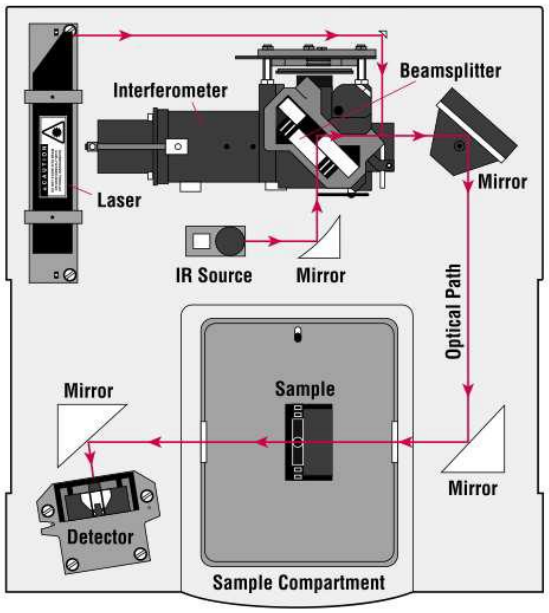

Figure 2.11 Schematic diagram of the optical layout of IR spectrometer.

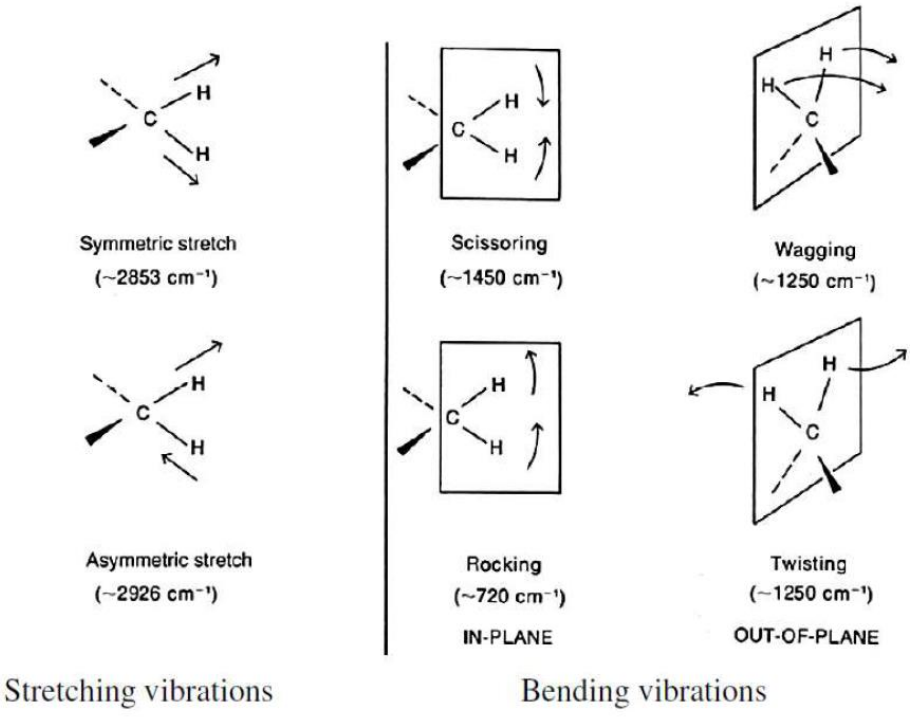

Figure 2.12 Stretching and bending vibrational modes for a CH_2 group.

There are various methods to determine the molar percentage of epoxide in epoxidized natural rubber (ENR). A common approach employs the Lambert-Beer

law and a standard curve, as described by Davey and Loadman [83]. This determination is based on analyzing the band areas of specific functional groups, such as methyl, hydroxyl, and epoxy groups. Typical infrared spectral data for ENR are presented in Table 2.1.

The FTIR spectra were captured over a wavenumber range of 400-4000 cm^{-1}, with a spectral resolution of 4 cm^{-1} and a scanning frequency of 20. The relative absorbance of specific functional groups-carbon-carbon double bonds (at 835 cm^{-1}), epoxy groups (at 870 cm^{-1}), methyl groups (at 1,375 cm^{-1}), and hydroxyl groups (at 3,460 cm^{-1}) was measured to calculate the molar percentage of epoxide. Table 2.1 presents an example of the infrared spectral data for ENR. The equations for calculating the molar percentage of epoxide in ENR, derived from the Lambert-Beer law, are outlined as follows.

$$\text{mol \% epoxide} = \frac{100k_1A_2}{A_1 + k_1A_2 + k_2A_3} \tag{2.1}$$

$$A_1 = A_{386} \tag{2.2}$$

$$A_2 = A_{870} - 0.14A_{836} \tag{2.3}$$

$$A_3 = A_{3460} - 0.019A_{1375} \tag{2.4}$$

Where A_{3460}, A_{1375}, A_{870}, and A_{836} are the absorption peaks corresponding to 3,460 cm^{-1}, 1,375 cm^{-1}, 870 cm^{-1}, and 836 cm^{-1} respectively. The k_1 and k_2, calculated using the ^{1}H-NMR method, are 0.77 and 0.34, respectively.

Davey [83] documented the standard curve correlating the absorbance ratio to the molar percentage of epoxide (as illustrated in Figure 2.13) for calculating the molar percentage of epoxide in ENR, as outlined in equation 2.5.

$$\text{Absorbance} = \frac{\log A/B}{\log A/B + \log C/D} \tag{2.5}$$

Where log A/B and log C/D are the absorbencies corresponding to 870 cm^{-1} and 836 cm^{-1}, respectively.

Table 2.1 The details of infrared spectral data of ENR

Frequency (cm^{-1})	Assignment
3,036	C-H (stretching of isoprene unit)
2,961, 2,727	C-H (asymmetric and symmetric stretching of -CH_3 group)
2,917, 2,852	C-H (asymmetric and symmetric stretching of the CH_2 group)
1,662, 1575	C=C (asymmetric and symmetric stretchings)
1,448	C-H (in-plane bending of CH_2 group)
1,376	C-H (in-plane bending of CH_3 group)
1,259, 1,018	C-O-C (stretching and bending of the epoxy ring)
870	C-H (bending of the epoxy ring)
836	C-H (bending of the isoprene unit)
740	C-H (out-of-plane bending of CH_3)
705	C-H (out-of-plane bending of CH_2)
690	C=C (out-of-plane bending)

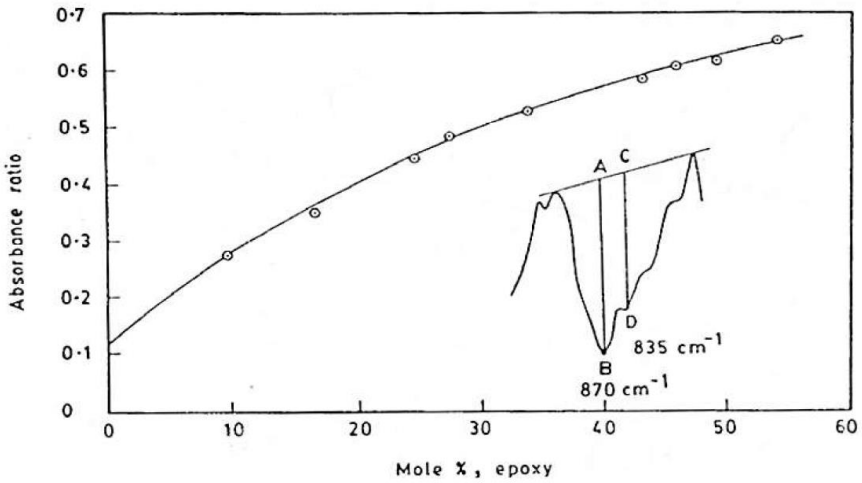

Figure 2.13 Standard curve of mol % epoxide via FTIR technique.

2.5.2 Nuclear magnetic resonance (^{1}H-NMR)

^{1}H-NMR spectroscopy is a highly effective method for analyzing molecular dynamics and structures. This technique leverages the magnetic properties of certain

atomic nuclei. The fundamental setup of a ^{1}H-NMR spectrometer is depicted in Figure 2.14. The atomic nucleus acts as a spinning charged particle, generating a magnetic field. In the absence of an external magnetic field, the nuclear spins are random and oriented in various directions. However, when an external magnetic field is applied, the nuclei align either with or against the direction of the external field. This process results in a locator number known as the Chemical Shift, measured in parts per million (ppm) and typically represented by the symbol δ. The structural analysis of epoxidized natural rubber has been investigated in this manner [84].

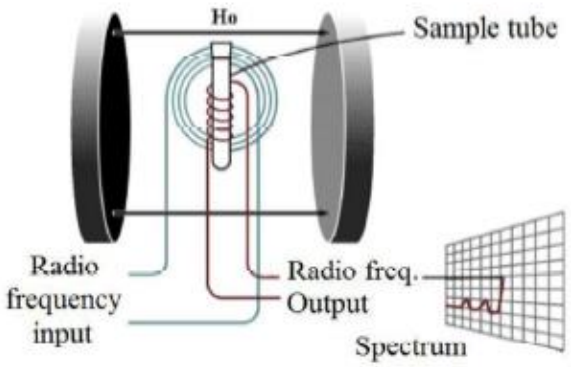

Figure 2.14 The basic arrangement of the 1H-NMR spectrometer.

^{1}H-NMR was employed to determine the chemical structure of the rubbers following the hydrogenation process. The percentage of hydrogenation (%HD) can be calculated using Equation 2.6

$$\text{Degree of hydrogenation} = \frac{I_{0.8\text{-}2.3} - 7I_{5.1}}{I_{0.8\text{-}2.3} + 7I_{5.1}} \times 100\% \qquad (2.6)$$

Where, A0.8-2,3 and A5.1 denote the integrated areas of the proton signals linked to the oxirane ring and the double bond, respectively.

2.5.3 Differential scanning calorimetry (DSC)

Differential Scanning Calorimetry (DSC) instruments detect the heat released or absorbed when the temperature of a material changes, or when a reaction occurs isothermally at a set temperature. They can also measure specific heat while

maintaining a steady temperature ramp. DSC is useful for observing phenomena such as salt precipitation and studying phase transitions including melting, glass transitions, exothermic decompositions, solidification onset, re-crystallization onset, and evaporation temperatures. These processes involve changes in energy or heat capacity that DSC can detect with high sensitivity. The calorimeter comprises a sample holder and a reference holder, as illustrated in Figure 2.15.

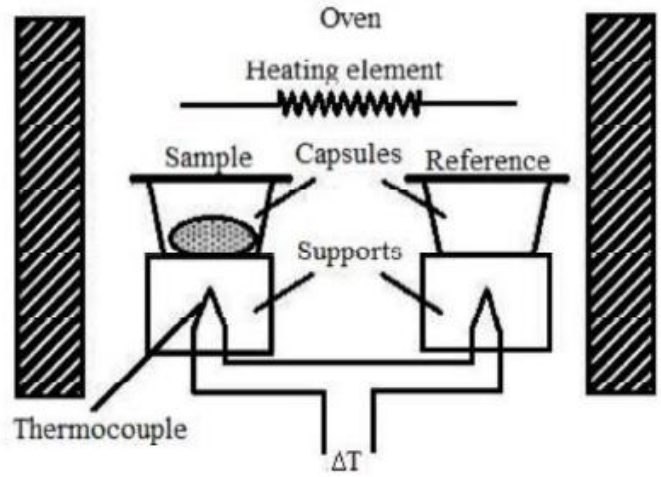

Figure 2.15 Schematic diagram of a DSC apparatus.

DSC measures the variation in the heat flow rate between a sample and a reference when subjected to a controlled temperature program. The reference material is typically an inert substance like alumina or an empty aluminum pan. Both the sample and the reference are heated at a consistent rate. Since the DSC operates under constant pressure, the heat flow corresponds to enthalpy changes. The difference in the power required to maintain both holders at the same temperature is used for calculations. This process helps determine the temperature at which a polymer transitions from a hard, glass-like state to a rubbery state, which is marked by a change in heat capacity. This transformation from a glassy to a rubbery state is defined as the glass transition temperature [85]. The glass transition appears as a step change rather than a peak on a DSC thermogram. Figure 2.16 displays a DSC thermogram highlighting four key points: the glass transition temperature (T_g), the

crystallization temperature (T_c), the melting temperature (T_m), and the curing temperature.

DSC provides precise measurements of the glass transition temperature (T_g). For epoxidized natural rubber (ENR), T_g shows a linear relationship with the epoxide group content. The method's calibration typically involves titration with HBr. Studies have indicated that T_g increases by 0.85 K per mol % of epoxide [86]. Another study by Davey and Loadman [83] similarly reported an increase of 0.92 K per mol % epoxide. The relationship between mol % epoxide and T_g is expressed as follows (Equation 2.1):

$$\text{mol \% epoxide} = \frac{T_g \text{ of ENR} + 70}{0.92} \tag{2.7}$$

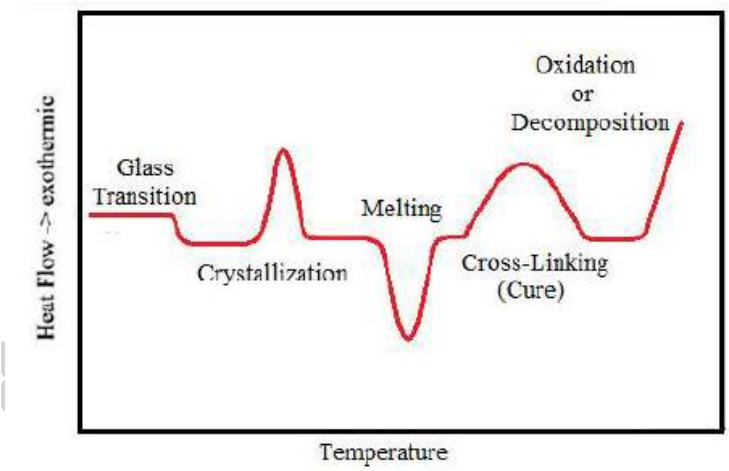

Figure 2.16 Schematic DSC curve demonstrating the appearance of several common

2.5.4 Viscosity average molecular weight ($\bar{M}_v$)

The dynamic viscosities of ENR and [η] were determined using kinematic viscosities measured with a Ubbelohde capillary viscometer (Cannon Instrument Co.), following ASTM D446-07 and ASTM D445-74, respectively. For diluted polymer solutions, the relationship between specific viscosity and concentration is described by Huggin's equation (Equation 2.8):

$$\text{mol \% epoxide} = \frac{T_g \text{ of ENR} + 70}{0.92} \tag{2.8}$$

Typically, the intrinsic viscosity is derived by extrapolating the plot of η_{sp}/C versus C to infinite dilution. However, for monitoring changes in molecular weight during rubber degradation, [η] can be determined from a single viscosity measurement using the following equation (Equation 2.9):

$$[\eta] = \frac{\eta_{sp}/C}{1 + 0.333\eta_{sp}} \tag{2.9}$$

The intrinsic viscosity correlates with the viscosity-average molecular weight according to the Mark-Houwink equation (Equation 2.10) [87]:

$$[\eta] = k\overline{M}_v^{\alpha} \tag{2.10}$$

Which allows the molecular weight to be determined if k and are α known.

For achieving precise outcomes, several key considerations should be taken into account. Firstly, ensure the viscometer is thoroughly cleaned to prevent contamination from previous solutions, which could alter the current solution's viscosity. Additionally, ensure the viscometer is free from dust particles as these can act as hard spheres with significant hydrodynamic volumes, potentially increasing viscosity and influencing results, especially in highly diluted solutions. For a viscometer where the flow time exceeds 100 seconds, allowing kinetic energy terms to be disregarded. This facilitates straightforward calculation of relative viscosity and specific viscosity by comparing the solution's flow time, t, with that of the pure solvent, t_0.

2.5.5 Gel tester

The gel content (insoluble fraction) of a polymer correlate directly with its mechanical property changes. Gel content of the samples was assessed following ASTM D 3616 standards. Each sample, weighing approximately 0.4 ± 0.05 g, was placed on screens inside a borosilicate bottle and treated with 100 cm^3 of toluene. The gel content was calculated using the following equation (Equation 11):

$$\text{Gel content (\%)} = \frac{A - B}{A} \times 100 \tag{2.11}$$

The equation uses A to denote the initial mass of the samples and B to represent the remaining mass after the solvent has evaporated. Each reported result represents the average of five separate determinations.

2.5.6 Mooney viscosity

Mooney viscosity, named after Melvin Mooney, is a crucial viscosity measurement method used for rubbers at specific temperatures. It is determined using a Mooney viscometer, where torque on the instrument's rotating spindle within heated dies is measured. ASTM D 1646 provides the procedure to convert this torque into Mooney Units (MU). The Mooney viscometer consists of a motor-driven disk housed in a die cavity formed by two shearing dies maintained under controlled temperature and closure force conditions. This method assesses the viscosity of rubber or compounds by measuring the torque needed to rotate the disk embedded in a specimen within the die cavity, demonstrating how temperature and time affect viscosity. Viscosity significantly influences the processing characteristics of rubber or compounds in various manufacturing processes such as calendering, extruding, or injection molding. Maintaining viscosity within specified limits is essential for ensuring optimal processability and quality of the final rubber products in the industry.

Figure 2.17 Viscometer dies and rotor.

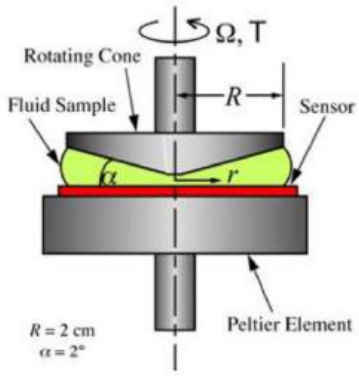

Figure 2.18 The cone and plate rheometer.

2.5.7 Cure characteristic

The curing process of rubber materials significantly influences the properties of rubber composites. Achieving optimal performance relies on controlling curing parameters such as cure time, temperature, and degree of vulcanization. Scorch time, the duration before crosslinking begins, is critical for successful molding and shaping. Sufficient scorch resistance allows for adequate mixing, shaping, and molding processes before vulcanization. Various instruments fall under rheology to measure these essential properties, with the moving die rheometer (MDR) being among the most advanced versions. In an MDR, the sample is positioned between two dies where the lower die oscillates within a range of ± 0.5 degrees as per ISO-3414 standards. The upper die is equipped with a torque sensor to measure the torque response of the rubber during deformation, as depicted in Figure 2.18. Typically, the operating temperature of the MDR ranges from 100°C to 190°C.

2.5.8 Mechanical properties

2.5.8.1 Tensile properties

The rubber vulcanized sheet, produced by compressing the rubber compound in a heated compression mold, was shaped into a dumbbell form using a punching machine, illustrated in Figure 2.19. The stress-strain characteristics of the specimen were evaluated according to ASTM D412. Tensile tests serve multiple purposes. They aid in material selection for engineering applications and are often included in

material specifications to ensure quality. These tests are crucial during the development of new materials and processes, enabling comparison between different materials and processes. Additionally, tensile properties are valuable for predicting how a material will behave under various loading conditions beyond uniaxial tension.

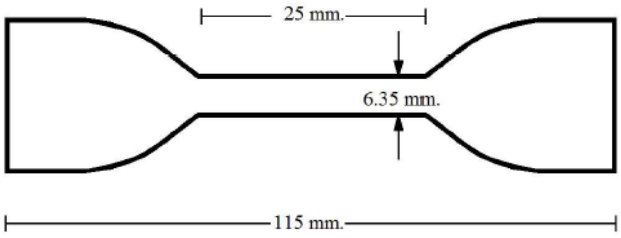

Figure 2.19 Typical dumbbell specimen.

In a tensile test, the specimen is positioned in a machine and stretched to apply tension. Tensile stress (σ) and strain (ε) are defined by Equations 2.12 and 2.13, respectively.

$$\sigma = F/A_0 \tag{2.12}$$

$$\varepsilon = \Delta L/L_0 \tag{2.13}$$

When a solid material undergoes tension in a tensile test, the tensile force F and the initial cross-sectional area A_0 of the specimen's gage section determine the tensile stress (σ), as described in Equation 2.12. The change in gage length ($L-L_0$) relative to the initial gage length L_0 defines the strain (ε) in Equation 2.13. Small stresses cause reversible stretching of atomic bonds, termed elastic deformation, which returns the material to its original shape when the stress is released. At higher stresses, atomic planes slide past each other, causing plastic deformation that persists after removing the stress. In most materials, the initial part of the stress-strain curve is linear, with the slope known as the elastic modulus or Young's modulus, illustrated in Figure 2.14.

$$E = \sigma/\varepsilon \tag{2.14}$$

The stress-strain curves from tensile tests are presented in Figure 2.20. The tensile strength, or ultimate strength, is identified as the peak value of engineering stress. Uniform deformation is expected across the gage section up to the maximum load. For ductile materials, tensile strength is associated with the onset of localized

deformation, leading to necking (see Figure 2.20a). In contrast, less ductile materials fracture before necking occurs (Figure 2.20b), in which case the fracture strength is equated to the tensile strength. Very brittle materials do not exhibit yielding prior to fracture (Figure 2.20c); these materials have a tensile strength but lack a defined yield strength.

2.5.9 Thermal and ozone resistant properties

The impact of aging on rubber has been investigated to understand how it affects rubber vulcanizates over time. Most research on rubber aging has focused on oxidative effects. These effects occur when oxygen targets the unsaturated bonds along the polymer chain. Ozone attacks, in particular, lead to static cracking, which is a common characteristic observed during this process.

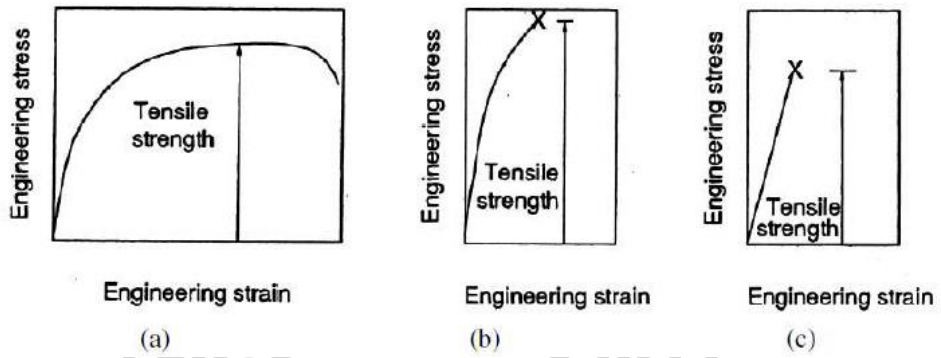

Figure 2.20 Stress-strain curves of (a) ductile, (b) semi-ductile, and (c) brittle materials.

2.5.10 Scanning electron microscope (SEM)

A scanning electron microscope (SEM) is a type of electron microscope that generates images by scanning a sample with a concentrated beam of electrons. The electrons interact with the sample's atoms, producing signals that provide information about the sample's surface topography and composition. The electron beam is typically scanned in a rapid, patterned manner, and the position of the beam is synchronized with the detected signals to create an image. SEM can achieve resolutions finer than 1 nanometer. Samples can be examined under various

conditions, including high vacuum, low vacuum, dry environments (such as in an environmental SEM), and at a broad range of cryogenic or elevated temperatures. The benefits of SEM include its extensive applications, detailed three-dimensional and topographical imaging capabilities, and the comprehensive information provided by different detectors. SEMs are relatively easy to operate with proper training, and modern advancements in computer technology and software have made them user-friendly. This instrument provides rapid analysis, often in less than five minutes. Moreover, technological advancements in contemporary SEMs enable data generation in digital form. While all samples need to be prepared before being placed in the vacuum chamber, most SEM samples require minimal preparation. Typically, data are gathered from a selected area of the sample's surface, producing a two-dimensional image that illustrates spatial variations in the sample's properties.

2.5.11 TG/DTA Simultaneous Thermal Analyzer

Thermogravimetric Analysis (TGA) measures weight changes in a material as a function of temperature (or time) under a controlled atmosphere. Its principal uses include measuring the thermal stability of material and composition. Differential thermal analysis (DTA) involves heating a material at a controlled rate to a pre-determined temperature and comparing any chemical emissions of heat (exothermic) or absorptions of heat (endothermic) from the material in comparison with a passive material such as alumina. This is most useful for determining the precise temperature at which a reaction occurs or identifying a phase change or reaction product. The TG/DTA Simultaneous Thermal Analyzer combines the flexibility of DTA with the capabilities of the TG measurement technology, providing property information for various samples. It simultaneously measures temperature and weight signals for studies concerning oxidation, heat resistance, amount of water, compositional analysis, and the measurement of mineral content in a sample. This instrument can analyze samples over a broad temperature range (RT to 1500ºC) with excellent performance at both low temperatures (<600ºC) and high temperatures (>1000ºC). It can be easily connected to equipment such as FTIR, MS, and GC-MS for hyphenated applications.

CHAPTER 3

MATERIALS AND METHODS

In this chapter, the experimental details were divided into three sections: (1) to prepare the LNR, a modified form of NR with a shorter polymeric chain, can be done via oxidative degradation using hydrogen peroxide (H_2O_2), sodium nitrite ($NaNO_2$), and formic acid (HCOOH) as reagents, (2) to synthesize the graft copolymer using cumene hydroperoxide/tetraethylenepentamine (CHPO/TEPA). The graft copolymerization was operated by preparing LNR as the core and methyl methacrylate (MMA) as the shell monomers in the emulsion process, and (3) finally, to improve the compatibility between the polylactide (PLA) and polypropylene (PP) blends by using the resulting graft product methyl methacrylate grafted liquid natural rubber (MMA-g-LNR) as compatibilizers. The details of material and methods for the preparation and characterization of LNR, graft copolymers, and PP/PLA (70/30 wt%) blend using MMA-g-LNR as a compatibilizer are described as follows.

3.1 Chemical and materials

1. Natural rubber latex with 60% dry rubber content (Bothong Natural Rubber Trade Co., Ltd., Chonburi, Thailand)

2. Polyoxyethylene styrenated phenyl ether ($C_{24}H_{22}O_2$) was used as a surfactant under the trade name Emulvin WA (Chemical and Materials Co., Ltd., Bangkok, Thailand)

3. Hydrogen peroxide (H_2O_2; Sigma-Aldrich; USA; purity ~ 50%)

4. Formic acid (HCOOH; Sigma-Aldrich; USA; purity ~ 85%)

5. Sodium nitrite ($NaNO_2$; Sigma-Aldrich; USA; purity ~ 97%)

6. Sodium sulfide (Na_2SO_3; Sigma-Aldrich; USA; purity ~ 98%)

7. Methanol (CH_3OH; commercial grade, Facobis Co., Ltd., Bangkok, Thailand)

8. Toluene ($C_6H_5CH_3$; commercial grade, Facobis Co., Ltd., Bangkok, Thailand)

9. Methyl methacrylate monomer was purified by washing with 10% sodium hydroxide solution to remove the inhibitor, followed by deionized water and by distillation under reduced pressure (MMA; $C_5H_8O_2$; Sigma-Aldrich; USA; purity ~ 99%).

10. Sodium dodecyl sulfate (SDS; $NaC_{12}H_{25}SO_4$; KemAus; Australia; purity ~ 95%)

11. Tetraethylene pentaamine (TEPA; $C_8H_{23}N_5$; Sigma-Aldrich; USA; purity ~ 99%)

12. Cumene hydroperoxide (CHPO; $C_9H_{12}O_2$; TCI; USA; purity ~ 20%)

13. Sodium hydroxide (NaOH; Q ReC; New Zealand; purity ~ 99%)

14. Potassium hydroxide (KOH: Q ReC; New Zealand; purity ~ 85%))

15. Isopropanol (C_3H_8O; Loba Chemie^{TM}; India; purity ~ 99.5%)

16. Acetone (C_3H_6O; commercial grade, Facobis Co., Ltd., Bangkok, Thailand)

17. Deionized water (DI water)

18. 2-L, a five-necked glass reactor equipped with a condenser, stirrer, and thermocouple, was used for the experimental reactor setup.

19. The Soxhlet extraction apparatus setup.

20. Viscometer.

21. The gel test apparatus.

22. Gel permeation chromatography (GPC, Alliance, Waters e2695 separations)

23. Fourier transform infrared Spectrophotometer (FTIR, PerkinElmer Frontier)

24. Field scanning electron microscopy (FE-SEM, Tescan, Mira3)

25. Transmission electron microscopy (TEM, Hitachi, HT7700)

26. Thermogravimetric analysis (TGA, Perkin Elmer, Pyris 1)

27. Internal mixer (MX105-D40L50)

28. Compression molding machine

29. Universal tensile testing (EZ-LX, Shimadzu)

30. Izod impact testing (GOTECH, GT-7045-MD)

3.2 Methods and experimental

3.2.1 Preparation of liquid natural rubber

227 g of NR latex (High ammonia with 60% dry rubber content (DRC)) was mixed with 136 g of 10% Emulvin WA solution in the experimental reactor setup, as shown in Figure 3.1. 50% aqueous H_2O_2 was added in NR latex, and then 10% solution of $NaNO_2$ was added, followed by the mixture being adjusted using 5% formic acid to the required pH. The mixture was diluted to approximately 1000 mL with distilled water and stored in latex. The reaction was carried out at 55 to 70 °C for 12 h. After the gradation reaction, a 5% solution of Na_2SO_3 was added to the mixture to remove excess H_2O_2 [88] and cooled down to room temperature. The degraded NR was coagulated with methanol, and the LNR obtained was washed two times with distilled water and dried in a vacuum oven at 40 °C. The LNR was then dried in a vacuum oven to a constant weight. Figure 3.2 shows the flowchart of the preparation and characterization of LNR. The process variables for the preparation of LNR are summarized in Table 3.1.

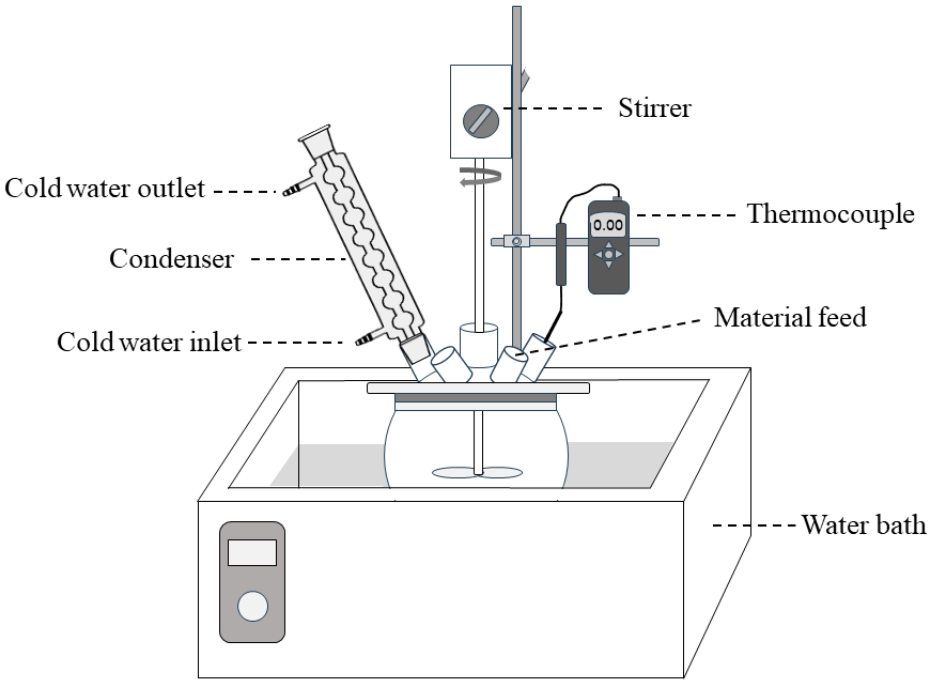

Figure 3.1 The experimental reactor setup.

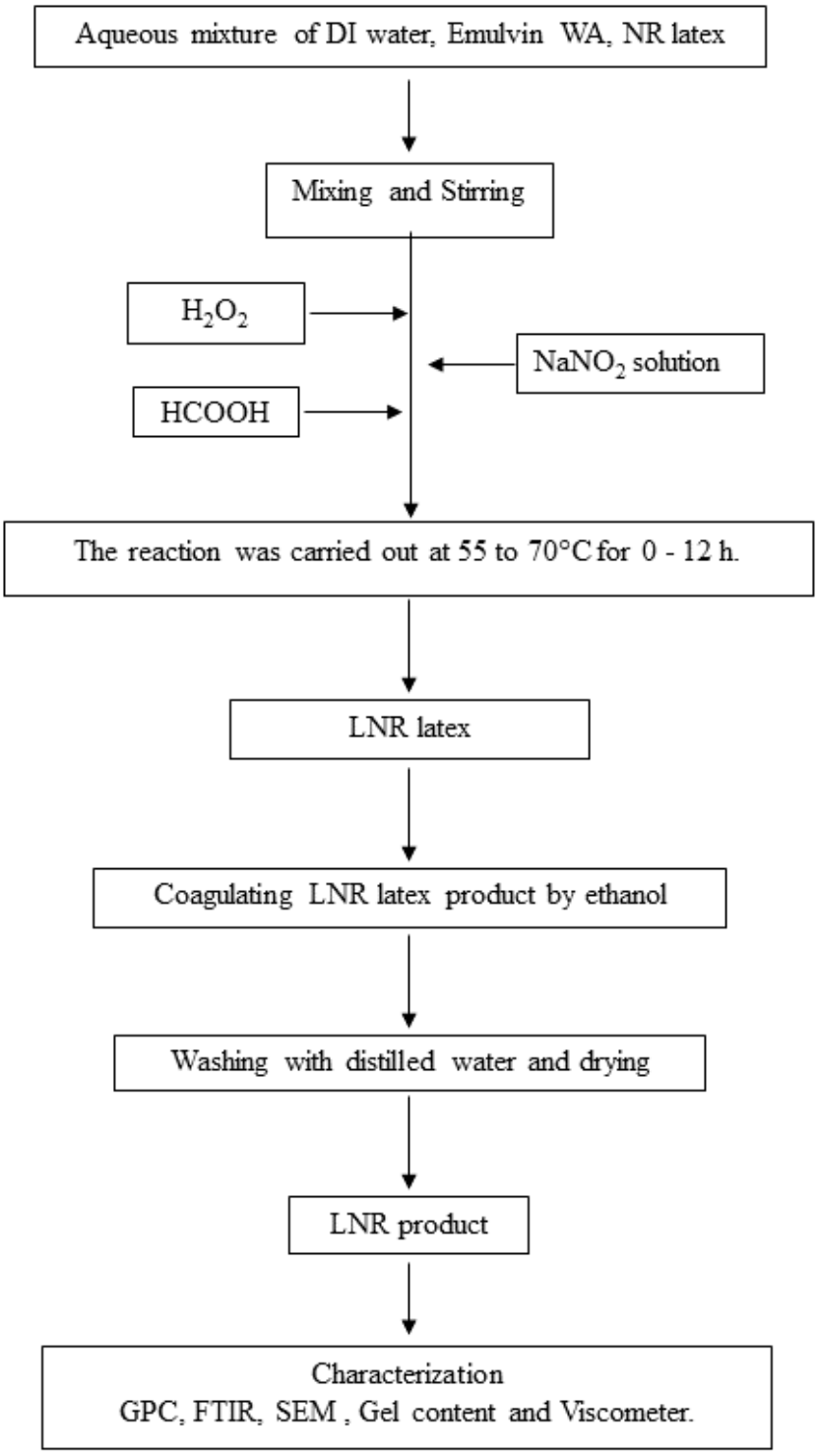

Figure 3.2 Flowchart for the preparation and characterization of LNR.

Table 3.1 The process variables for the preparation of LNR.

Sample	H_2O_2 (mol)	pH	$NaNO_2$ (mol)	Temperature (°C)	Time (h)
LNR01	0.1	5	0.02	65	0 – 12
LNR02	0.2	5	0.02	65	0 – 12
LNR03	0.3	5	0.02	65	0 – 12
LNR04	0.4	5	0.02	65	0 – 12
LNR05	0.4	7	0.02	65	0 – 12
LNR06	0.4	9	0.02	65	0 – 12
LNR07	0.4	11	0.02	65	0 – 12
LNR04	0.4	5	0.02	65	0 – 12
LNR08	0.4	5	0.05	65	0 – 12
LNR09	0.4	5	0.10	65	0 – 12
LNR10	0.4	5	0.15	65	0 – 12
LNR11	0.4	5	0.20	65	0 – 12
LNR12	0.4	5	0.02	55	0 – 12
LNR13	0.4	5	0.20	60	0 – 12
LNR04	0.4	5	0.02	65	0 - 12
LNR04	0.4	5	0.02	65	0 - 12

3.3.2 Graft copolymer of MMA onto LNR latex

The graft polymerization was conducted in the experimental reactor setup, as shown in Figure 3.1. Before graft copolymerization, NR latex was modified to LNR with a shorter chain. Then, the latex was left to cool down at room temperature. 1200 g LNR latex (18.3134% DRC) was taken in a five-necked reactor. Then, 0.5487 - 2.1950 mol of the MMA monomer, 4 ml of isopropanol, and 10 ml of 10% KOH solution that was added to keep the LNR latex's pH above 10 were charged in the reactor. LNR latex was soaked with the MMA monomer for 24 h at room temperature, followed by the addition of the redox initiation system, consisting of 1.5034×10^{-3} – 5.7402×10^{-3} mol of CHPO/TEPA at a mole ratio of 1:1. The mixture was diluted to approximately 1,600 mL with distilled water. The graft copolymerization was carried out at a stirring speed of 400 rpm for the desired temperature range of 328.15 –

343.15 K. The reaction time was varied at 0 - 480 min. The sample was collected every 120 min by transferring approximately 100 mL of latex product to a glass bottle. Then the latex product was precipitated by using boiling water containing 5% formic acid. The gross product was then washed three times with DI water and then left to dry in a vacuum oven at 50°C until constant weight was obtained. The procedure to prepare the graft copolymer of MMA onto LNR is represented in Figure 3.3. The graft copolymerization recipes and variable factors are shown in Table 3.2.

The free polymethyl methacrylate (PMMA) was extracted in a Soxhlet extractor using acetone for 24 h. The residue was dried in a vacuum oven at 50 °C until a constant weight for 24 h.

Table 3.2 The recipes and variable factors for the graft copolymer of MMA-g-LNR.

Sample	LNR03 (mol)	CHPO (mol)	TEPA (mol)	MMA (mol)	T (K)	Time (min)
MGLNR01	3.23	1.5034×10^{-3}	1.5034×10^{-3}	2.1950	343.15	0 - 480
MGLNR02	3.23	2.8700×10^{-3}	2.8700×10^{-3}	2.1950	343.15	0 - 480
MGLNR03	3.23	4.3735×10^{-3}	4.3735×10^{-3}	2.1950	343.15	0 - 480
MGLNR04	3.23	5.7402×10^{-3}	5.7402×10^{-3}	2.1950	343.15	0 - 480
MGLNR05	3.23	4.3735×10^{-3}	4.3735×10^{-3}	0.5487	343.15	0 - 480
MGLNR06	3.23	4.3735×10^{-3}	4.3735×10^{-3}	1.0975	343.15	0 - 480
MGLNR07	3.23	4.3735×10^{-3}	4.3735×10^{-3}	1.6462	343.15	0 - 480
MGLNR03	3.23	4.3735×10^{-3}	4.3735×10^{-3}	2.1950	343.15	0 - 480
MGLNR08	3.23	4.3735×10^{-3}	4.3735×10^{-3}	2.1950	328.15	0 - 480
MGLNR09	3.23	4.3735×10^{-3}	4.3735×10^{-3}	2.1950	333.15	0 - 480
MGLNR10	3.23	4.3735×10^{-3}	4.3735×10^{-3}	2.1950	338.15	0 - 480
MGLNR03	3.23	4.3735×10^{-3}	4.3735×10^{-3}	2.1950	343.15	0 - 480

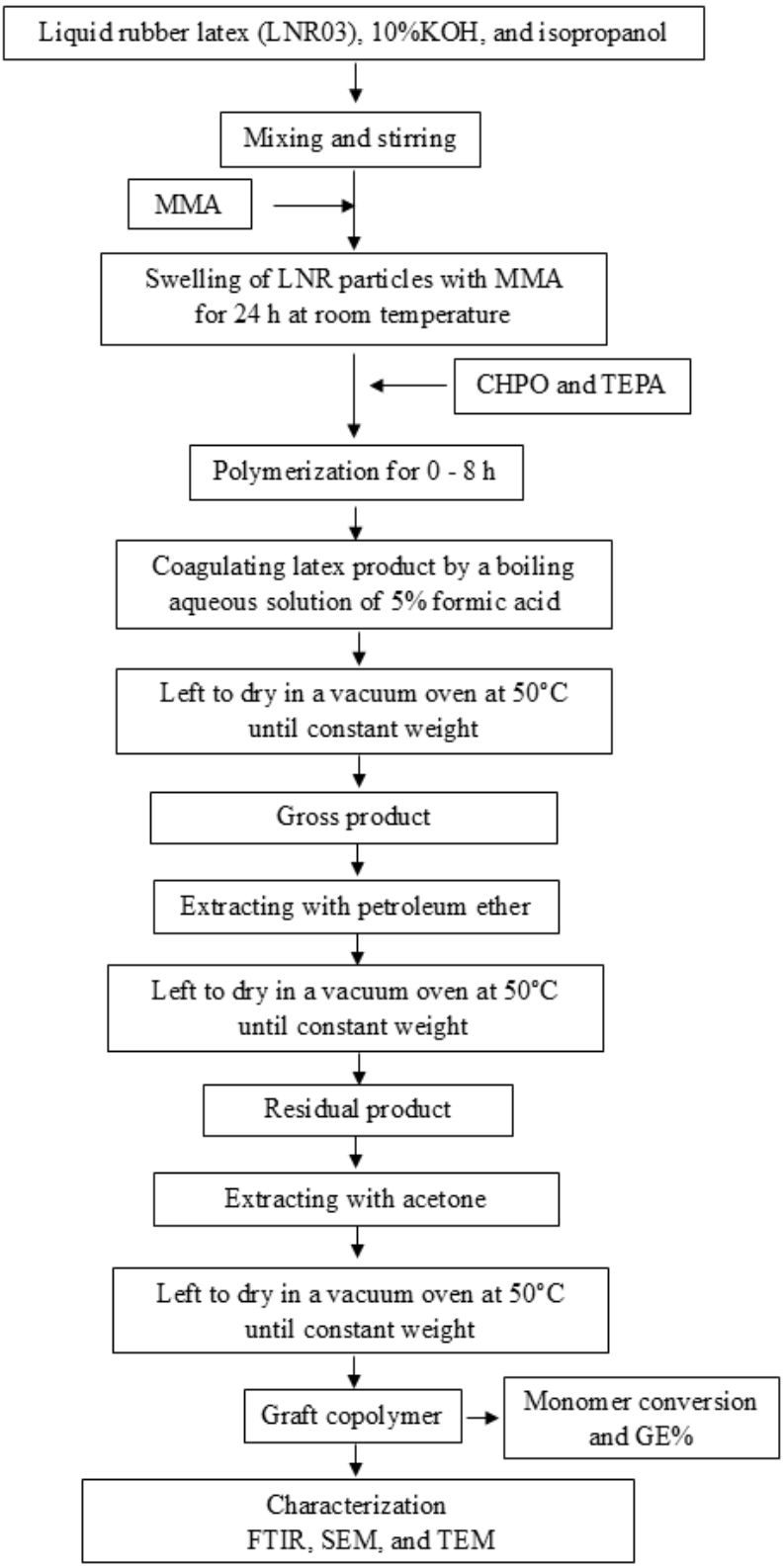

Figure 3.3 Flowchart for the preparation and characterization of MMA-g-LNR.

3.2.3 Blend preparation

The pure PLA and PP, and PLA/PP in a ratio of 70:30 wt% without and with MMA-g-LNR as compatibilizer with a content of 0.0, 2.5, 5.0, and 10.0 phr, all blends were prepared using an internal mixer (MX105-D40L50) at 180 °C, as shown in Figure 3.4. The polymer blend was operated at a rotor speed of 70 rpm for 13 min. Before mixing, the pure PLA and PP pellets were dried in a vacuum oven at 80 °C for 4 h. MMA-g-LNR looked like powder (Figure 3.5) as a compatibilizer and was also dried in an oven at 50 °C under vacuum for 4 h. Material formulations in blend preparation are shown in Table 3.3. After blending, the polymer is introduced into a compression molding machine by using to mold the samples into dumbbell and bar shapes (Figure 3.4). The flowchart for the preparation and characterization of the polymer blend is shown in Figure 3.6.

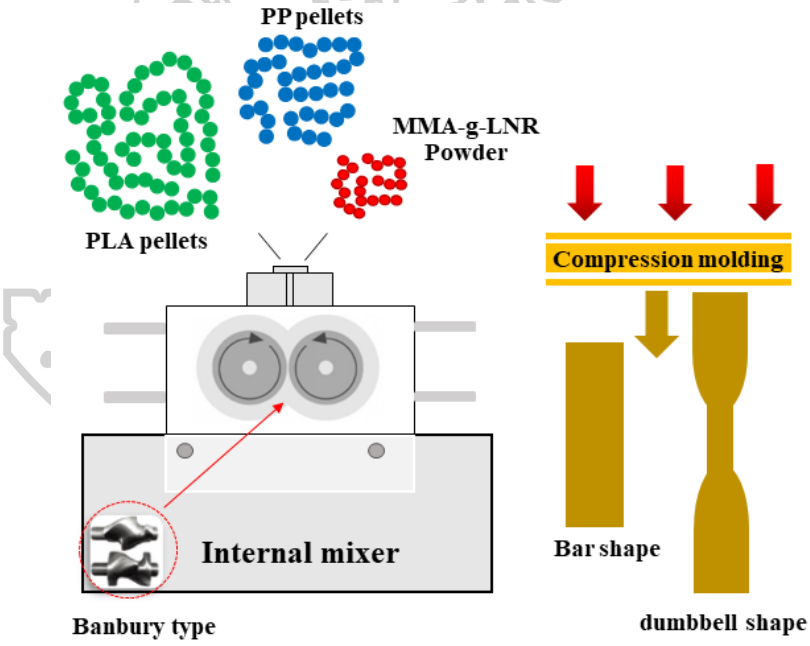

Figure 3.4 The experimental apparatus for polymer blend.

Figure 3.5 MMA-g-LNR powder image obtained from graft copolymerization using as compatibilizers for PLA/PP blend.

.

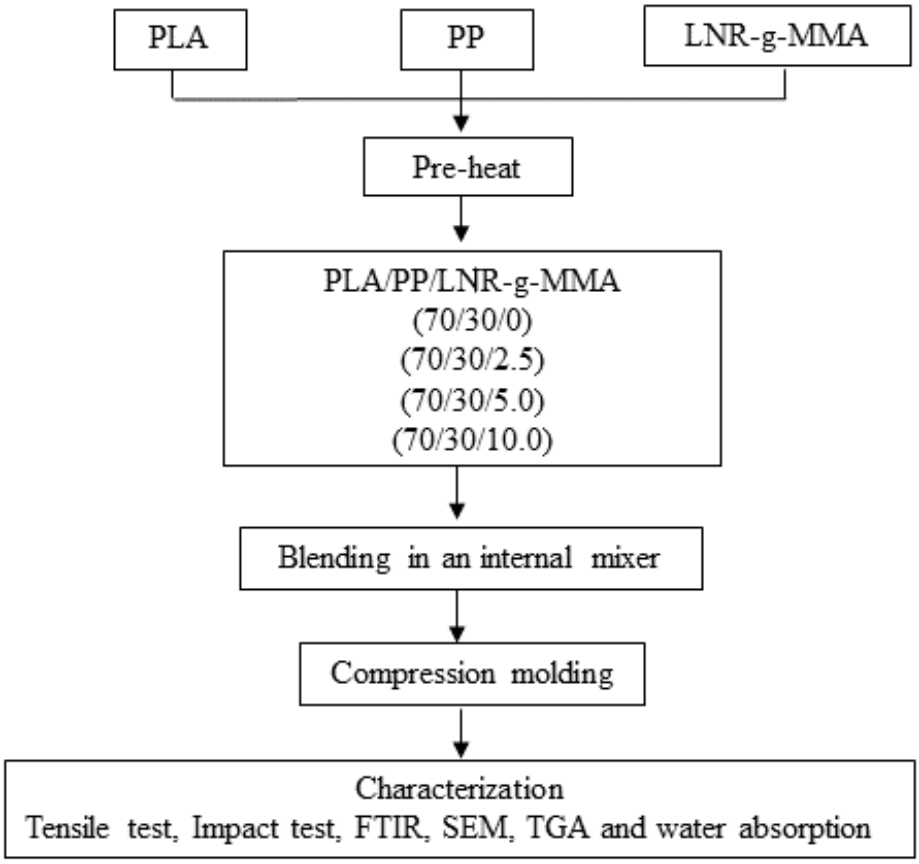

Figure 3.6 Flowchart for the preparation and characterization of polymer blend.

Table 3.3 Material formulations in blend preparation.

Sample	PLA (wt.%)	PP (wt.%)	MGLNR (phr)
PLA	100	-	-
PP	-	100	-
PLA/PP (70:30)	70	30	0
PLA/PP (70:30)	70	30	2.5
PLA/PP (70:30)	70	30	5.0
PLA/PP (70:30)	70	30	10.0

3.3 Characterization

3.3.1 Intrinsic viscosity

The intrinsic viscosity ([η]) of rubber samples was determined using an Ubbelohde viscometer (as shown in Figure 3.7) with toluene solution at 30°C. According to ASTM D445, the capillary diameter of the viscometer was 0.53 mm, and the rubber was weighed approximately 0.1 g/dL in toluene solution. The dilution type is determined by extrapolation to zero concentrations of specific intrinsic viscosity measurements acquired at five different concentration levels. The condition of the LNR rubber in toluene solution at 30°C [89]. The corrections for kinetic energy and shear were negligible.

3.3.2 Gel permeation chromatography (GPC)

Gel permeation chromatography (GPC, Alliance, Waters e2695 separations) was used to determine the number-average molecular weight ($\bar{M}_n$), weight-average molecular weight ($\bar{M}_w$), and Z-average molecular weight ($\bar{M}_z$) of the prepared rubber samples. The measurement was operated using the polystyrene for standard calibration and tetrahydrofuran (THF) as eluent at 30 °C. The rubber sample was dissolved in THF for 24 hours and filtered through a 0.45 μm syringe filter prior to injection into a chromatograph.

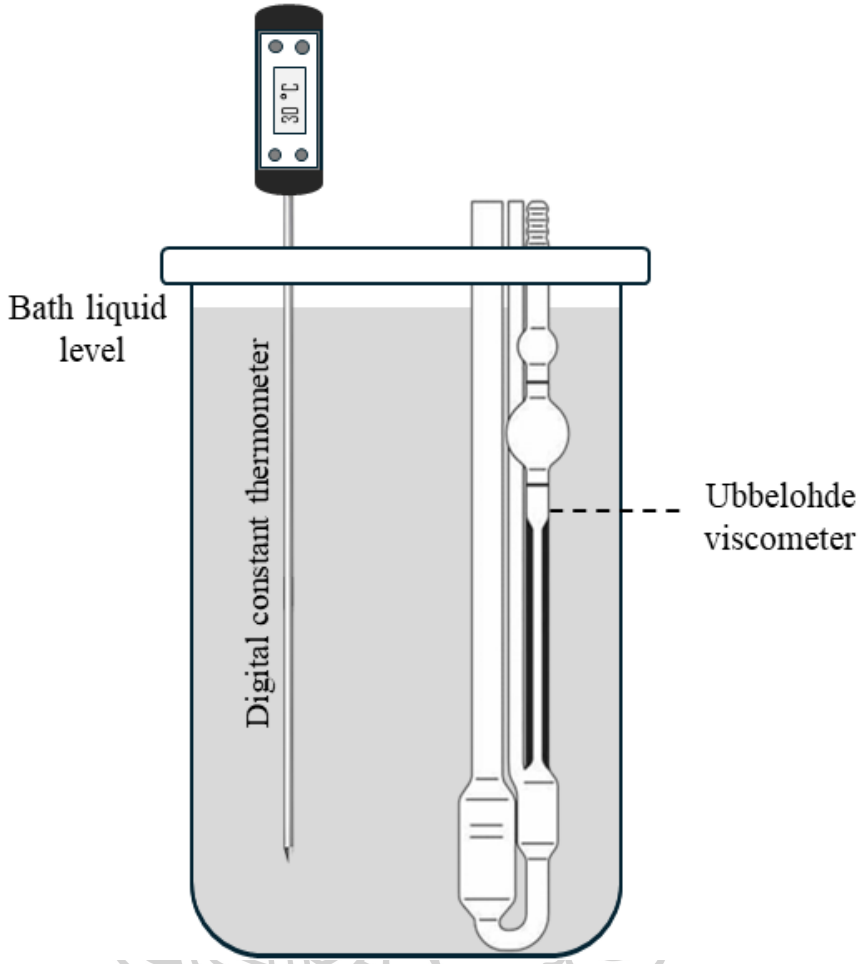

Figure 3.7 Ubbelohde viscometer apparatus.

.

3.3.3 Gel content

Gel content was determined by using the gel test by weighing approximately 0.4 ± 0.05 g of rubber sample into place on a screen rack (50 mesh) in a borosilicate bottle, and 100 ml of toluene was added. Then, The rubber sample was soaked for 20 h in a dark place, according to ASTM D3616 -95 (2004) which is shown in Figure 3.8. The liquid was pipetted to determine the gel content, as shown in the Equation below.

$$\text{Gel content (\%)} = \frac{C - B}{C} \times 100 \qquad (3.1)$$

where A is the amount of rubber present in 25 mL of the sol, B = 4×A = mass of total dried solvents, and C is the amount of rubber initially taken to make the rubber solution (100 ml).

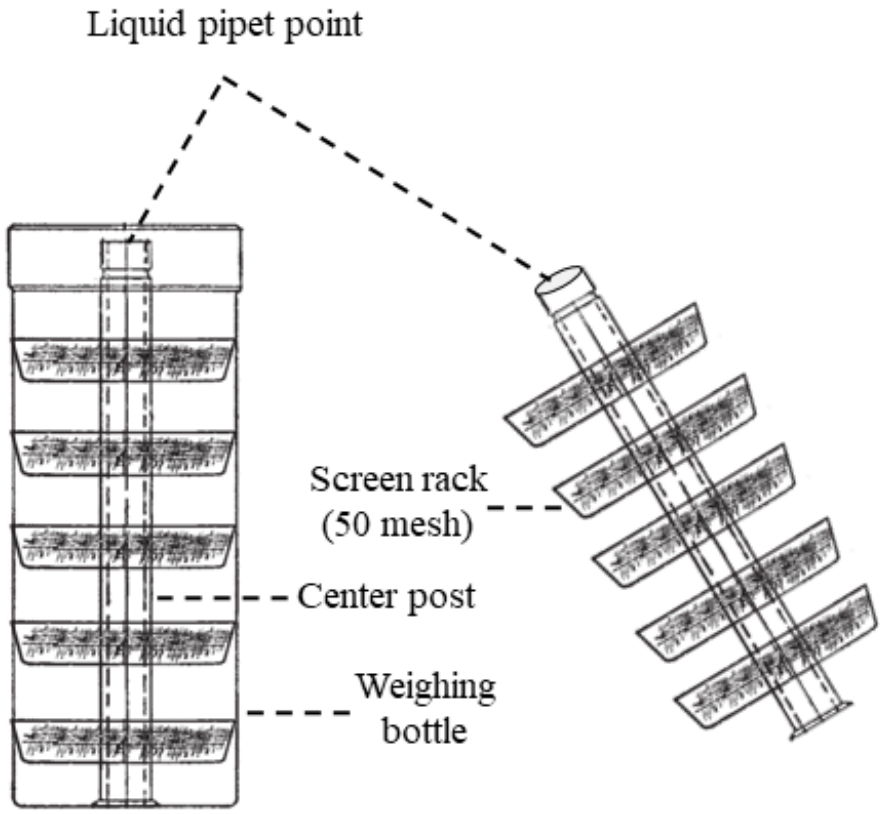

Figure 3.8 The gel test apparatus.

3.3.4 Fourier Transform Infrared Spectrophotometer (FTIR)

The presence of functional groups of the rubber samples was characterized using attenuated total reflectance-Fourier transform infrared spectroscopy (ATR-FTIR, Perkin Elmer Frontier). The spectra were recorded at room temperature with a resolution of 4 cm^{-1} and 16 scans in the spectral range of 4000 to 600 cm^{-1}.

3.3.5 Scanning electron microscopy (SEM)

The morphology of the samples was measured using a field emission-scanning electron microscope (FE-SEM, Tescan, Mira3). Prior to the observation, the dried latex grids prepared were placed onto a specimen stub and were sputter-coated with a thin layer of gold. The backscattered electrons detected all grids with an acceleration of 5 kV.

3.3.6 Transmission electron microscope (TEM)

The morphology of the rubber latex and grafted rubber latex were studied. The latex sample was diluted 200 times with DI water. A drop of diluted solution is placed on microscope grids (300-mesh copper grid) and then exposed to a vapor of 1 ml of 2% osmium tetroxide (OsO_4) solution overnight before observation. The stained grids were measured by Transmission electron microscopy (TEM, Hitachi, HT7700, Hitachi Naka, Ibaraki, Japan.) with a magnification of 20,000 – 40,000 at an accelerating voltage of 80 kV.

3.3.7 Thermogravimetric Analysis (TGA)

The thermal degradation of samples was performed using a thermogravimetric analyzer (TGA, Perkin Elmer, Pyris 1). 5.0 - 10.0 mg samples were weighed in alumina crucibles. The samples were operated at heating rates of 10, 20, 30, and 40 °C/min under air with a flow rate of 20 mL/min with a temperature range of 25°C to 850 °C to estimate the thermal stability and kinetic degradation.

3.3.8 Monomer conversion

At a given reaction time, the weight of the latex sample was weighted both before coagulation and after drying, was collected and used to calculate monomer conversion (x_p), related to the weight fraction of unreacted monomer and the overall weight fraction of monomer by using the following relationships:

$$\text{Monomer conversion } (x_p) = \frac{\text{weight of monomer polymerized}}{\text{weight of initial monomer}} \qquad (3.2)$$

The free rubber was removed from the gross product by using soxhlet extraction with petroleum ether and dried in a vacuum oven at 50 °C for another 24 hours, was recorded and used to determine the conversion of the graft of rubber (x_{GR}) and free rubber (x_{FR}) as follows:

$$\text{Free rubber conversion } (x_{FR}) = \frac{\text{weight of rubber ungrafted}}{\text{weight of gross polymer}} \qquad (3.3)$$

$$\text{Grafing of rubber conversion } (x_{GR}) = \frac{\text{weight of rubber grafted}}{\text{weight of gross polymer}} \qquad (3.4)$$

The residual product was then extracted with acetone for 24 hours and dried in a vacuum oven at 50 °C for another 24 hours, as shown in Figure 3.9, was recorded and used to determine the grafting of monomer (x_g) and free homopolymer (x_f), as well as grafting efficiency (GE) and grafting level (GL). All calculations are presented as follows:

$$\text{Grafting of monomer conversion } (x_g) = \frac{\text{weight of monomer grafted}}{\text{weight of initial monomer}} \quad (3.5)$$

$$\text{Free of monomer conversion } (x_f) = \frac{\text{weight of monomer ungrafted}}{\text{weight of initial monomer}} \quad (3.6)$$

$$\text{Grafting effiency (GE, \%)} = \frac{\text{weight of monomer grafted}}{\text{weight of monomer polymerized}} \times 100 \quad (3.7)$$

$$\text{Grafting level (GL, \%)} = \frac{\text{weight of graft copolymer}}{\text{weight of rubber grafted}} \times 100 \quad (3.8)$$

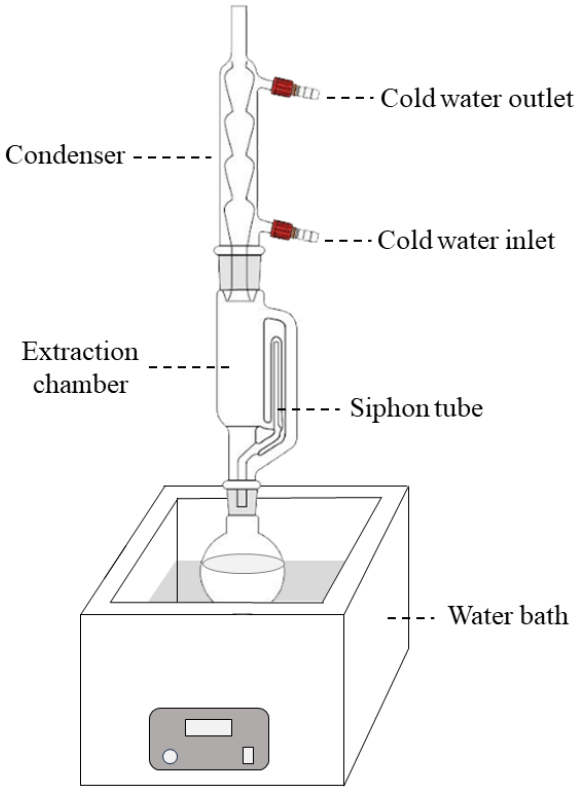

Figure 3.9 The Soxhlet extraction apparatus setup.

3.3.9 Universal tensile testing

Tensile testing and elongation at break were investigated at room temperature using a universal tensile testing machine (EZ-LX, Shimadzu, Tokyo) according to ASTM D638. Specimens were tested with a load cell of 10 N and a crosshead speed of 50 mm/min. Dumbbell-shaped specimens were prepared following type IV, with an overall width of 25.7 mm, an overall length of 115 mm, a thickness of 3 mm, and a gage width of 6 mm. The reported values were the average value of six samples and the standard deviation (SD) of the data around the average value.

3.3.10 Impact testing

The impact strength of the samples was conducted according to ASTM D256. The impact test of specimens was prepared by using the compression molding process. The dimensions of 12.7 × 3.2 × 63.5 mm (width × length × thickness) are used as a standard specimen. Before testing, all specimens were notched and tested using an impact tester (GOTECH, GT-7045-MD) with a pendulum energy of 2.7 J at room temperature. The value of impact strength was represented as energy lost per unit cross-section area at the note (J/m^2). The test results are reported as the average of four specimens of each condition and the standard deviation (SD) of the data around the average value.

3.3.11 Water absorption

A water absorption test was performed following ASTM D570. All samples were immersed in distilled water at room temperature for a period of 24 h. After every 24 hours, the specimen was removed from the distilled water and dried with a cloth. The content of water absorbed was weighed with a precise 4-digit balance. An average of three specimens for the water absorption percentage was weighed of the weights of dry specimens and the weights of fully saturated specimens, as the following Equation (3.9):

$$\%W_w = \frac{W_2 - W_1}{W_2} \times 100 \qquad (3.9)$$

where $\%W_w$ represents the percentage of water absorption, w_1 is the weight of the dry specimen (g), and w_2 denotes the weight of the fully saturated sample (g). The test results were the average weight of five specimens of each condition and the standard deviation (SD) of the data around the average value [90].

CHAPTER 4

RESULTS AND DISCUSSIONS

4.1 Liquid natural rubber (LNR)

LNR consisting of shorter chains, was prepared via oxidative degradation using $NaNO_2$ and H_2O_2 degrading agents in the presence of the HCOOH. The influence of reagent concentrations, temperature, and reaction time on the number-average molecular weight ($\overline{M}_n$), gel content, chemical structure using FTIR, and the morphology of the latex particles using SEM were studied. The degradation kinetics of NR that generate the LNR have been assessed using molecular weight data.

4.1.1 Average molecular weight

The results of the NR degradation were determined by measuring average molecular weights, as shown in Figure 4.1, and the [η] is summarized in Figure 4.2. The relationship between the average molecular weight and the [η] can be described by the Mark-Houwink-Sakurada (MHS) Equation [49-51, 91] as follows:

$$[\eta] = K\overline{M}_n^{a} \tag{4.1}$$

$$[\eta] = K\overline{M}_v^{a} = K(\overline{M}_v/\overline{M}_w)^{a}\,\overline{M}_w^{a} = Kq_{MHS}\,\overline{M}_w^{a} \tag{4.2}$$

where *a* and K are constant, and the q_{MHS} is the polydispersity correction factor for a certain temperature and solvent [51]. The *a* and K values for rubber samples were evaluated by using eleven samples of different average molecular weights. Figure 4.3 represents the plot of ln [η] against the log $\overline{M}_n$ of rubber samples yielded a straight line. Thus, it was found that the plot of log [η] and log $\overline{M}_n$ showed a straight line with a slope and an intercept equal to 0.6382 and -2.8837, respectively, obtained by the least square linear regression method (R^2 = 0.9745). Then, the following MHS Equation can be obtained:

$$[\eta] = 1.3071 \times 10^{-3}\,\overline{M}_n^{0.6382} \tag{4.3}$$

where $\bar{M}_n$ is the number-average molecular weight, a preliminary estimate of the q_{MHS} for LNR samples was calculated for each LNR sample, assuming *a* is equal to 0.6382 (the exponent in Equation (4.1)) and substituted in Equation (4.2) was obtained from

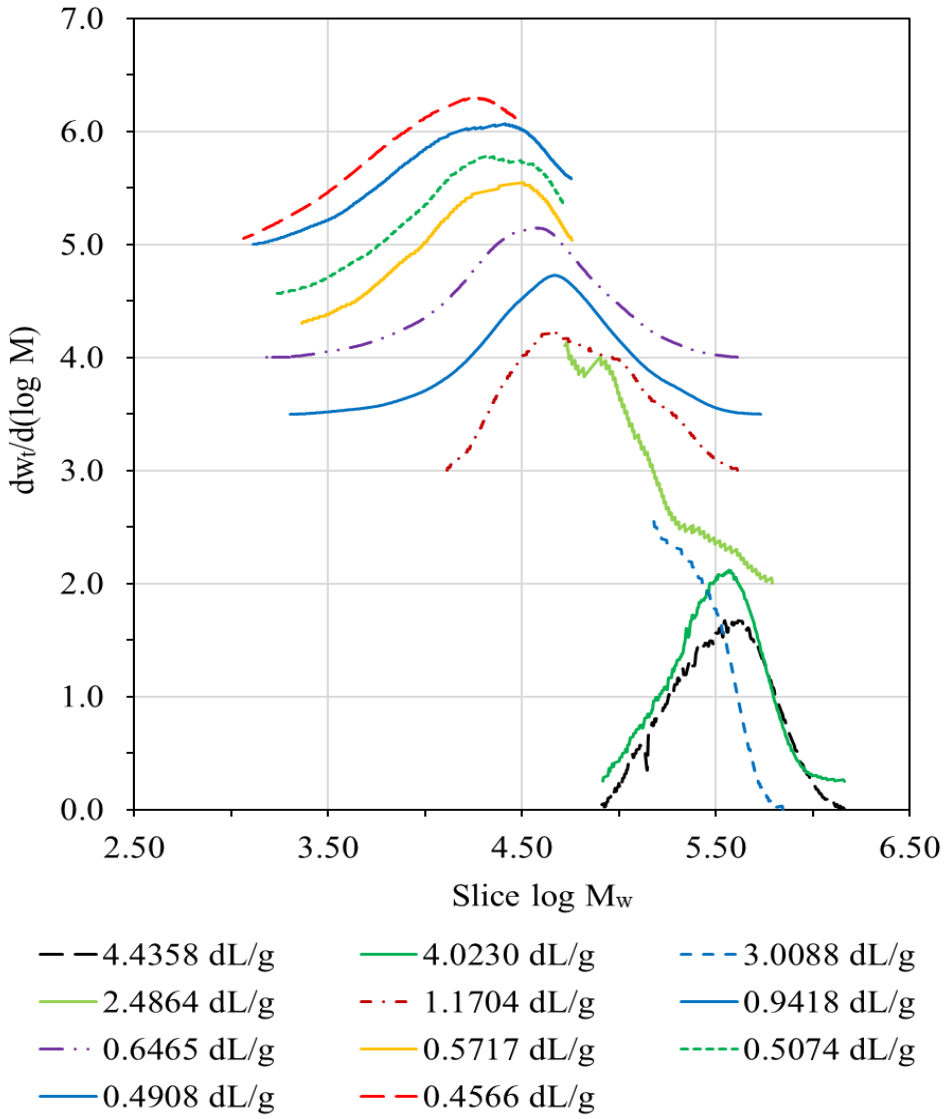

Figure 4.1 Molecular weight distribution curves from GPC analysis of rubber samples.

Equation (4.2). A new value of *a* was calculated from the slope of the line by plotting (log [η] - log q_{MHS}) against log $\bar{M}_w$ to produce a straight line. The procedure was repeated until two continuous values differed by less than 0.001 [50, 91]. Lastly, the plot of (log [η] - log q_{MHS}) against log $\bar{M}_w$ as shown in Figure 4.4, and the final values

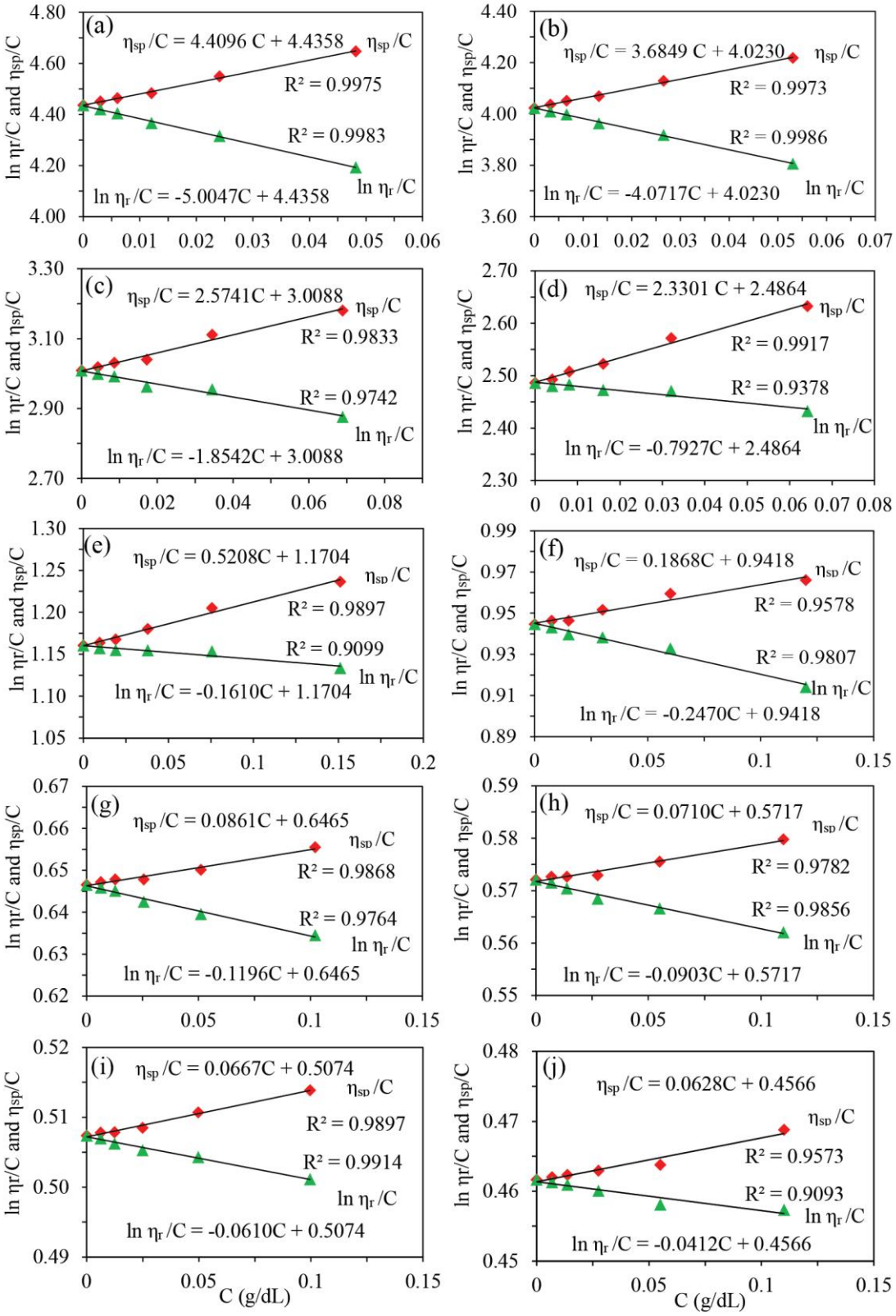

Figure 4.2 Intrinsic viscosity of rubber for different molecular weight.

of *a* and K constant were derived from the slope and the intercept of line [49]. The constants K and *a* were 1.2688×10^{-3} dL/g and 0.6191 for LNR samples and can be used to calculate the $\bar{M}_v$ by using Equation (4.2) as the summary in Table 4.1. The resulting MHS Equation for LNR samples in the $\bar{M}_w$ range of $1.24 \times 10^4 - 9.57 \times 10^5$ g/mol and the average value of 0.9521 for q_{MHS} were proposed:

$$[\eta] = 1.2688 \times 10^{-3} \bar{M}_v^{0.6191} = 1.2688 \times 10^{-3} q_{MHS} \bar{M}_w^{0.6191} = 1.2080 \times 10^{-3} \bar{M}_w^{0.6191} \quad (4.4)$$

Equation (4.2) can be calculated as $\bar{M}_v$ showing a plot of log [η] against log $\bar{M}_v$ of rubber samples, which yielded a straight line ($R^2 = 1.000$). The values of *a* and K constant were derived from the slope and intercept of the line to be 0.6191 and 1.2688×10^{-3} dL/g, as shown in Figure 4.5, in good agreement with the results shown above.

Table 4.1 Polydispersity Correction Factor (q_{MHS}), [η], $\bar{M}_n$, $\bar{M}_w$, and $\bar{M}_v$ for each LNR sample.

Sample	q_{MHS}	[η] (dL/g)	$\bar{M}_n$ (g/mol)	$\bar{M}_w$ (g/mol)	$\bar{M}_v$ (g/mol)
1	0.9582	4.4358	330,439	957,045	529,355
2	0.9695	4.0230	276,184	350,416	452,090
3	0.9823	3.0088	225,787	253,633	282,782
4	0.9452	2.4864	95,389	127,762	207,813
5	0.9339	1.1704	50,023	80,016	61,532
6	0.9078	0.9418	22,408	46,351	43,318
7	0.9750	0.6465	22,143	27,796	23,591
8	0.9566	0.5717	17,139	23,254	19,342
9	0.9521	0.5074	12,853	21,007	15,951
10	0.9404	0.4908	10,825	19,882	15,117
11	0.9522	0.4566	7,465	12,354	13,452

Generally, the values of *a* and K depend on the nature of the polymer, the temperature, the range of molecular weight, the quality of solvent, and MWD. However, the value of K is more sensitive to the MWD of polymers. In this work, for thermodynamically suitable solvents, the value of a (0.6191) lies between 0.50 and 0.75 for flexible-chain polymers [92]. From the results above, it is clearly seen that the value of *a* and K was equal when compared between plotting log [η] against log $\bar{M}_v$ and log [η] - log q_{MHS} against log $\bar{M}_w$. According to Equation (4.4), it can be observed that the coefficients in MHS Equations differ for $\bar{M}_v$ and $\bar{M}_w$. This indicates that the value of q_{MHS} slightly influences the correlation of rubber samples.

The results shown above that these *a* and K values of the MHS equation were further used for the transformation of the [η] of other samples into $\bar{M}_n$, $\bar{M}_w$, and $\bar{M}_v$ by using Equations (4.3) and (4.4) as shown in Table 4.1.

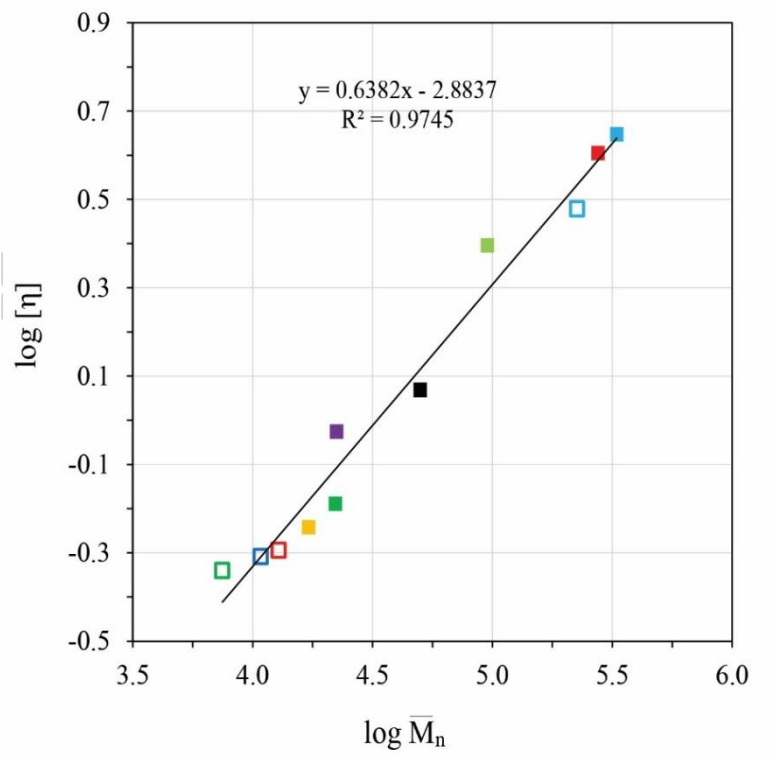

Figure 4.3 Relation of log [η] and log $\bar{M}_n$ for rubber samples in toluene at 30°C.

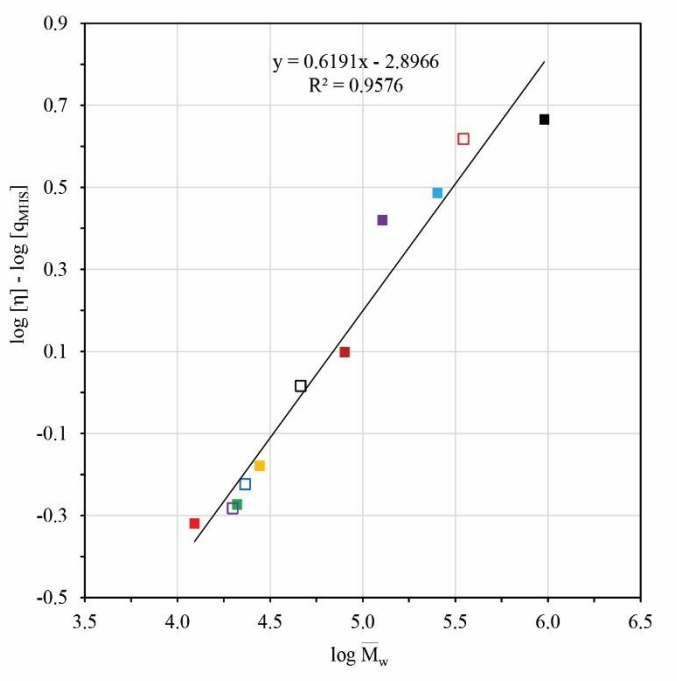

Figure 4.4 Relation of log [η] -log [q_{MHS}] and log $\bar{M}_w$ for LNR samples in toluene at 30°C.

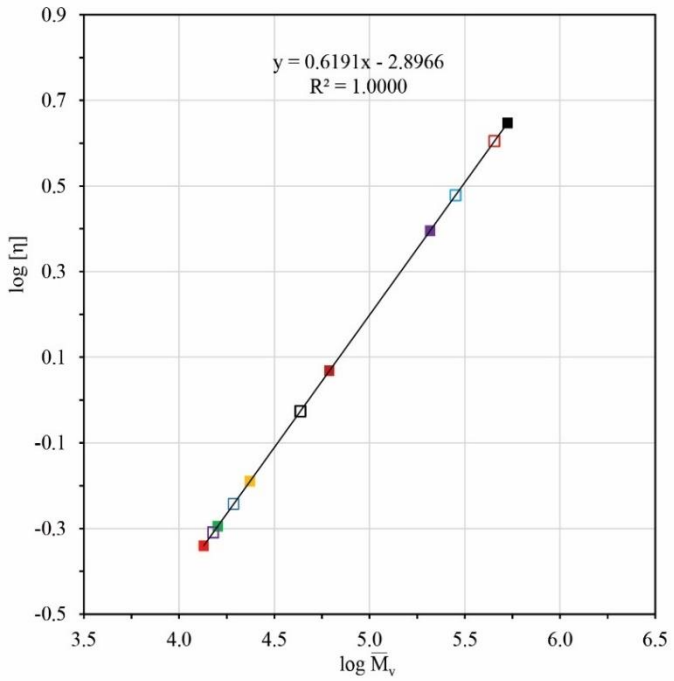

Figure 4.5 Relation of log [η] and log $\bar{M}_v$ for LNR samples in toluene at 30°C.

4.1.2 Effect of the reaction time

The effect of reaction time on the $\bar{M}_n$ and gel content of the LNR samples was studied at various reaction times from 3 to 12 h. It was evident that the $\bar{M}_n$ values of the LNR samples showed an exponential increase with the increasing reaction time, as shown in Figure 4.6a. When an increase in reaction time, the trend of the $\bar{M}_n$ values decreased significantly during the first 3 h, followed by a gradual decrease after a reaction time of 3 up to 12 h. In part of the gel content, it can seen that the gel value continued to decrease significantly as the time increased from 3 to 12 hours , as shown in Figure 4.6b. Therefore, after 12 h of reaction, the $\bar{M}_n$ and gel content of the NR sample were reduced from 83.04 $\times 10^{-4}$ to 10.83 $\times$ 10^3 g/mol and 26.26 to 9.25 %, respectively. The decrease of $\bar{M}_n$ and gel content indicates that the degradation reaction has broken the chains at both the gelling and linear part of NR, resulting in a decrease in the gel content of LNR compared to the starting material of NR [93].

Figure 4.7 shows the FTIR spectra of NR and LNR samples that were prepared at various reaction times from 3 to 12 h. In general, the spectra of the LNR sample showed a similar pattern to that of the NR spectrum. It can observed that the absorption peaks of 1665, 1446, and 836 cm^{-1}, which correspond to the C=C, C–C, and =CH bonds, some groups decreased with increased reaction time after degradation reaction [94]. This may indicate that the chain breaking of NR at the C-C bond, which has a labile proton, is the weak point that can be broken by radical species such as OH. However, the chains of NR were broken during the degradation reaction for 3 to 12 h, and the chain scission of NR latex was increased, resulting in the formation of hydroxyl and carbonyl groups, which correspond to absorption peaks of 3400 and 1740 -1715 cm^{-1} on the cis-1,4 - polyisoprene chain of LNR [7, 18, 21].

The morphology of the NR and LNR particles at varying molecular weights was examined using SEM micrographs, as illustrated in Figure 4.8a-d. Significant differences were observed in the morphology of latex particles. Before degradation, the particles exhibited the largest sizes [95], with spherical and pear shapes, and NR particle sizes ranged between 1.06 and 1.44 μm, as depicted in Figure 4.8a.

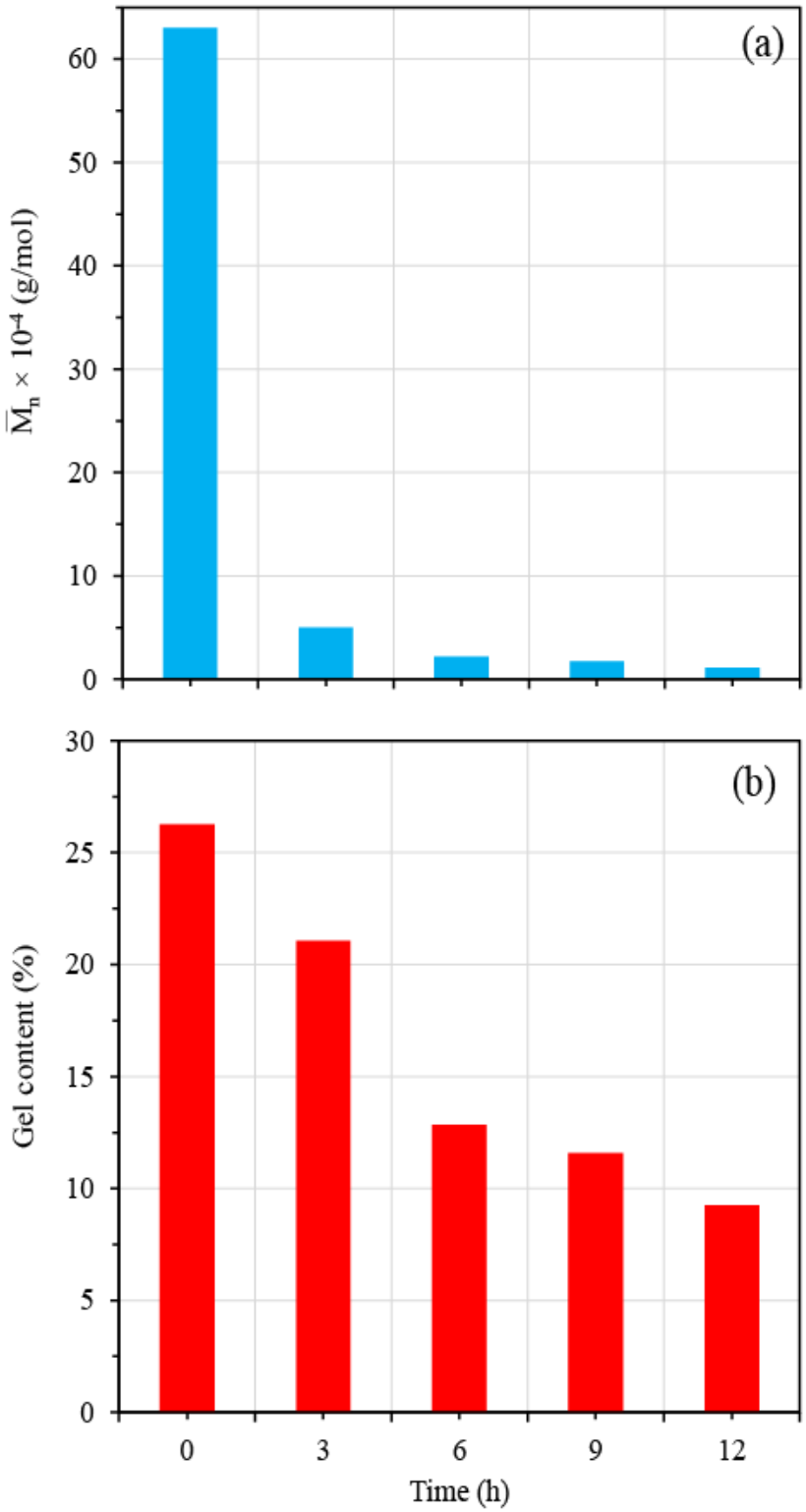

Figure 4.6 $\bar{M}_n$ and gel content of LNR over time with H_2O_2 0.4 mol, $NaNO_2$ 0.02 mol, at pH 5 and 65°C.

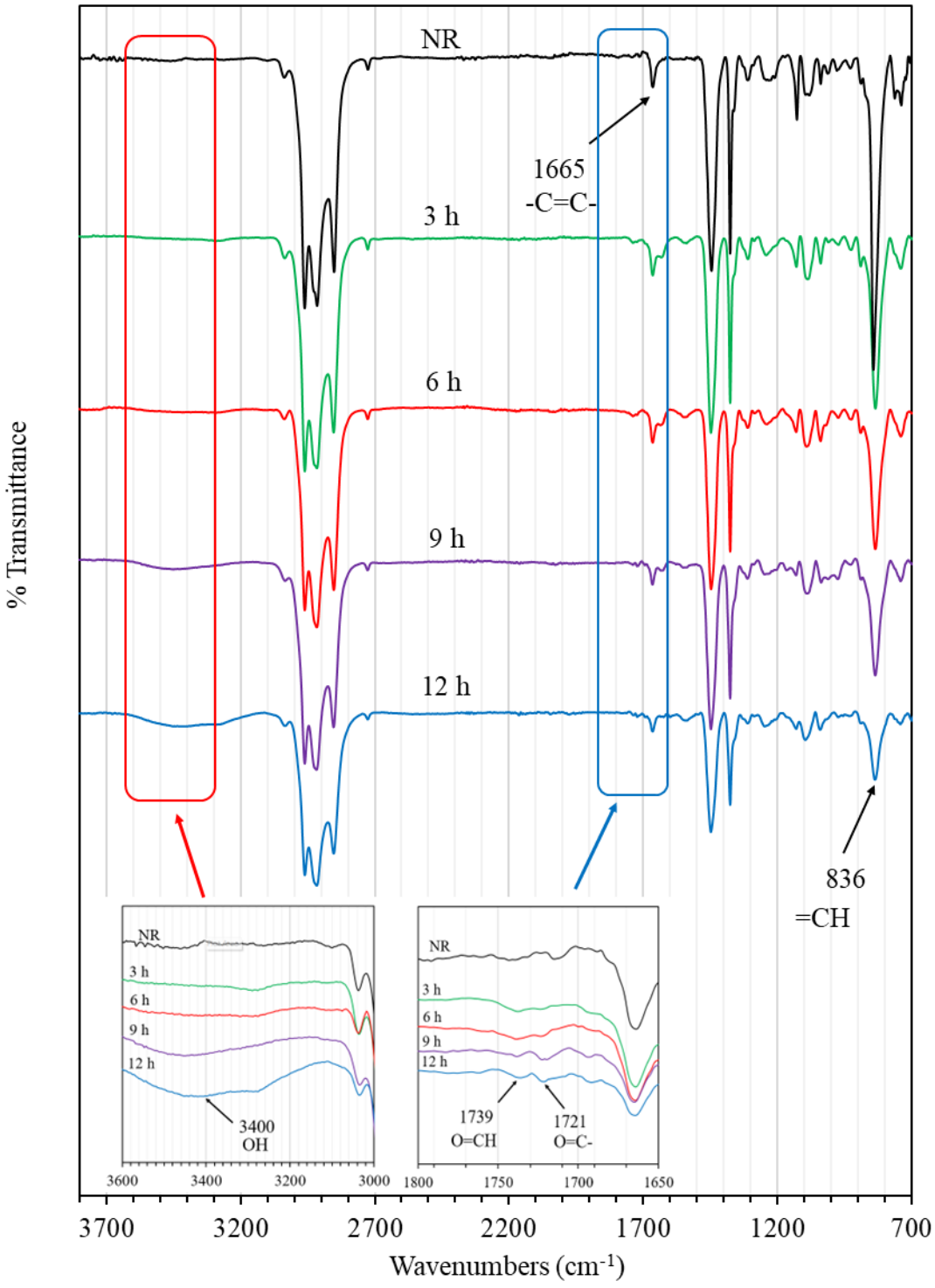

Figure 4.7 FTIR spectra (700 – 3800 cm^{-1}) of NR and LNR samples prepared at various reaction times with amounts of H_2O_2 0.4 mol, $NaNO_2$ 0.02 mol, and pH.

Factors such as extended reaction times facilitated further degradation of the rubber chains, resulting in smaller particles. It was noted that after a 3 h degradation reaction, some latex particles became spherical, smaller, and displayed a broader size range compared to the NR particles (Figure 4.8b). After a 12 h degradation process, as shown in Figure 4.8d, the latex particles were nearly uniform and had shrunk to sizes ranging from 0.13 to 0.29 μm [89].

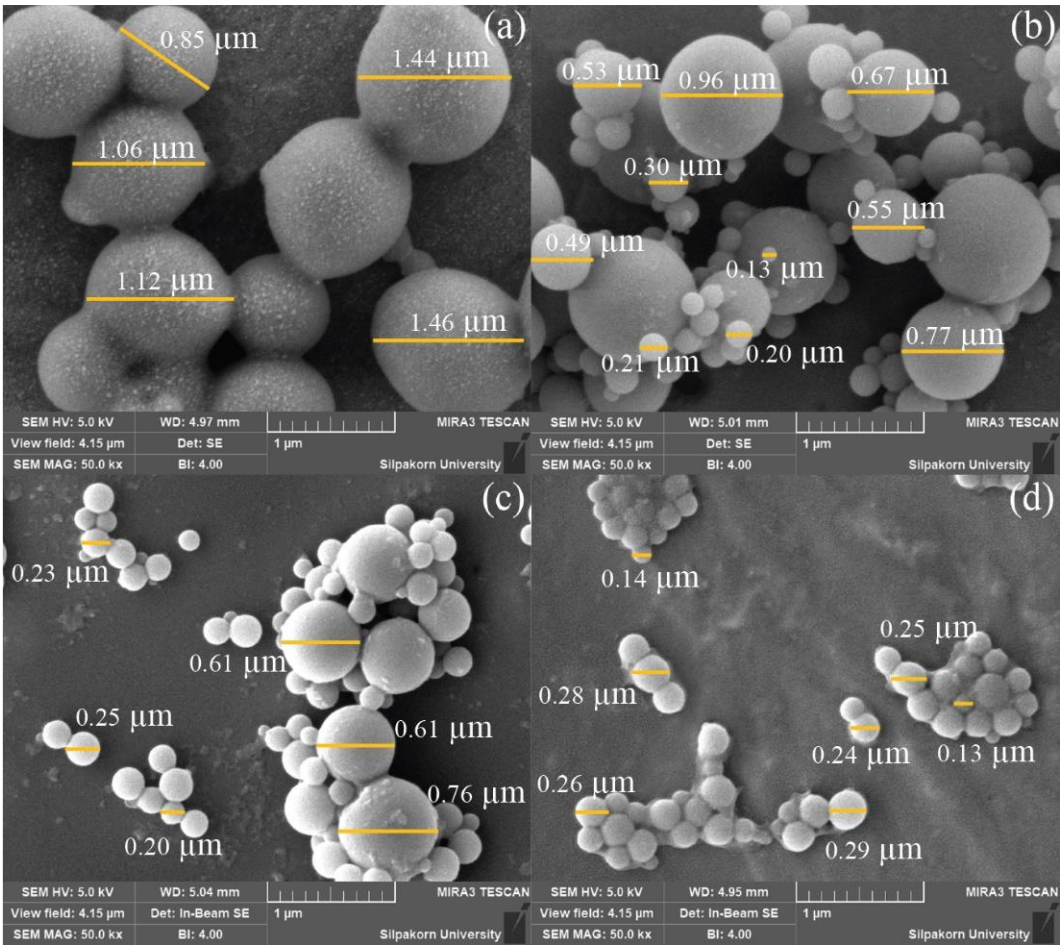

Figure 4.8 SEM micrographs (50,000×) of the rubber particles after degradation reaction at different reaction times: (a) NR, (b) 3 h, (c) 6 h, and (d) 12 h for amounts of H_2O_2, 0.4 mol, $NaNO_2$ 0.02 mol, and pH 5 at 65 °C. (The yellow line is diameters)

4.1.3 Effect of the concentration of hydrogen peroxide

It is generally known that the concentration of chemicals related to a reaction is one of the main factors affecting the reaction yield. Figure 4.9 shows the $\overline{M}_n$ and gel contents of LNRs that were prepared with various amounts of H_2O_2 with $NaNO_2$ 0.02 mol and pH 5 at 65°C for 3 - 12 h. The value of the $\overline{M}_n$ and gel content of LNR revealed to decrease with an increase in the amounts of H_2O_2 from 0.1 to 0.4 mol at the same time, which has been reduced from 80.64 $\times 10^{-3}$ to 10.83 $\times 10^{-3}$ g/mol, as shown in Figure 4.9a. The gel content also decreased with an increase in the amounts of H2O2 from 0.1 to 0.4 mol, as shown in Figure 4.9b. This suggests that the NR underwent degradation. The observed trend can be attributed to the increased presence of H_2O_2, which generated more hydroxyl radicals during the degradation reaction, thereby enhancing the chain scission of NR [93, 96]. Consequently, a higher concentration of H_2O_2 results in a more rapid oxidative degradation of the NR.

The FTIR spectra of NR and LNR samples were performed at various amounts of H_2O_2 with $NaNO_2$ 0.02 mol and pH 5 at 65 °C for 12 h, as shown in Figure 4.10. It can be seen that absorption peaks at 1665, 1446, and 836 cm^{-1} correspond to the C=C, C-C, and =CH bonds decreased after the degradation reaction for all the LNR samples. On the other hand, the LNR samples appeared to have new absorption peaks at 3400, 1739, and 1721 cm^{-1}, which were higher absorption peaks than those of the NR. A broad absorption peak at 3400 cm^{-1} indicates the presence of the OH group, which gradually increases on the LNR chain with an increase in the amount of H_2O_2 0.1 - 0.4 mol. Meanwhile, small peaks at 1739 and 1721 cm^{-1} correspond to carbonyl groups. Both of these groups occur on LNR chains as a result of chain scission in the degradation reaction [94, 97]. Hydroxyl and carbonyl groups were expected to form during the chain breakage when labile hydrogens were attacked at α-carbons on the NR chain, which could easily undergo free radical substitution by hydroxyl radicals [18]. Or may occur the breaking at C=C due to being very sensitive to oxidation and quickly react with oxidizing agents [98].

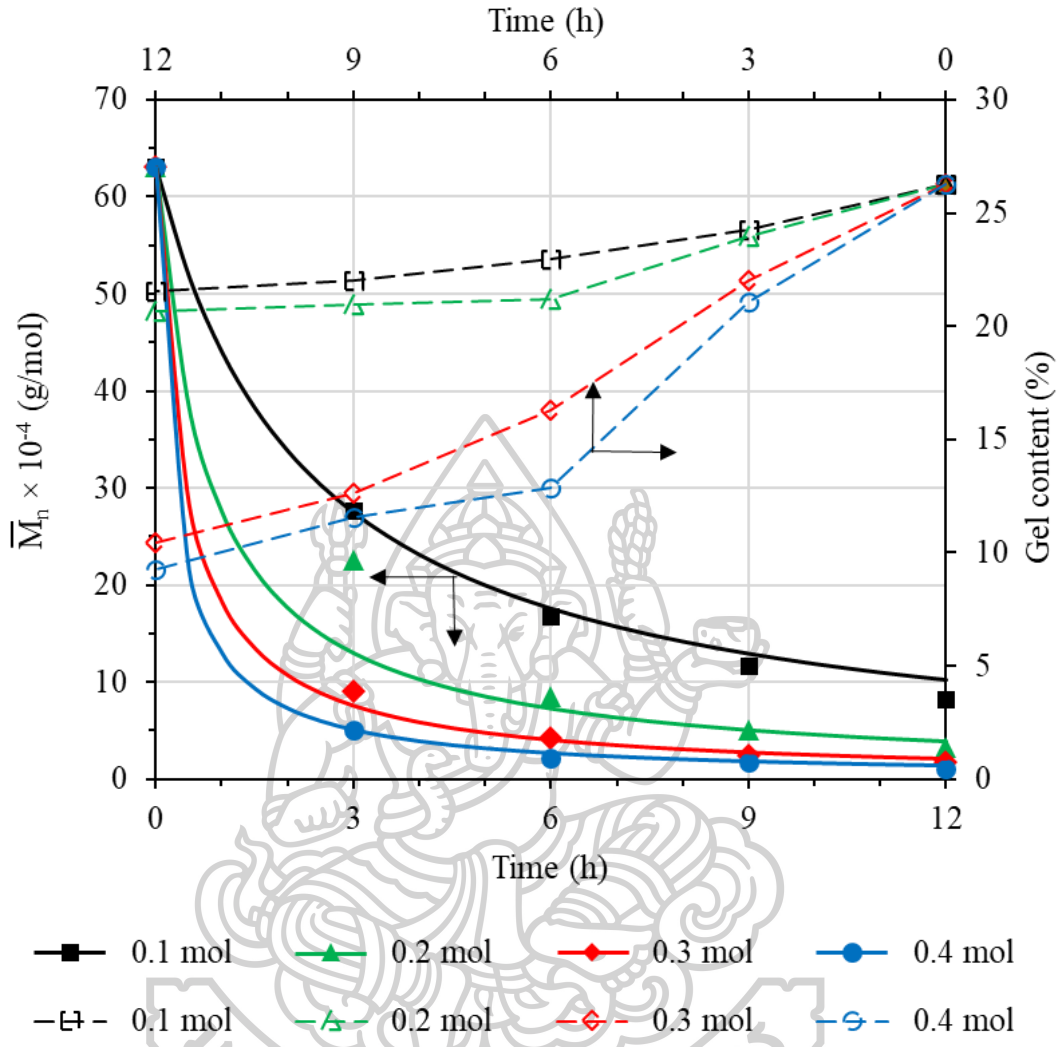

Figure 4.9 Effect of amount of hydrogen peroxide on (a)) $\overline{M}_n$ (close symbols) and (b) Gel content (open symbols) at various times. And the solid line is the kinetic model.

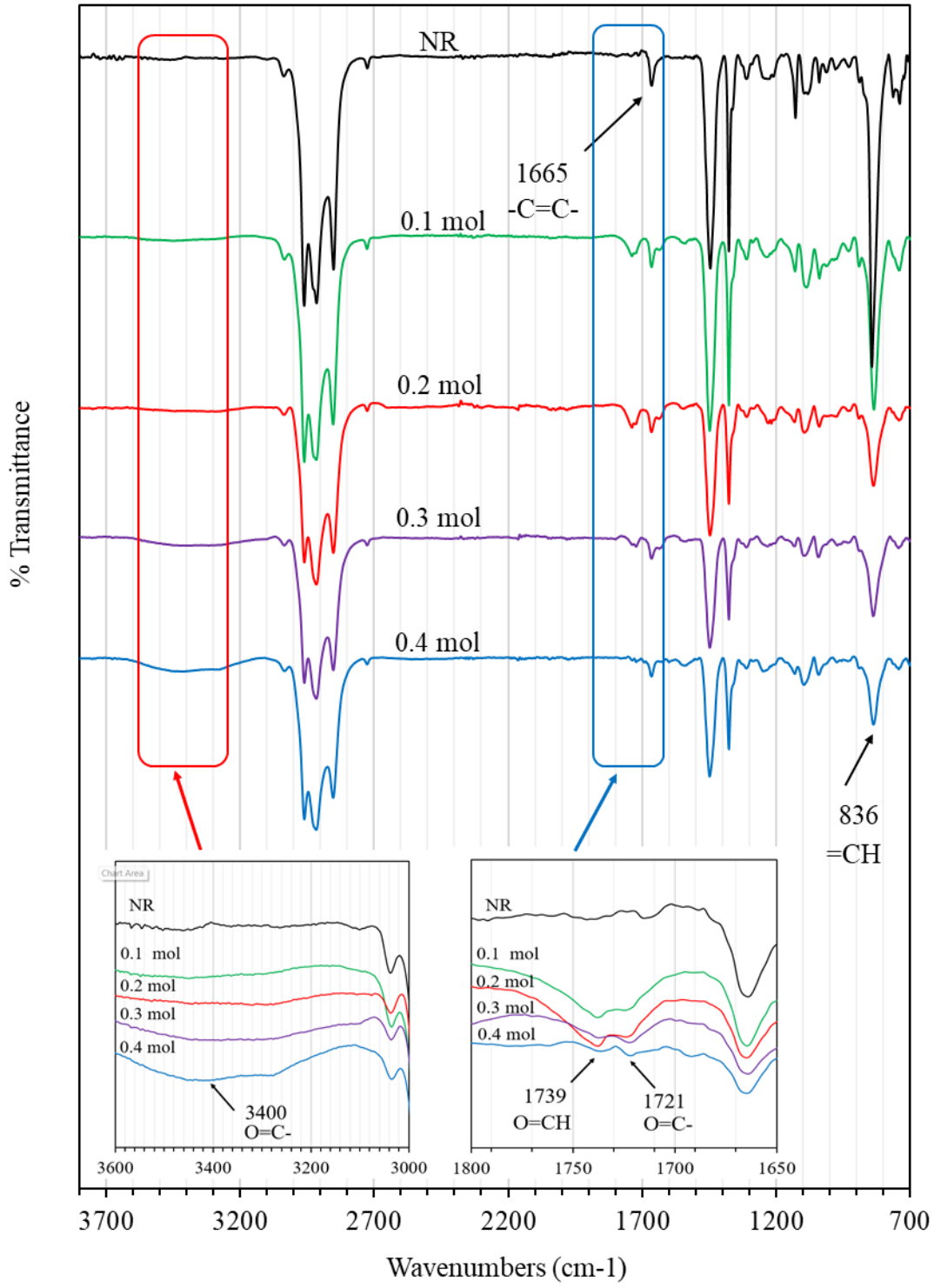

Figure 4.10 FTIR spectra (700 – 3800 cm^{-1}) of NR and LNR samples prepared at various amounts of H_2O_2 with $NaNO_2$ 0.02 mol and pH 5 at 65°C for 12 h.

4.1.4 Effect of the concentration of formic acid

Figure 4.11 shows the $\overline{M}_n$ and gel content of NR and LNR samples prepared at various pH with amounts of H_2O_2 0.4 mol and $NaNO_2$ 0.02 mol at 65 °C for 3 -12. The amount of HCOOH used was adjusted to the required range of pH 5 to 11 for the degradation reaction. It is generally known that hydrogen peroxide and sodium nitrite do not interact chemically under neutral and alkaline conditions but react spontaneously to produce peroxynitrite acid in acidic conditions [69, 99]. At lower pH levels, a greater amount of formic acid (HCOOH) provided more hydrogen ions, leading to an increased formation of peroxynitrous acid, which in turn released hydroxyl ($^{\bullet}OH$) and nitrogen dioxide ($^{\bullet}NO_2$) radicals. This resulted in a higher rate of degradation of latex natural rubber (LNR). According to Figure 4.11a, degradation of natural rubber (NR) in acidic conditions was more effective than in alkaline conditions, producing LNR with a lower the $\overline{M}_n$. As mentioned above, the $\overline{M}_n$ of LNR samples was reduced from 46.64 $\times 10^{-3}$ (pH 11) to 10.83 $\times 10^{-3}$ g/mol (pH 5). The gel content of LNR also decreased when the $\overline{M}_n$ of LNR was reduced in the oxidation degradation reaction, as shown in Figure 4.11b. This indicates that NR's linear and gelling parts have broken the chain during the degradation reaction.

The chemical structures of NR and LNR samples were analyzed at different pH levels using FTIR, as depicted in Figure 4.12. The LNR exhibited absorption peaks corresponding to C=C, C-C, and =C-H bonds at 1665, 1446, and 836 cm^{-1}, respectively, which are similar to those found in NR. The FTIR spectra of LNR samples prepared at various pH levels revealed a few additional peaks not present in the NR spectra. For the LNR sample prepared in an acidic condition, a broad absorption peak at 3400 cm^{-1} was attributed to the stretching mode of hydroxyl groups on the LNR chains. In contrast, the LNR samples prepared in neutral and alkaline conditions showed carbonyl peaks (C=O) at 1721 cm^{-1} and 1739 cm^{-1}, corresponding to ketone and aldehyde groups, respectively [89].

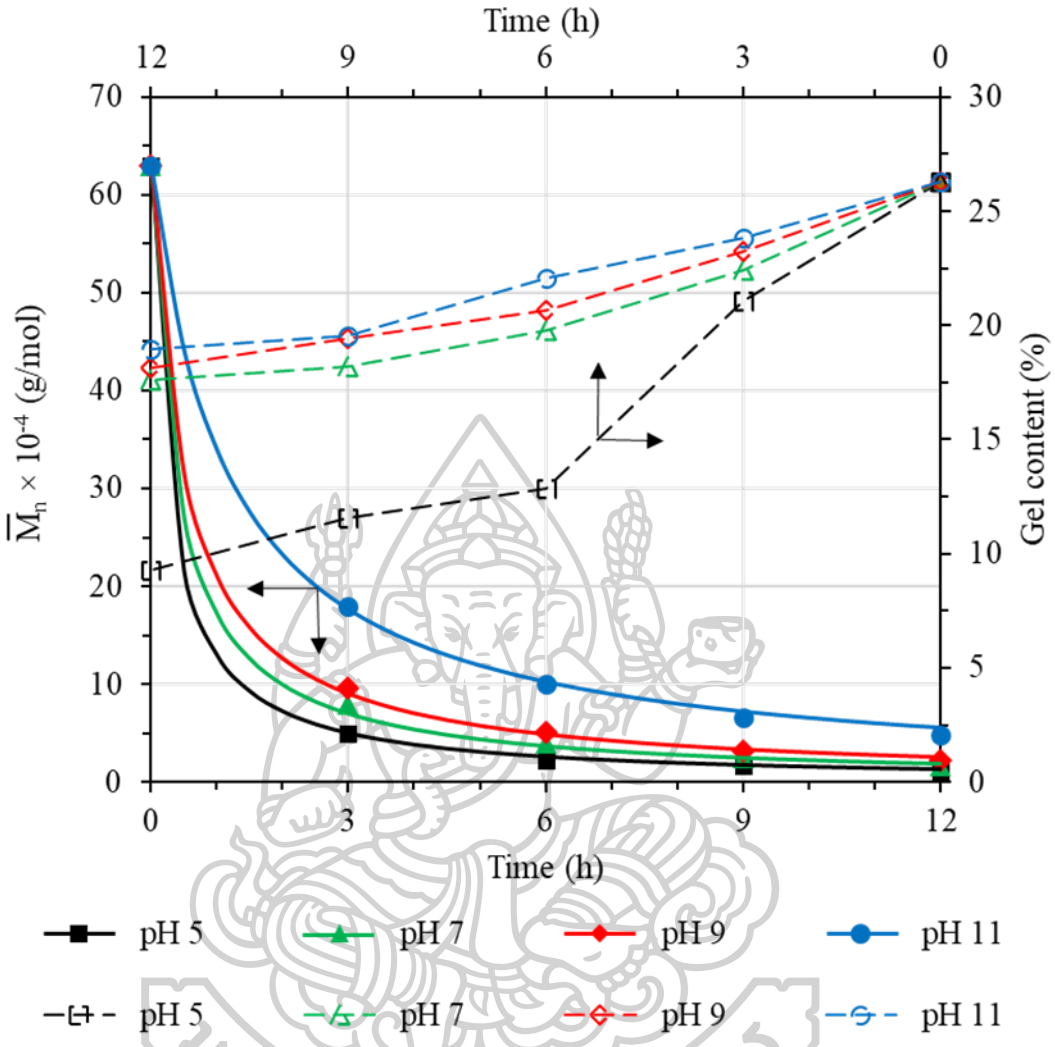

Figure 4.11 Effect of different pH on (a) $\overline{M}_n$ (close symbols) and (b) gel content (open symbols) at various times. And the solid line is the kinetic model.

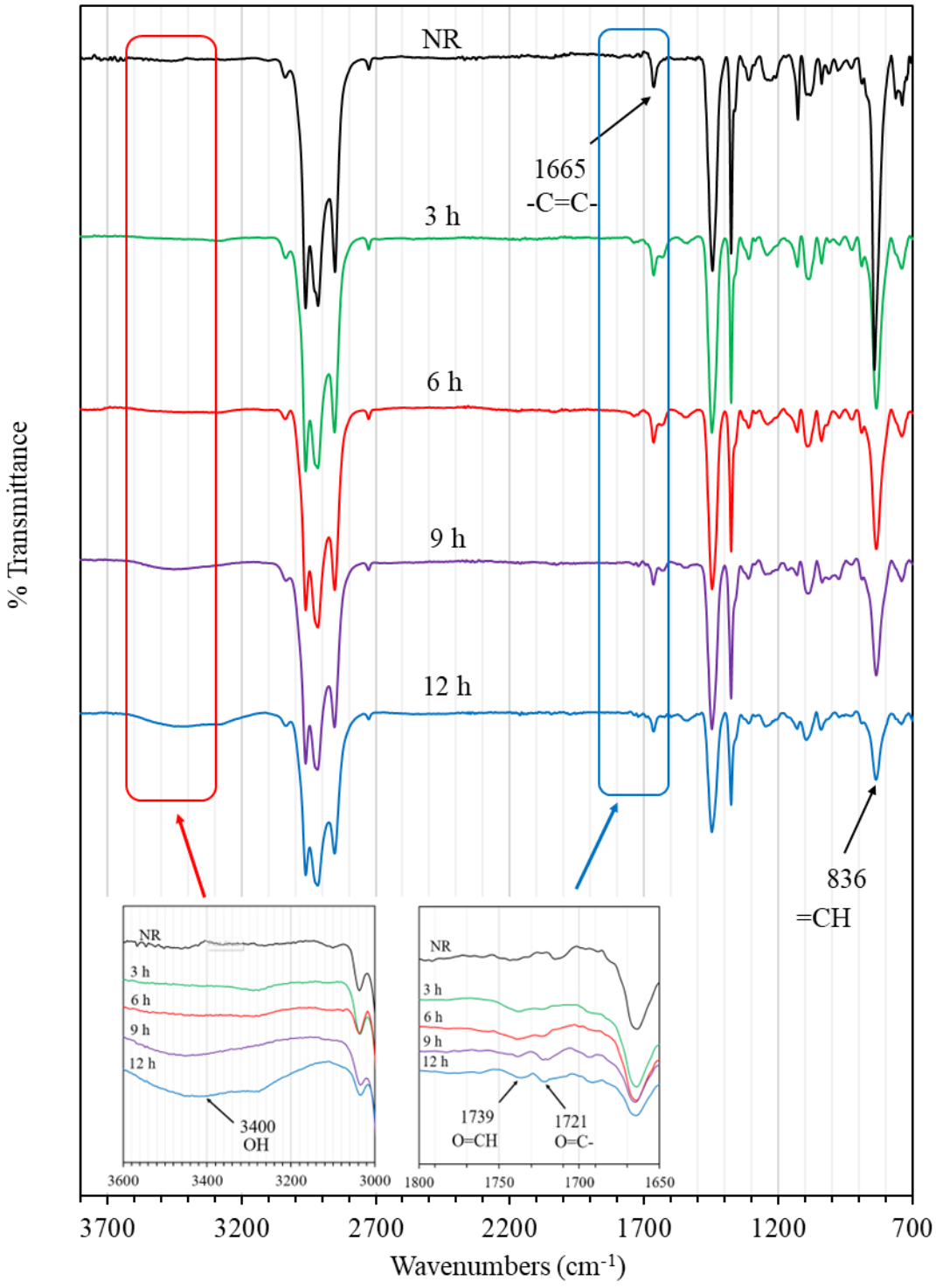

Figure 4.12 FTIR spectra (700 – 3800 cm^{-1}) of NR and LNR samples prepared at various pH, with amounts of H_2O_2 0.4 mol and $NaNO_2$ 0.02 mol at 65°C for 12 h.

4.1.5 Effect of the concentration of sodium nitrile

The influence of varying amounts of $NaNO_2$ on the $\bar{M}_n$ and gel content of LNR samples was studied over a range from approximately 0.02 to 0.2 mol, using 0.4 mol of H_2O_2 at pH 5 and a reaction temperature of 65°C. The results indicated that increasing the amount of $NaNO_2$ led to an increase in the $\bar{M}_n$ of LNR at the same reaction time, as shown in Figure 4.13. This increase in $\bar{M}_n$ was attributed to the higher concentration of nitrite ions, which were oxidized by hydroxyl radicals ($^{\bullet}OH$), resulting in an excess of nitrogen dioxide radicals ($^{\bullet}NO_2$) and hydroxide ions (OH^-). The $^{\bullet}NO_2$ radicals were highly unstable in an aqueous solution [100, 101], leading them to pair with each other to form dinitrogen tetroxide (N_2O_4). The hydrolysis of N_2O_4 in water produced nitrous acid (HNO_2), which reacted with $^{\bullet}OH$ to regenerate $^{\bullet}NO_2$ radicals. These side reactions reduced the availability of $^{\bullet}OH$ radicals, thereby inhibiting the degradative reaction or promoting crosslinking at higher $NaNO_2$ concentrations [94]. As discussed above, the $\bar{M}_n$ and gel content of LNR samples was increased from 10.83×10^{-3} to 40.84×10^{-3} g/mol and 9.25% to 14.48%, respectively. With an increased amount of $NaNO_2$ 0.02 to 0.2 mol, as shown in Figure 4.13(a,b). The gel content of LNR samples was found to increase significantly. So, the increase in gel content of LNR samples was expected due to either reconnecting the chain or the crosslink between radical chains [102, 103].

FTIR spectra of LNR samples were prepared at various amounts of $NaNO_2$ with H_2O_2 0.4 mol and pH 5 at 65°C for 12 h, as shown in Figure 4.14. In general, the spectra of the LNR samples showed a similar pattern to that of the NR spectrum. However, the spectra of the LNR samples appeared to have new absorption peaks at 3400, 1739, and 1721 cm^{-1}, which showed the presence of hydroxyl and carbonyl groups. Indicating the breaking of chains and an increase in a few absorption peaks, indicating the presence of terminal groups as a result of the chains breaking. For all LNR samples. When the amount of $NaNO_2$ was increased from 0.02 to 0.2 mol. It can seen that the peaks at 1739 and 1721 cm^{-1}, corresponding to the carbonyl group, were increased after increasing $NaNO_2$. Meanwhile, no significant change was shown for the hydroxyl groups as the broad peak at 3400 cm^{-1} remains unchanged or very little has changed [94].

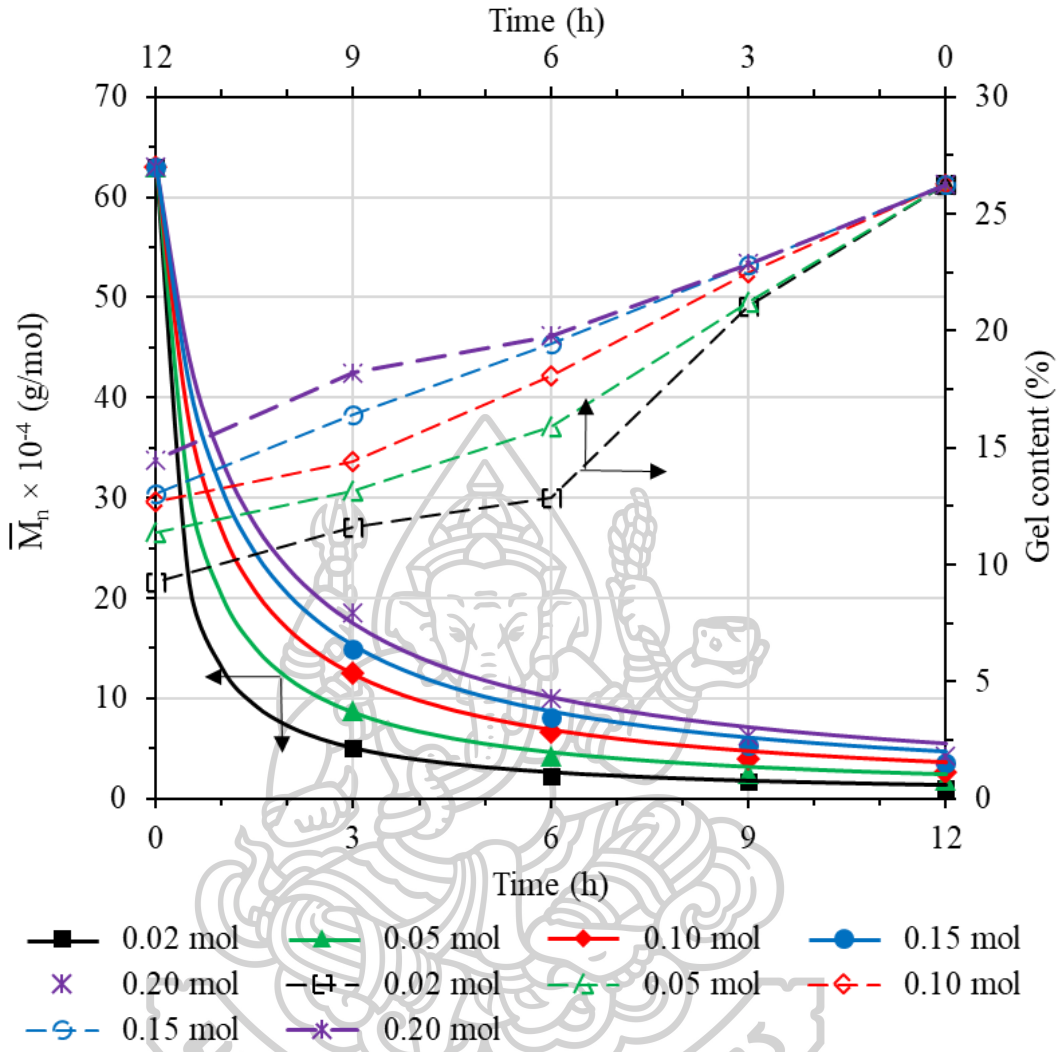

Figure 4.13 Effect of amount of sodium nitrite on (a) $\bar{M}_n$ (close symbols) and (b) gel content (open symbols) at various times. And the solid line is the kinetic model.

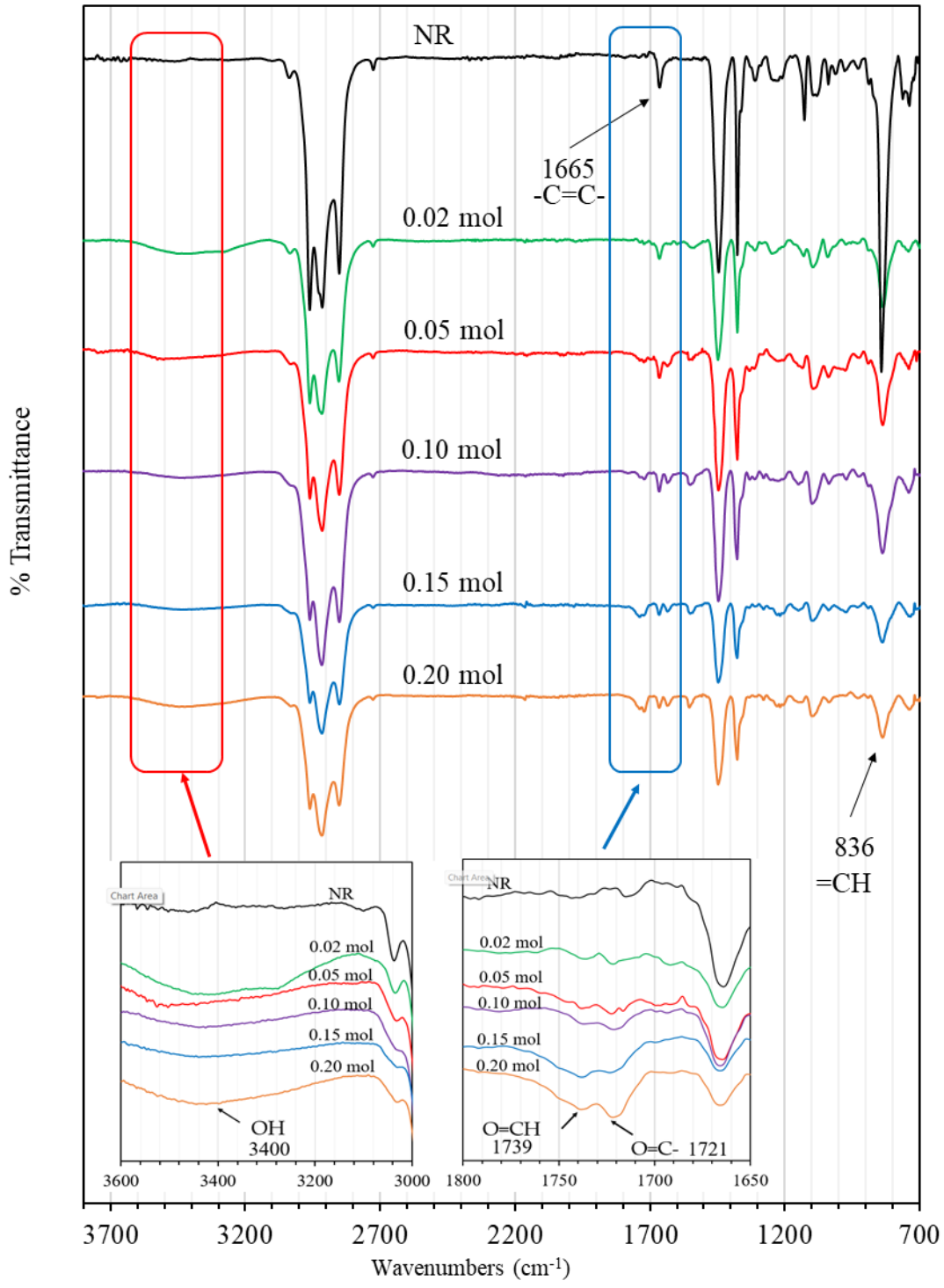

Figure 4.14 FTIR spectra (700 – 3800 cm^{-1}) of NR and LNR samples prepared at various amounts of $NaNO_2$ with H_2O_2 0.4 mol and pH 5 at 65°C for 12 h.

4.1.6 Effect of the reaction temperature

The effect of the temperature degradation on the $\bar{M}_n$ and gel content was performed at 55, 60, 65, and 70 °C for various reaction times with amounts of H_2O_2, 0.4 mol, $NaNO_2$, 0.02 mol, and pH 5. as shown in Figure 4.15. The reaction temperature affects the efficiency of the initiator and the rate of the degradation reaction [16, 21]. Higher temperatures provide more energy to activate the molecules, leading to faster chain-breaking reactions. Consequently, higher reaction temperatures accelerate the degradation rate of NR. As discussed above, the $\bar{M}_n$ and gel content of the LNR samples decreased significantly at the same time. So, the $\bar{M}_n$ of the LNR samples was reduced from 26.92×10^{-3} to 7.47×10^{-3} g/mol when the increase in reaction temperature at 12 h, as shown in Figure 4.15a. The gel content then continued to decrease when the temperature was raised to 65 °C due to an increase in reaction rate at higher temperatures [104, 105]. However, when the reaction was operated at 70 °C, the solution coagulated after 9 h of degradation reaction, as shown in Figure 4.15b. At high temperatures, the latex particle's thermal motion was accelerated. Then, the collisions among the rubber particles were more violent and trended to aggregate or re-connect rubber chains, resulting in the coagulation in the latex solution during the degradation reaction [106].

FTIR spectra of NR and LNR samples were prepared at various temperatures with amounts of H_2O_2 0.4 mol, $NaNO_2$, 0.02 mol, and pH 5 for 12 h. Figure 4.16 shows three absorption peaks at 3400, 1721, and 1089 cm^{-1}, which correspond to the hydroxyl, carbonyl, and ester groups, respectively. However, the broad absorption peak at 3400 cm^{-1}, which corresponds to the OH group, increased at a higher temperature. Only one absorption peak at 1089 cm^{-1} was found to be the presence of the ester group at a high temperature (70 °C). which was expected to have been formed during chain breaking by degradation reaction and may be one of the factors that cause crosslink.

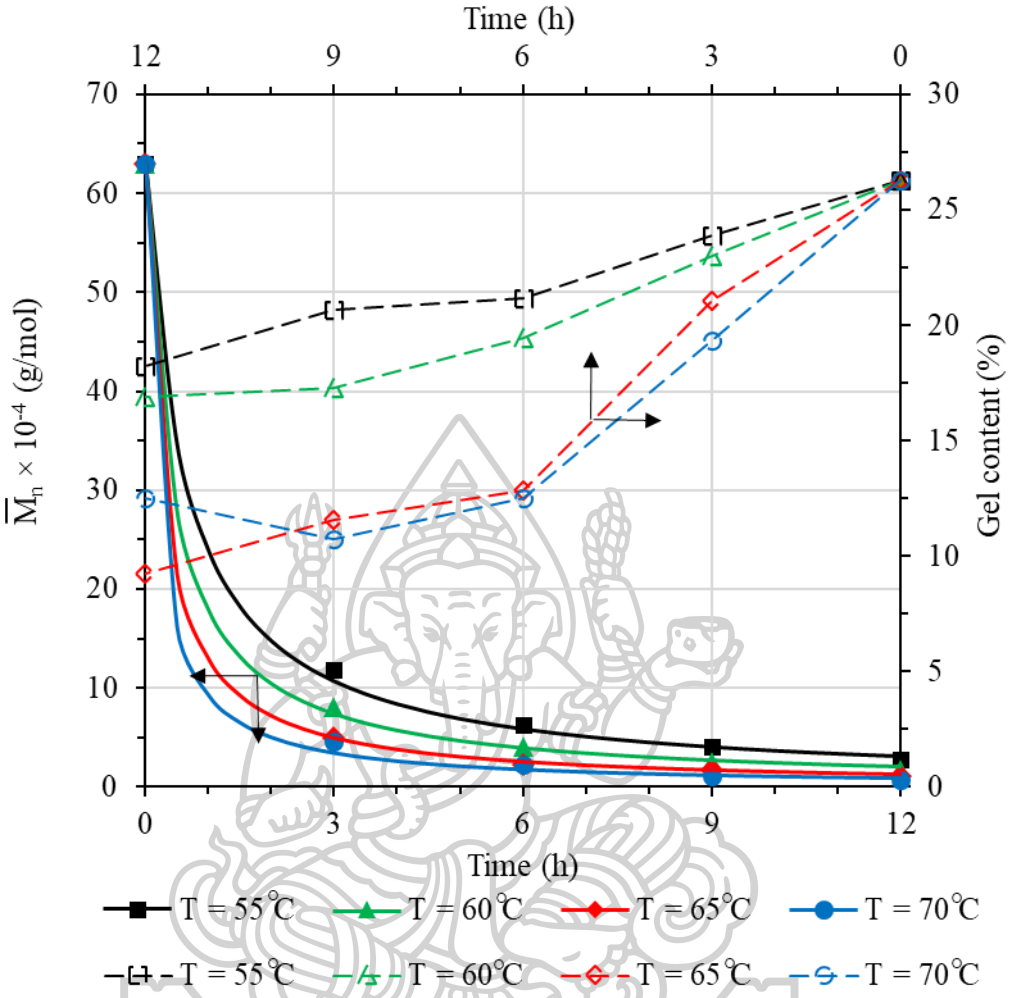

Figure 4.15 Effect of reaction temperature on (a) $\overline{M}_n$ (close symbols) and (b) gel content (open symbols) at various times. And the solid line is the kinetic model.

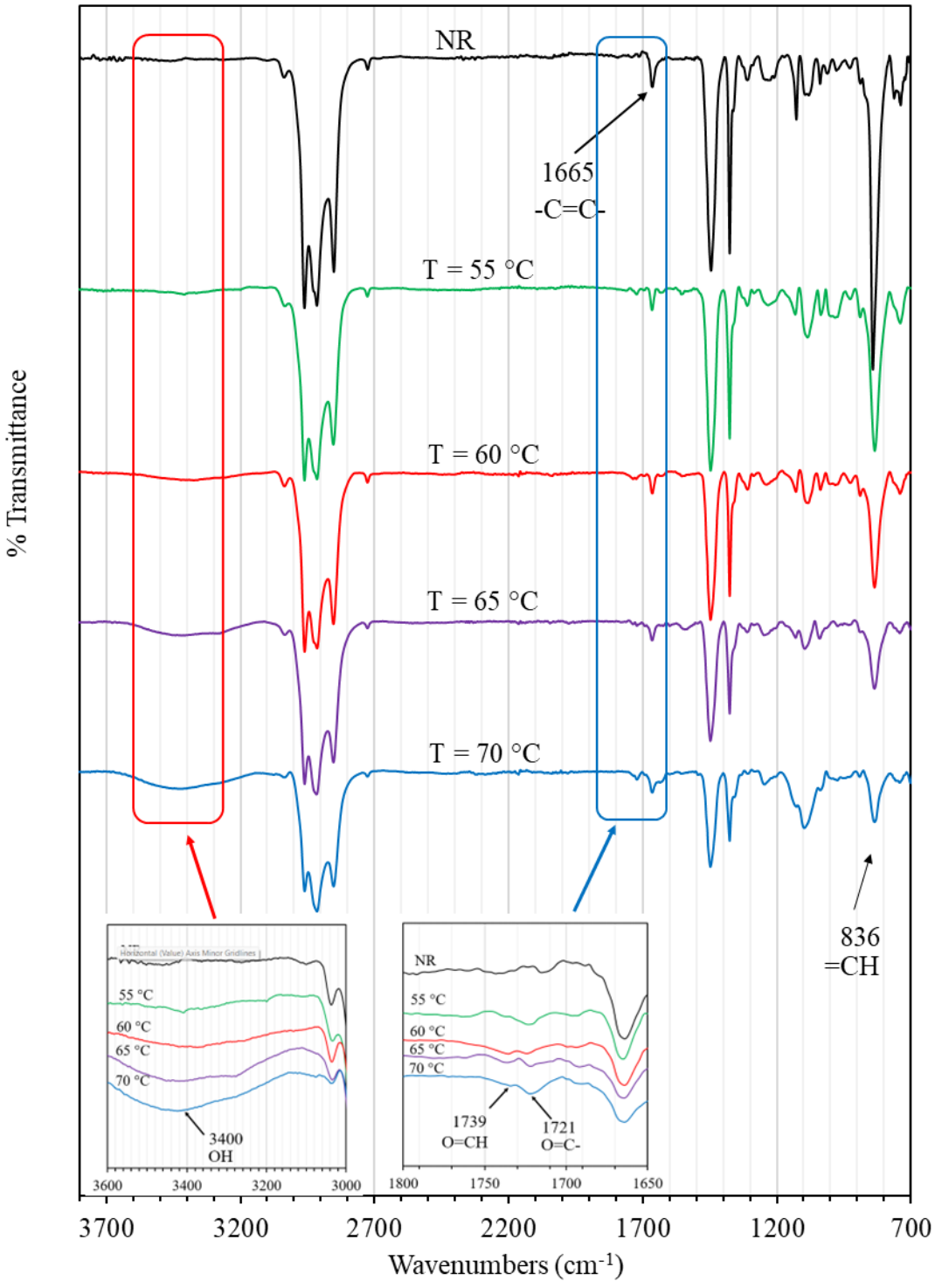

Figure 4.16 FTIR spectra (700 – 3800 cm^{-1}) of NR and LNR samples prepared at various reaction temperatures with amounts of H_2O_2 0.4 mol, $NaNO_2$, 0.02 mol, and pH 5 for 12 h.

4.1.7 The degradation kinetics

The reaction mechanisms represented in Schemes 4.1 were proposed to explain the formation of hydroxyl and carbonyl groups on LNR backbone chains generated in an acidic and alkaline media, respectively. The breaking of NR chains at the C-C bond typically occurs due to radical attacks, resulting in a hydroxyl end group. Conversely, an oxidizing agent can oxidize a broken C=C bond in the NR chains, leading to a carbonyl end group. The mechanisms of LNR degradation using $NaNO_2$ and H_2O_2 revealed that the end groups, either hydroxyl or carbonyl, varied depending on the pH of the system. At a pH below 7, H_2O_2 and $NaNO_2$ react to form peroxynitrous acid, which decomposes to produce the $^{\bullet}OH$. These radicals attack the C-C bonds in polyisoprene chains, leading to the formation of LNR with hydroxyl end groups, as illustrated in Scheme 4.1a. At a pH ≥ 7, hydrogen peroxide tends to oxidize the C=C bonds to form epoxy rings. During degradation, these rings are attacked by nitrite ions (NO_2^-), causing the polyisoprene chains to break and resulting in shorter chains with carbonyl end groups, as depicted in Scheme 4.1b [89]. Similar mechanisms involving different end groups for LNR prepared under various pH conditions were suggested by Ibrahim et al. [18].

The degradation of LNR chains can be described as a second-order reaction involving the breaking of the number of bonds during the depolymerization process [107-109]. The [η] of the LNR obtained can be calculated to the $\bar{M}_n$ values, which refer to Equation (4.3). A model for the random chain scission of LNR macromolecules can be applied, as described by Equation (4.5).

$$\frac{1}{\bar{M}_{n(t)}} - \frac{1}{\bar{M}_{n(0)}} = \frac{kt}{\bar{M}_0} \qquad (4.5)$$

where $\bar{M}_{n(0)}$ is $\bar{M}_n$ the of NR at time = 0, $\bar{M}_{n(t)}$ is the $\bar{M}_n$ of LNR at time = t, M_0 is the $\bar{M}_n$ of the isoprene unit (68 g/mol), and k is the rate constant. As previously discussed, the degradation process is significantly affected by various parameters including the concentrations of H_2O_2, HCOOH, $NaNO_2$, and the reaction temperature.

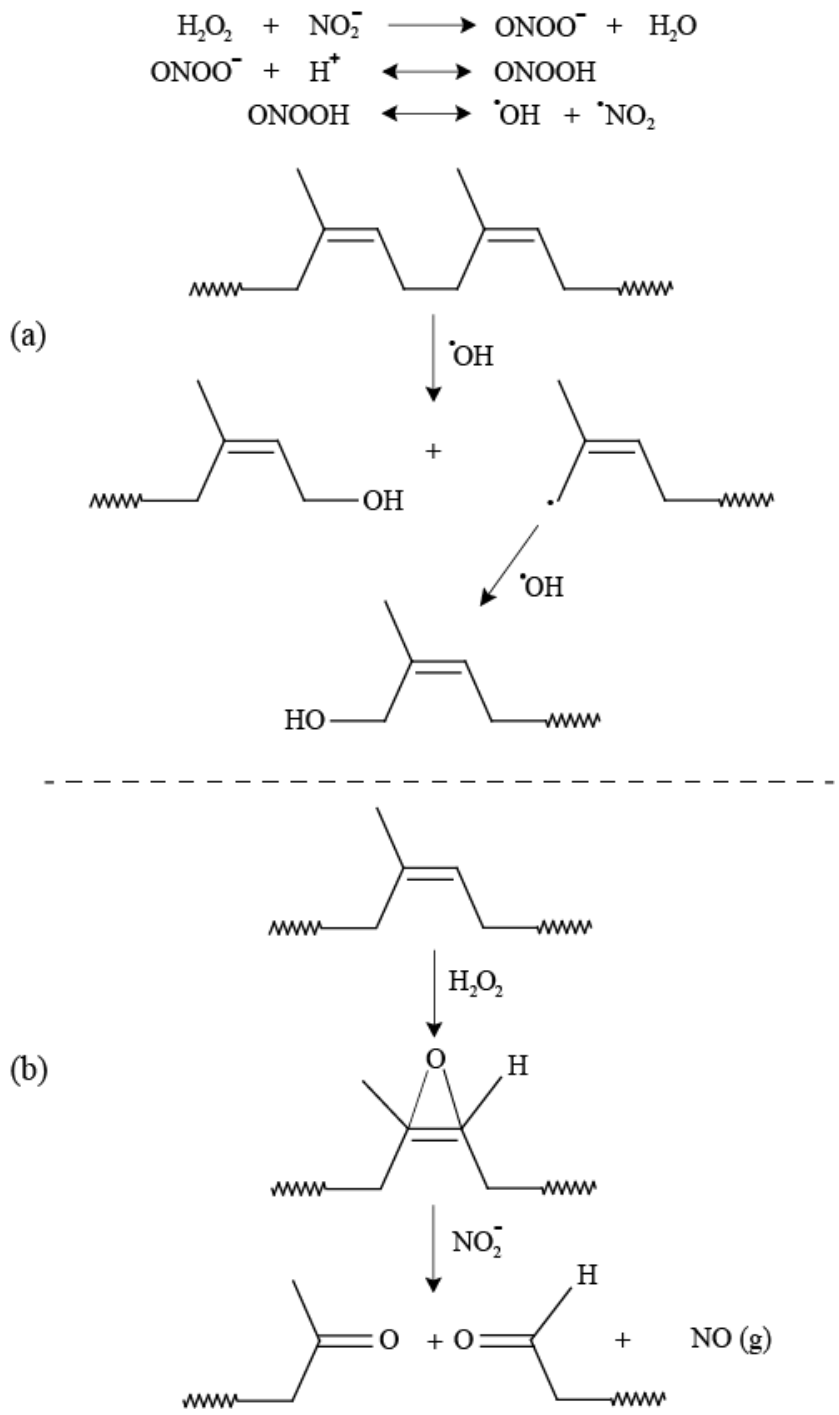

Scheme 4.1 The degradation of the NR chain using H_2O_2 and $NaNO_2$ in (a) acid medium, and (b) neutral and alkaline media [18].

Based on the Arrhenius equation, $k = A \times e^{(-Ea/RT)}$ where E_a is the activation energy, A is the pre-exponential factor, R is the universal gas constant, and T is the reaction temperature. These parameters can be expressed as a power function in the kinetic model. Consequently, Equation (4.5) can be rearranged to form Equation (4.6).

$$\frac{\overline{M}_0}{\overline{M}_{n(t)}} - \frac{\overline{M}_0}{\overline{M}_{n(0)}} = A \times e^{\frac{-E_a}{RT}} [H_2O_2]^m [CH_2O_2]^n [NaNO_2]^o \times t \qquad (4.6)$$

where $[H_2O_2]$, [HCOOH], and $[NaNO_2]$ denote the initial concentrations of the reagents in mol/L. The exponents m, n, and o are known as the partial orders of the reaction and indicate the influence of each reactant's concentration on the reaction rate. These partial orders must be determined experimentally by varying the concentration of one reactant while keeping the concentrations of the other reactants constant.

In general, the kinetic model, expressed as a power function of the process variables, is independent of time. The partial orders can be calculated by using a logarithm plot of $[(\overline{M}_0/\overline{M}_{n(t)} - \overline{M}_0/\overline{M}_{n(0)})/t]$ against log [reactant] and the linear regression technique, as demonstrated in Figures 4.17 - 4.19. The slopes corresponded to the partial orders provided by m, n, and o, respectively. Based on Figure 4.20a, a natural logarithm plot of $\ln [(\overline{M}_0/\overline{M}_{n(t)} - \overline{M}_0/\overline{M}_{n(0)})/([0.4]^{1.58}[0.1247]^{0.79}[0.02]^{-0.65} \times t)]$ against 1000/T provide a straight line, and the E_a value can be estimated from the slope ($-1000E_a/R$) of that line, whose intercept with the y axis is equal to ln A, as presented in Figure 4.20. The reaction orders for the concentrations of H_2O_2 and HCOOH deviated from 1, suggesting a nonlinear relationship in the degradation reactions. Increasing the concentrations of H_2O_2 and HCOOH, as well as raising the reaction temperature, accelerated the chain-scission reaction. Conversely, the negative exponent for $NaNO_2$ concentration indicated that the reduction in the $\overline{M}_n$ was inversely related to the concentration of $NaNO_2$. Thus, increasing the concentration of $NaNO_2$ slowed down the depolymerization rate. The reaction orders of H_2O_2 concentration, HCOOH concentration, and $NaNO_2$ concentration were 1.58, 0.79, and -0.65, respectively (Figures 4.17-4.19). According to Figure 4.20, the activation energy and pre-exponential factor were found to be 78.66 kJ/mol and 1.04×10^9

$M^{-1.72}\ t^{-1}$, respectively, the kinetic model for the random scission of NR using H_2O_2, HCOOH, and $NaNO_2$ as reagents can be summarized by Equation (4.7).

$$\frac{\overline{M}_0}{\overline{M}_{n(t)}} - \frac{\overline{M}_0}{\overline{M}_{n(0)}} = 1.04\times10^{9}\ M^{-1.72}\ t^{-1}\ e^{\frac{-78.66\ kJ\cdot mol^{-1}}{RT}}[H_2O_2]^{1.58}[CH_2O_2]^{0.79}[NaNO_2]^{-0.65}\times t \qquad (4.7)$$

Figure 4.21 illustrates a strong correlation between the predicted values and the experimental results obtained from Equation (4.7) for the degradation of NR. The kinetic parameters were assessed using experimental data, showing a high degree of linearity with an R^2 value of 0.9771. This indicates that the predicted values from Equation (4.7) closely match the experimental data, demonstrating good performance and a high correlation.

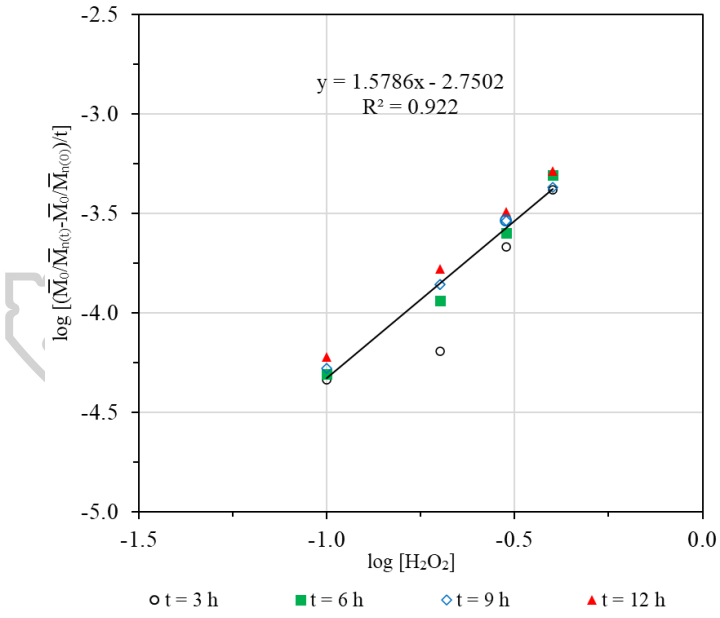

Figure 4.17 A log-log plot of $[(\overline{M}_0/\overline{M}_{n(t)} - \overline{M}_0/\overline{M}_{n(0)})/t]$ versus H_2O_2 concentration at different reaction times. Condition: pH = 5, $NaNO_2$ = 0.02 M, and T = 338 K.

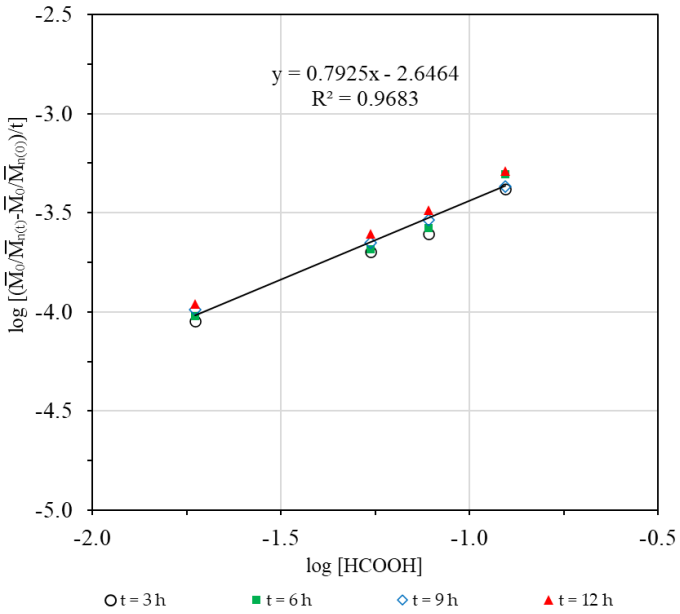

Figure 4.18 A log-log plot of $[(\bar{M}_0/\bar{M}_{n(t)} - \bar{M}_0/\bar{M}_{n(0)})/t]$ versus HCOOH concentration at different reaction times. Condition: H_2O_2 = 0.4 M, $NaNO_2$ = 0.02 M, and T = 338 K.

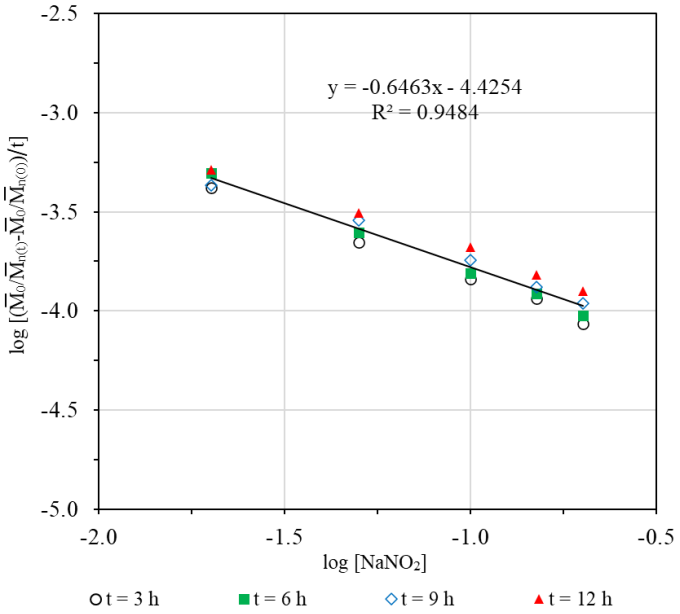

Figure 4.19 A log-log plot of $[(\bar{M}_0/\bar{M}_{n(t)} - \bar{M}_0/\bar{M}_{n(0)})/t]$ versus $NaNO_2$ concentration at different reaction times. Condition: H_2O_2 = 0.4 M, pH = 5, and T = 338 K.

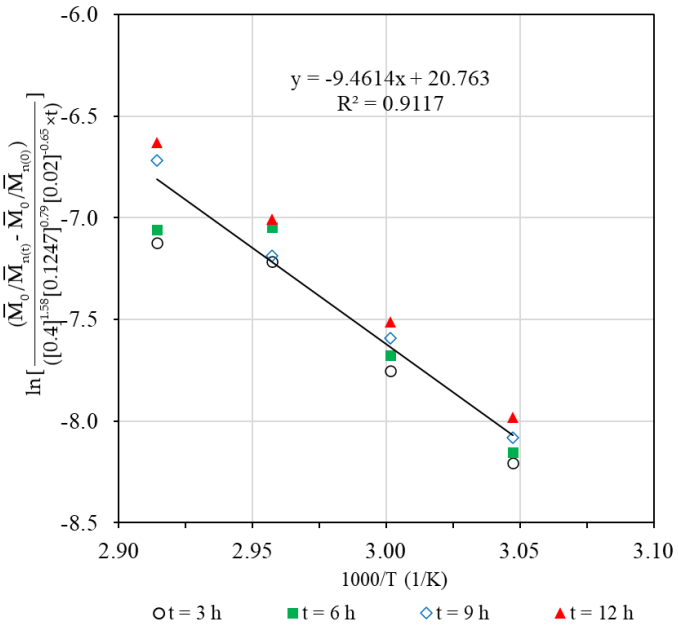

Figure 4.20 A natural logarithm plot of $[(\bar{M}_0/\bar{M}_{n(t)} - \bar{M}_0/\bar{M}_{n(0)})/ ([0.4]^{1.58} [0.1247]^{0.79} [0.02]^{-0.65}\times t)]$ versus 1000/T at different reaction times. Condition: H_2O_2 = 0.4 M, pH = 5, and $NaNO_2$ = 0.02 M.

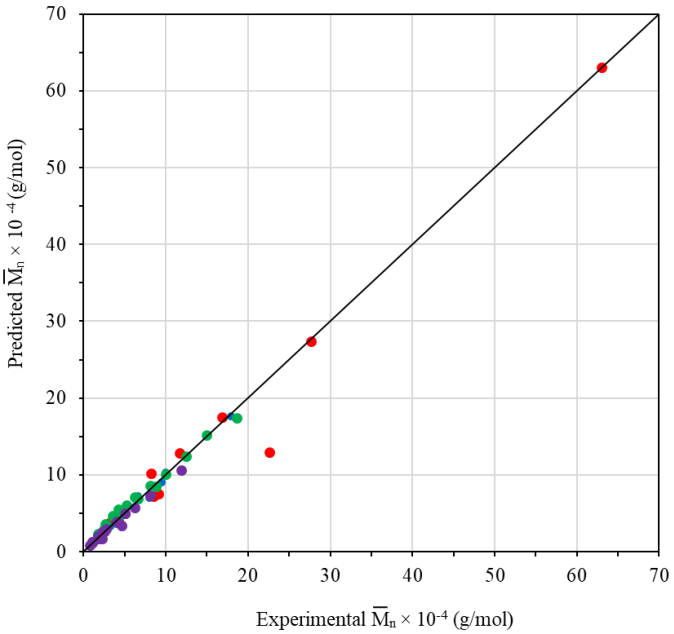

Figure 4.21 Correlation between the predicted values obtained from Equation (4.5) and experimental data with R^2 = 0.9771

4.2 Graft copolymers

The grafting of an olefinic monomer like methyl methacrylate onto liquid natural rubber (LNR) was carried out by using cumene hydroperoxide redox initiator to enhance the new chemical groups on the NR backbone and, in turn, to develop the newer grades of NR that have inherent multifunctional additive activity. The present study involves the grafting reaction conditions such as the initiator content, monomer content, reaction temperature, and reaction time followed by the study of the individual effect of the aforesaid parameters on the grafting reaction. Kinetic analysis of the graft copolymers also has been discussed.

Mechanism of graft copolymers

The graft copolymer of MMA onto LNR particles, initiation of polymerization is due to free radicals produced by the interaction of CHPO dissolved in the monomer swollen rubber particles and TEPA in the aqueous phase of the LNR latex. Either interaction between the CHPO and TEPA or the CHPO probably decomposes to yield radicals (RO$^{\bullet}$) formed at the particle-water interface (Scheme 4.2a), which might interact with the rubber molecule or the monomer, producing a macroradical that initiates grafting. The radicals can not only abstract α-methylenic hydrogen atoms to produce polyisoprene radicals, which initiate monomers to form the graft copolymers, but also initiate monomers to form polymeric radicals, which combine with polyisoprenyl radicals to terminate or transfer to LNR to form graft copolymers. Some of the free polymer radicals still terminate to form free copolymers. As mentioned above, the probable grafting mechanism of grafting MMA-g-LNR using CHPO and TEPA as initiators, the cumyloxyl [110], dimethylphenyl carbinol or hydroxyl radicals [111] (produced from cumene hydroperoxide) preferentially abstract α-methylenic hydrogen atoms from the allylic carbon in the polyisoprene backbone. This process leads to the formation of polyisoprene radicals, which initiate the graft copolymerization of MMA, as shown in Scheme 4.2b [40, 112]. Figure 4.22 illustrates one hypothetical pathway for creating core-shell particles, where newly formed oligomers adhere to seed particles through hetero-coagulation, growing until they merge and form a unified shell.

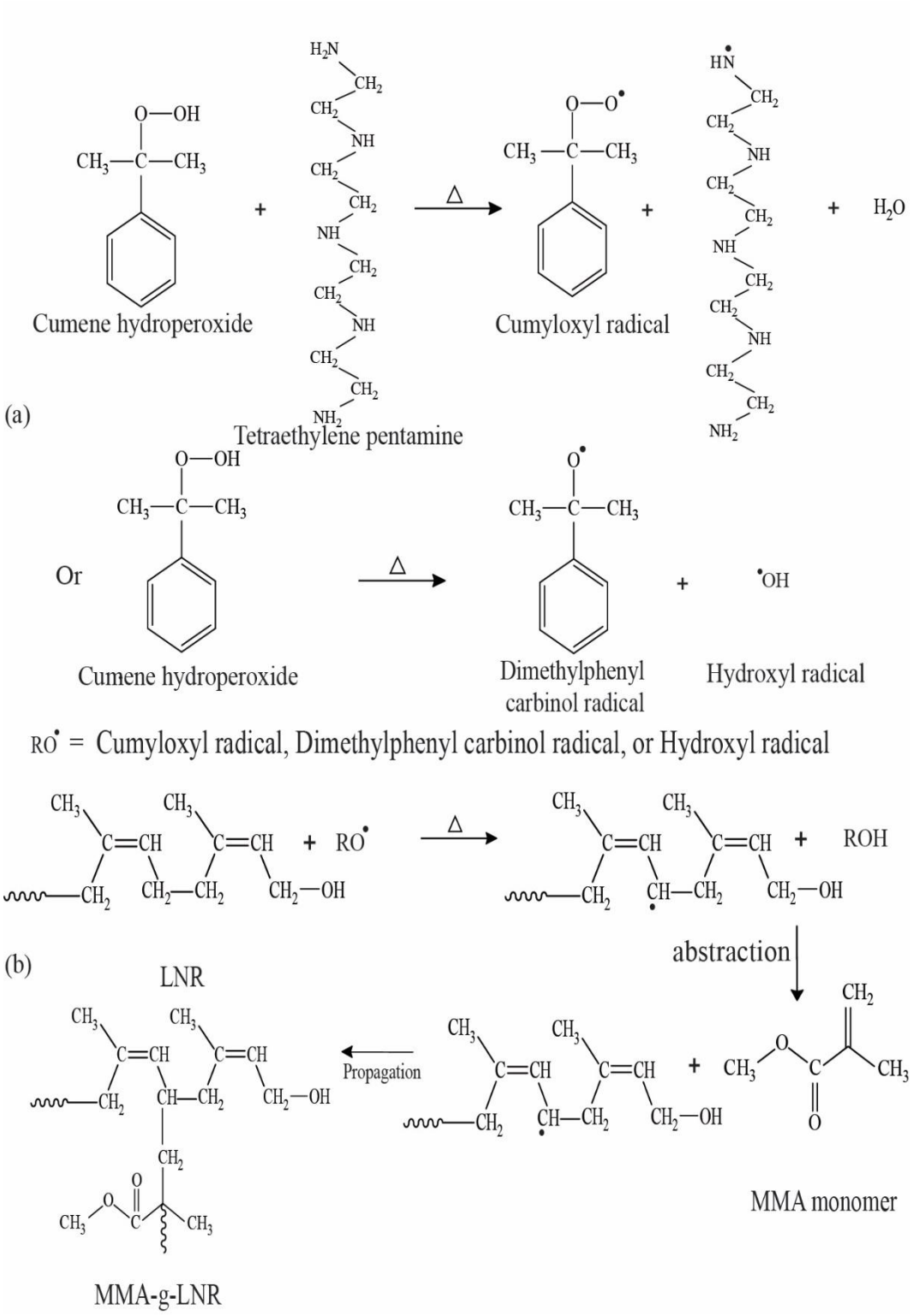

Scheme 4.2 Possible mechanism for graft copolymer of MMA onto LNR via radical polymerization [113].

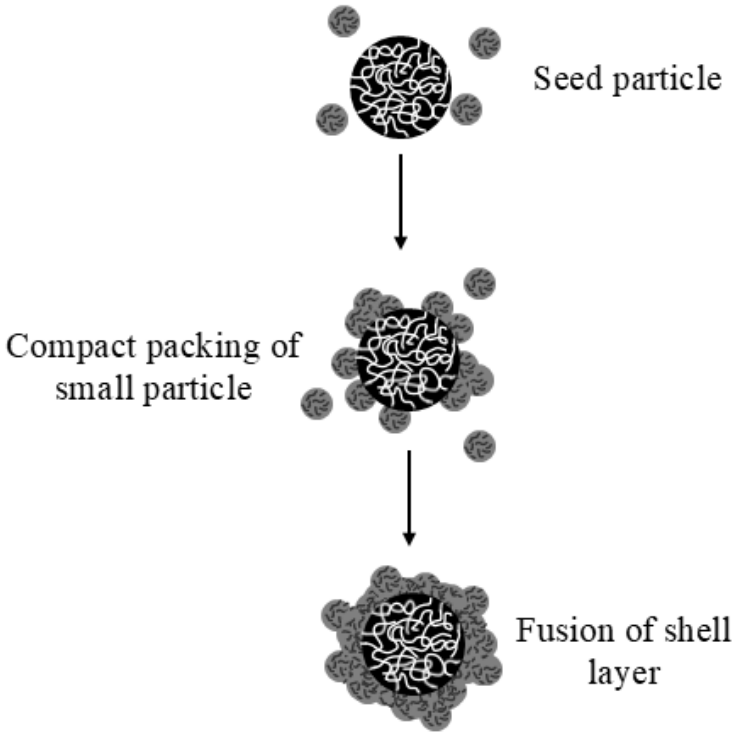

Figure 4.22 Pathway to prepare core/shell particle [114] .

4.2.1 Effect of the molecular weight

The effect of the $\bar{M}_n$ on the conversion of monomer (x_p), graft of monomer (x_g), free homopolymer (x_f), graft of rubber (x_{GR}), free rubber (x_{FR}), and grafting efficiency (GE,%) and grafting level (GL,%) have been investigated, as shown in Figure 4.23-4.26. The reaction was performed with the concentration of CHPO 2.7484×10^{-3} M and MMA 1.3794 M at 343.15 K for 0 - 480 min (MGLNR03). Figure 4.23-4.24 shows the difference in molecular weight on the x_p, x_g, x_f, x_{GR}, and x_{FR} of graft copolymerization of MMA and NR and LNR. It was observed that the value of x_p, x_g, and x_{GR}, for a graft of MMA onto LNR is greater than that of a graft of MMA onto NR. Maybe the molecular weight of LNR is less than that of NR, as the resulting MMA-grafted LNR is easier. On the other hand, the value of x_f, and x_{FR}, for the graft of MMA onto LNR is less than the graft of MMA onto NR. It reveals that the grafting increases, resulting in lower rubber and monomer ungrafted.

Figure 4.25 shows GE increased with increasing reaction time for GNR and MGLNR03 from 11.14, 27.79, 31.40, and 82.38% and 34.07, 30.13, 68.38, and 85.42%, respectively. It is observed that the GE increases with a decrease in the $\bar{M}_n$ of the LNR. This trend can be explained by the low molecular weight of the LNR, which has plenty of active sites for grafting reactions on the LNR backbone chain, giving significant increases in the grafting MMA at the active site of the LNR chain. It may be described by a mechanism involving a surface-controlled process [115]. On the other hand, at high molecular weight, it has a meager number of active sites for grafting reaction on the LNR backbone. This results in a decrease in the grafting of MMA at the active site of the LNR chain. It is generally known that high molecular weight also leads to high intrinsic viscosity [116].

In the same way, the variation of the GL of grafted rubber depends on the $\bar{M}_n$. The GL of grafted NR increased from 31.99, 41.58, 41.32, and 65.38%, while the GL of grafted LNR increased from 49.39, 53.85, 75.51, and 96.35% for reaction time at 120, 240, 360, 480 min. It is noticed that when the $\bar{M}_n$ decreases, the GL also increases, as shown in Figure 4.26. The presence of the GL in LNR is more than in NR. Therefore, the graft product for graft of MMA onto the NR core particle resulted in graft copolymer particles with a heterogeneous structure (shell-core structures), as shown in Figure 4.27a. Similarly, the graft product for a graft of MMA onto the LNR core particle also resulted in graft copolymer particles with a heterogeneous structure (shell-core structures), which has the characteristics of graft product in the form of powder, as shown in Figure 4.27b. This can be indicated that the LNR (core particle) is a lower molecular weight ($\bar{M}_n$ =17,139), whereas NR (core particle) is a higher molecular weight ($\bar{M}_n$ = 630,439); this results in a low-molecule or small-sized grafting product for grafting MMA onto LNR as shown in Figure 4.27b. This may be one reason why the values of GE and GL of the graft MMA onto LNR core particle were higher when compared to the graft MMA onto NR core particle.

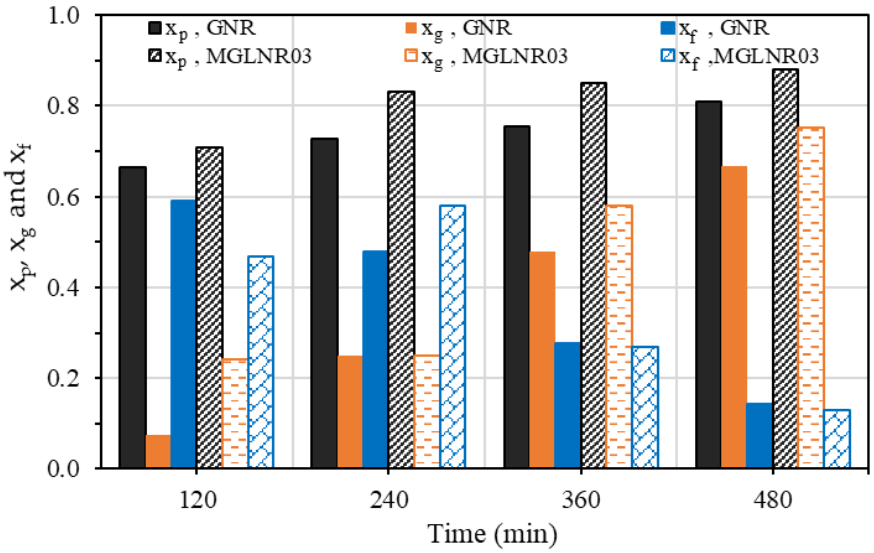

Figure 4.23 Effect of molecular weight on x_p, x_g, and x_f for MMA-g-NR and MMA-g-LNR with various reaction times.

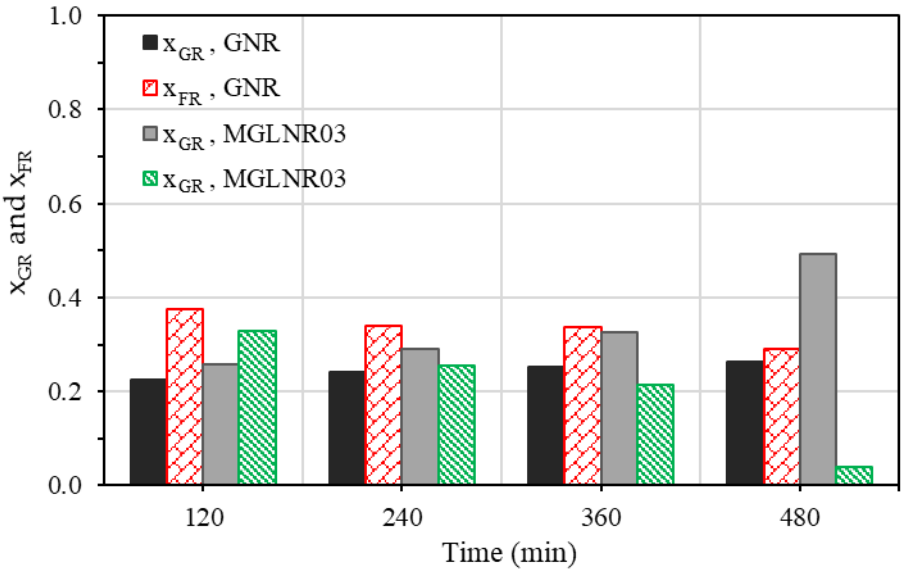

Figure 4.24 Effect of molecular weight on x_{GR} and x_{FR} for MMA-g-NR and MMA-g-LNR with various reaction times.

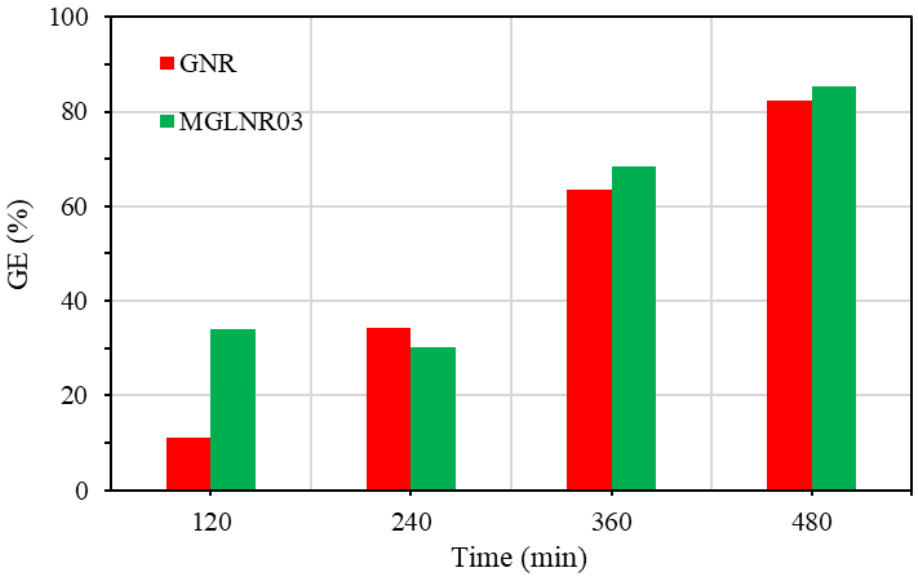

Figure 4.25 Effect of molecular weight on grafting efficiency for MMA-g-NR and MMA-g-LNR with various reaction times.

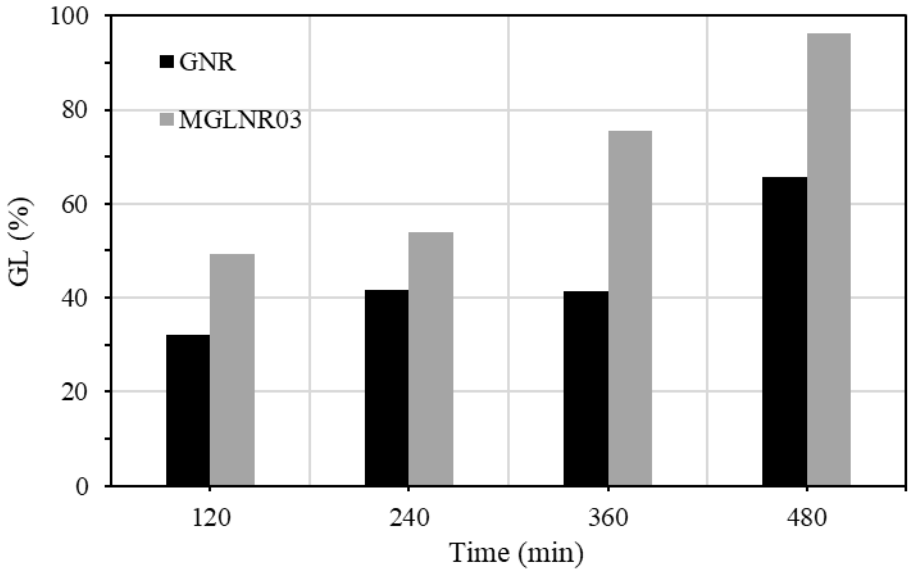

Figure 4.26 Effect of molecular weight on graft level for MMA-g-NR and MMA-g-LNR with various reaction times.

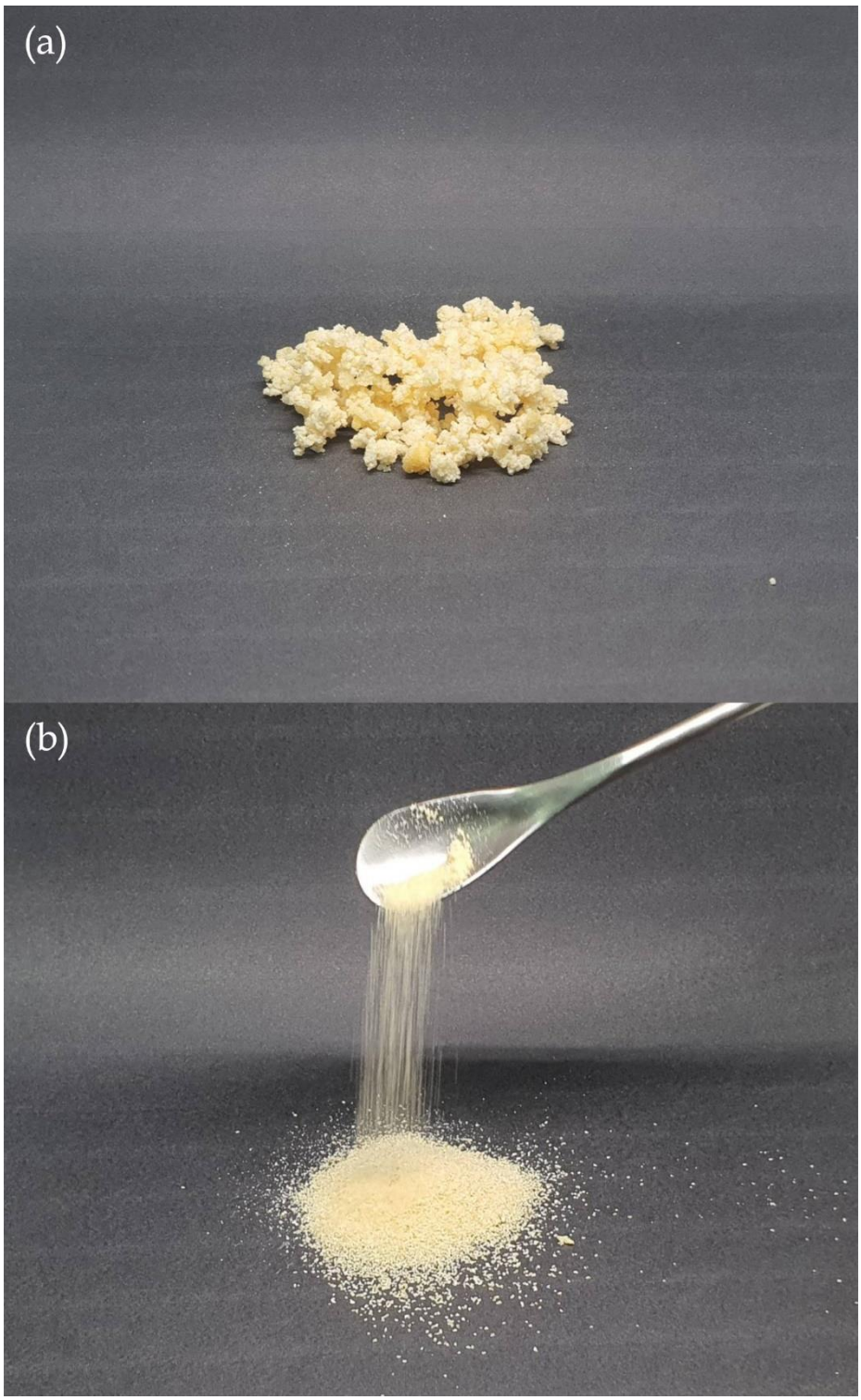

Figure 4.27 (a) MMA-g-NR and (b) MMA-g-LNR powder image obtained from graft copolymerization.

4.2.2 Effect of the reaction time

The influence of reaction time from 0 to 480 min on the monomer conversion (x_p), grafting of monomer conversion (x_g), and free homopolymer conversion (x_f). The reaction employed emulsion polymerization with an MMA concentration of 1.3719 M of rubber and CHPO 3.5876×10^{-3} M of MMA as the initiator at 343.15 K, as shown in Figure 4.28. In the early stages of the reaction (from 0 to 240 minutes), where there is a lot of the monomer, the x_f - t curve revealed a similar trend as x_p - t. x_p and x_f increased greatly with reaction time increase, but x_g slightly increased. Since x_p is the summation between x_g and x_f, it indicates that most of the monomer polymerizes to produce free homopolymeric radicals rather than being grafted onto LNR backbone chains during the early stages of the reaction. As a result, the observed free homopolymer conversion in the graft product increased tremendously with respect to the grafting polymer conversion in the graft product (Figure 4.28(a-c)), leading to a gradual increase of GE during this stage. After 240 minutes, the polymerization had into the end stage, where x_p started to level off and remain almost constant. It was found that x_g continuously increased with reaction time increase, but x_f decreased. This phenomenon suggests that a lot of free homopolymeric radicals produced in the early stage favorably form a chemical bond with the LNR backbone chains, producing graft copolymer. The use of free homopolymer by grafting with LNR resulted in a decrease in the free homopolymer in the graft product. This led to a significant increase in the grafting polymer in the graft product. Therefore, GE greatly increased at the end of the reaction.

The functional groups of the grafted LNR obtained after Soxhlet extraction were analyzed by FTIR spectroscopy and compared to the pure LNR. Figure 4.29 shows the spectra of the LNR and MGLNR04. The two major absorption peaks of LNR were detected at wave numbers 1665 and 836 cm^{-1} attributed to C=C stretching vibration of cis-1, 4-polyisoprene, and the =CH out-of-plane bending of cis-1,4-polyisoprene, respectively. In the spectra of grafted MMA onto LNR chains, A new absorption peak at wavenumbers of 1729 cm^{-1} was the presence of C=O stretching of ester groups of MMA [112, 117].

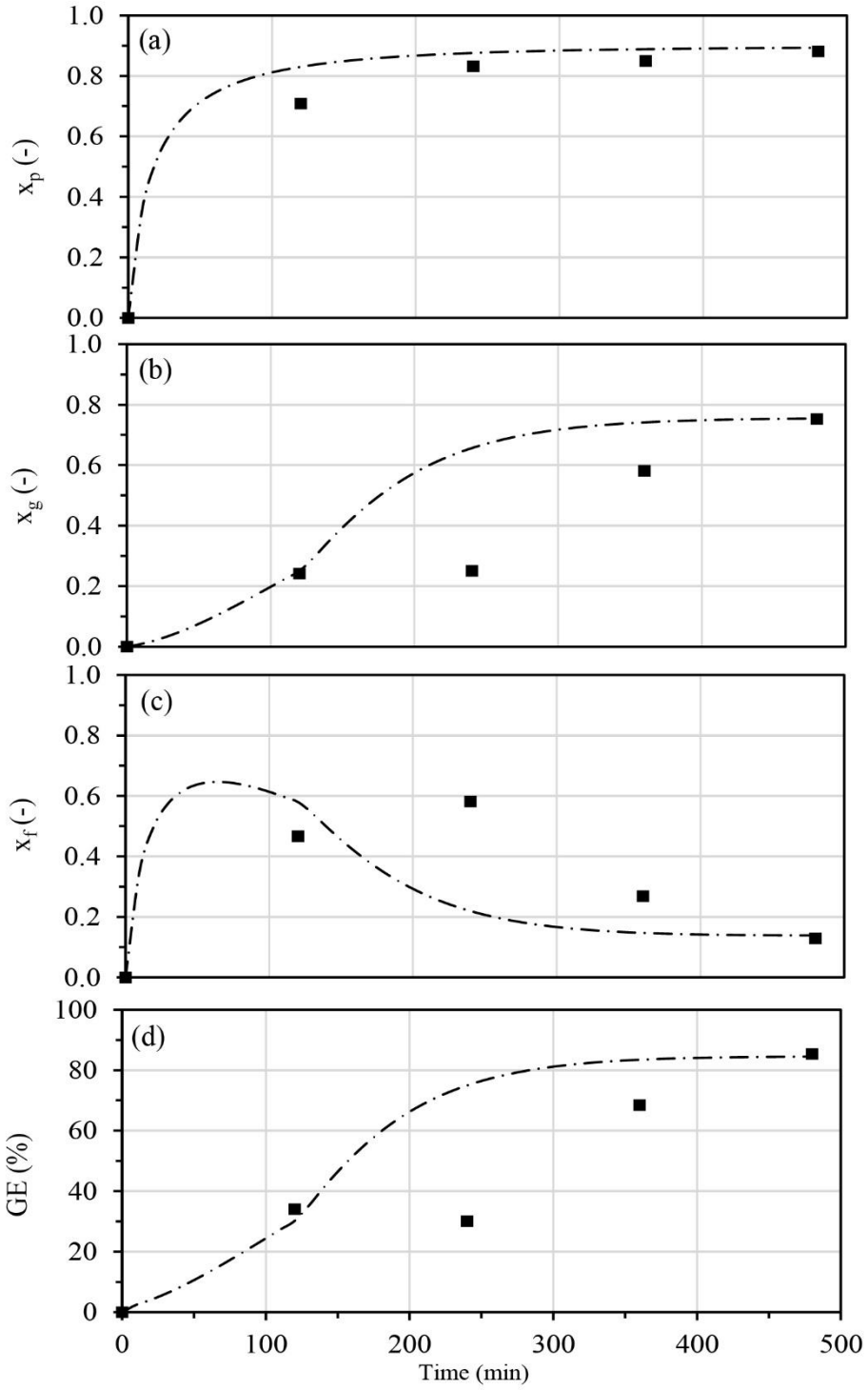

Figure 4.28 Effect of the reaction time on (a) x_p, (b) x_g, and (c) x_f (symbols) with concentration of MMA 1.3719 M, CHPO 3.5876×10^{-3} M and T = 343.15 K for MGLNR04. And the line is the kinetic model.

The observation of the new characteristic peak can confirm the formation of a grafting MMA onto LNR chains. However, the variations of the new absorption peak at wave number 1729 cm^{-1} depend on various reaction times at 2 - 8 h, as shown in Figure 4.29. It was found that the reaction time increases, increasing the amount of MMA grafted onto the LNR chain. This resulted in the absorption peak being higher, indicating a higher at 92.37 % GE for 8 h. Vanderhoff J et al. [114] proposed the a possible process for preparing core-shell particles based on the hetero-coagulation of newly generated oligomers onto seed particles, resulting in the formation of a fused shell. The morphologies of LNR and grafted LNR with MMA were examined using a TEM, which indicated that the seed particles are microspheres, as shown in Figure 4.30. Before being measured by TEM, the surface morphology of LNR and the grafted rubber was studied using OsO_4 staining at the carbon-carbon double bonds of the LNR to increase the contrast and gradation of the LNR particles. The observed LNR particles are spherical with a diameter of approximately 0.34 μm, as shown in Figure 4.30a. After graft copolymerization with the PMMA for 2, 4, and 8 h, the TEM image shows a light contrast of the two-phase polymer of the core/shell composites. The LNR core represented by a darker area is coated by the MMA layer (lighter area in Figure 4.30(b-c) on its outer surface. The grafted particle has a rough surface with a shell thickness of about 0.21 μm for grafting with MMA at 8 h with respect to the LNR particle (Figure 4.30d) [113, 117-119]. Therefore, the LNR core polymer shell composites were favorably prepared by the graft copolymerization process. The morphology of the particles during the period of polymerization and the thickness of the graft copolymer (the outer layer) on the surface of seed particles increased with the increasing reaction time. Therefore, the value of %GE increases from 35.32 to 92.37 with increasing time from 2 to 8 h, respectively. However, it can be explained that the level of shell thickness became larger, which indicates that the value of %GE was also higher. Moreover, at a low GE, A graft copolymer is recommended for adhesive applications [23]. On the other hand, Lee and Chang [120] reported that a graft copolymer with a higher GE was used for another application [27, 112]. Figure 4.31 reveals the SEM micrographs of LNR and the grafted LNR with various reaction times at 2, 4, and 8 h. The process of grafting MMA onto LNR involves emulsion copolymerization of the core-shell type.

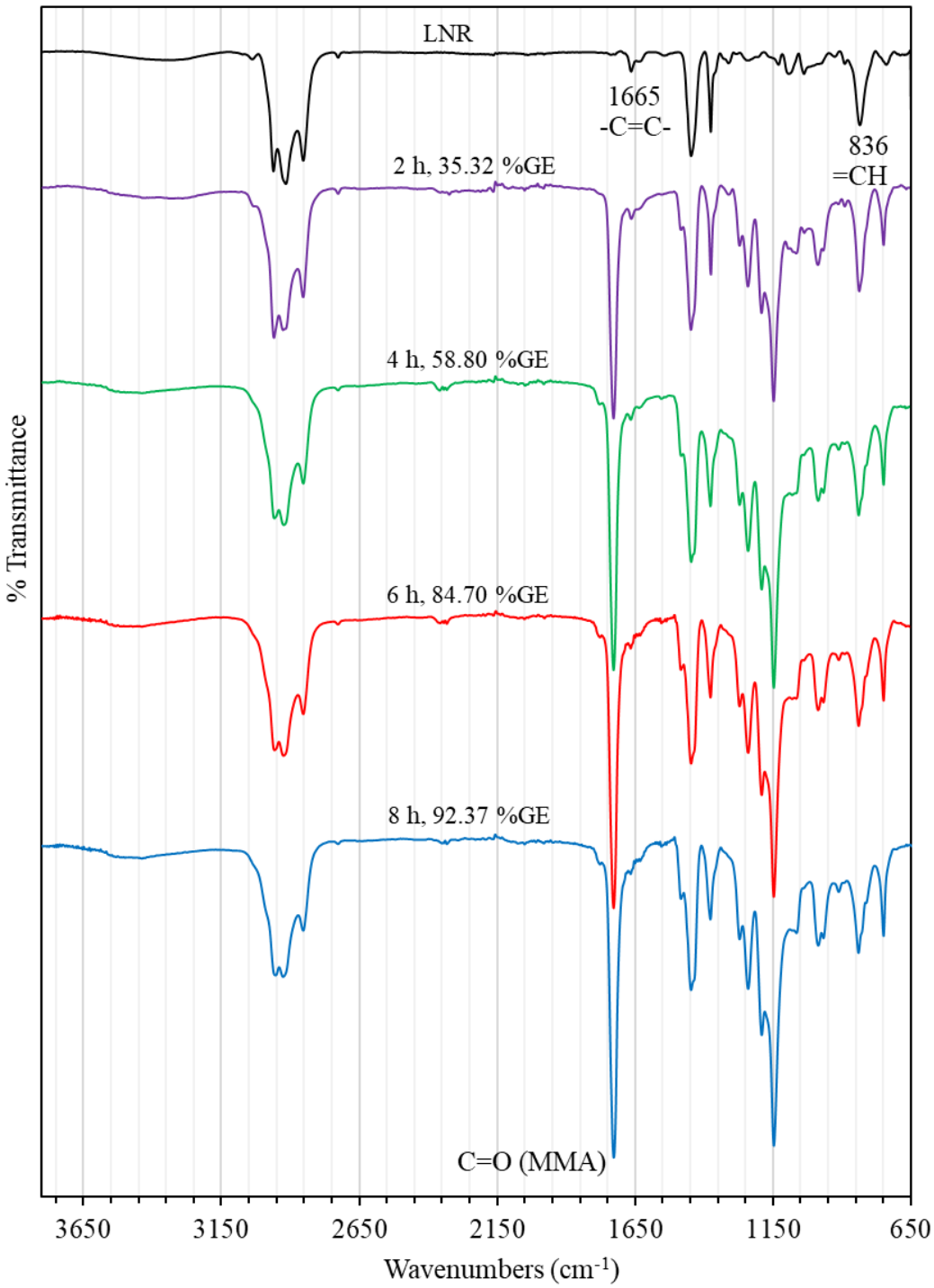

Figure 4.29 FTIR spectra (650 – 3800 cm^{-1}) of LNR and MGLNR04 samples at various times for graft copolymer of MMA onto LNR.

Most of the LNR particles were spherical to a few different sizes (diameter range of 0.24 - 0.29 µm) and were smaller than as compared to that of the grafted LNR particles (diameter range of 0.96 - 1.21 µm), as shown in Figure 4.31. The gloomy domain represents the LNR, whose surface is smooth, as shown in Figure 4.31a, and the bright domain represents the MMA. A rough layer on the surface is grafted onto the surface of the LNR particles, as shown in Figure 4.31(b-d). At the early reaction time, a few bright domains were dispersed in the gloomy matrix. As the reaction time increases, the bright domain grows to cover the gloomy sphere fully (Fig. 4.31c) and then fuses to give an excessively thickness shell layer (Fig. 4.31). This indicates that MMA is more grafted onto the LNR chain in the core-shell latex particles and results in a higher value of %GE.

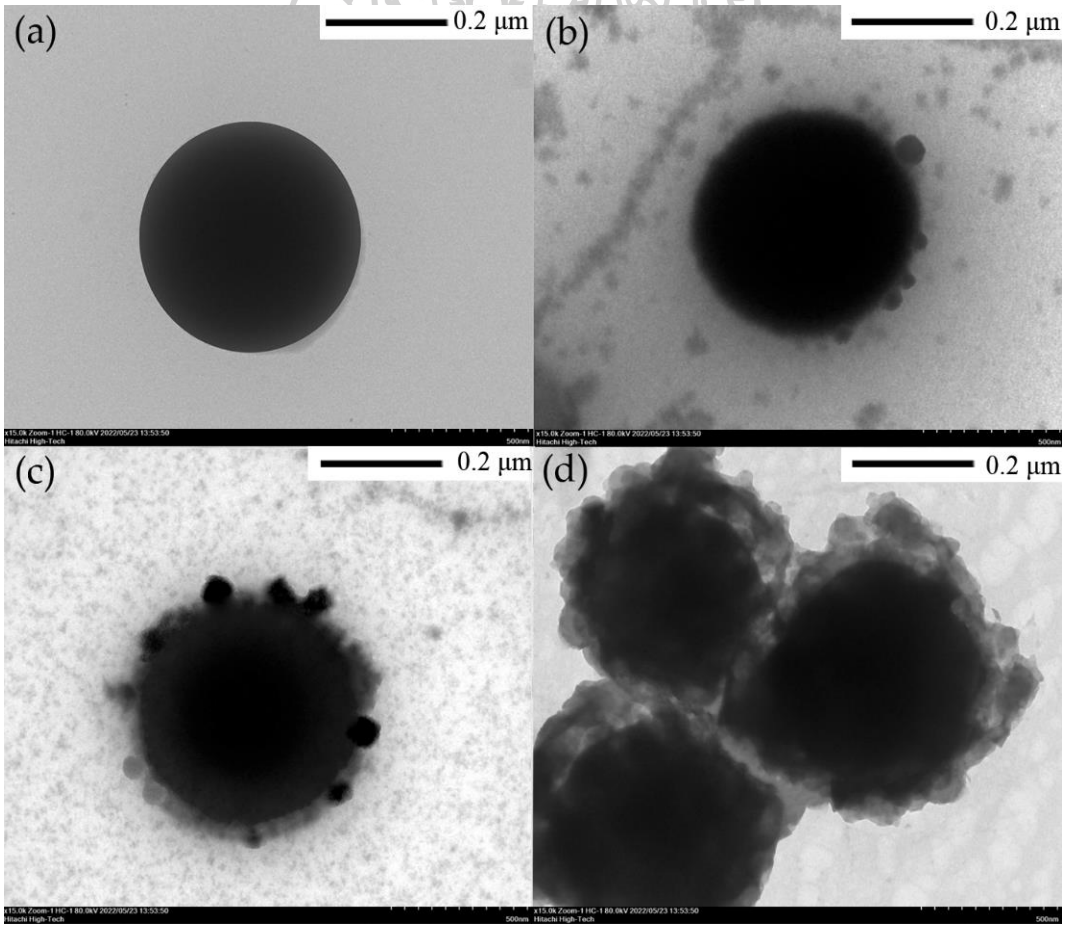

Figure 4.30 TEM micrographs (magnification 40,000×) of the polymers: (a) LNR, (b) MGLNR04 at 2 h, (c) MGLNR04 at 4 h and (d) MGLNR04 at 8 h.

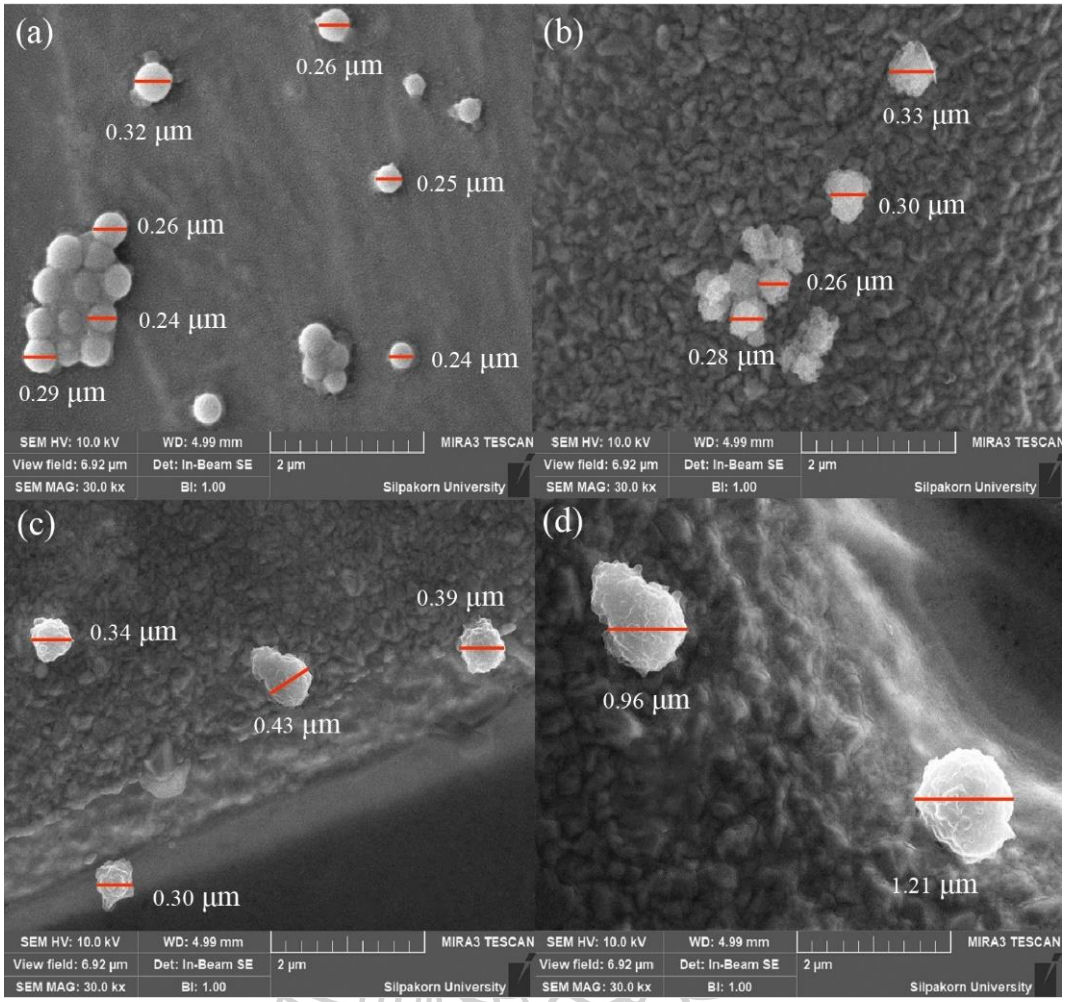

Figure 4.31 SEM micrographs (magnification 30,000×) of the polymers: (a) LNR, (b) MGLNR04 at 2 h, (c) MGLNR04 at 4 h and (d) MGLNR04 at 8 h.

4.2.3 Effect of the initiator

The effect of the amount of initiator on the GE was investigated within the range of approximately $9.3961 \times 10^{-4} - 3.5876 \times 10^{-3}$ M and constant MMA concentration of 1.3719 M at 343.15 K for 0 - 480 h. Figure 4.32 shows the influence of initiator concentration on conversion as the reaction proceeded. At a constant x_p, an increase in initiator concentration resulted in a greater number of total radicals on the core and shell phases. This trend could be explained by the fact that an increase of initiator concentration provides more generation of cumyloxy radicals in the system. The cumyloxy radicals can further transferred to either LNR or monomer to produce

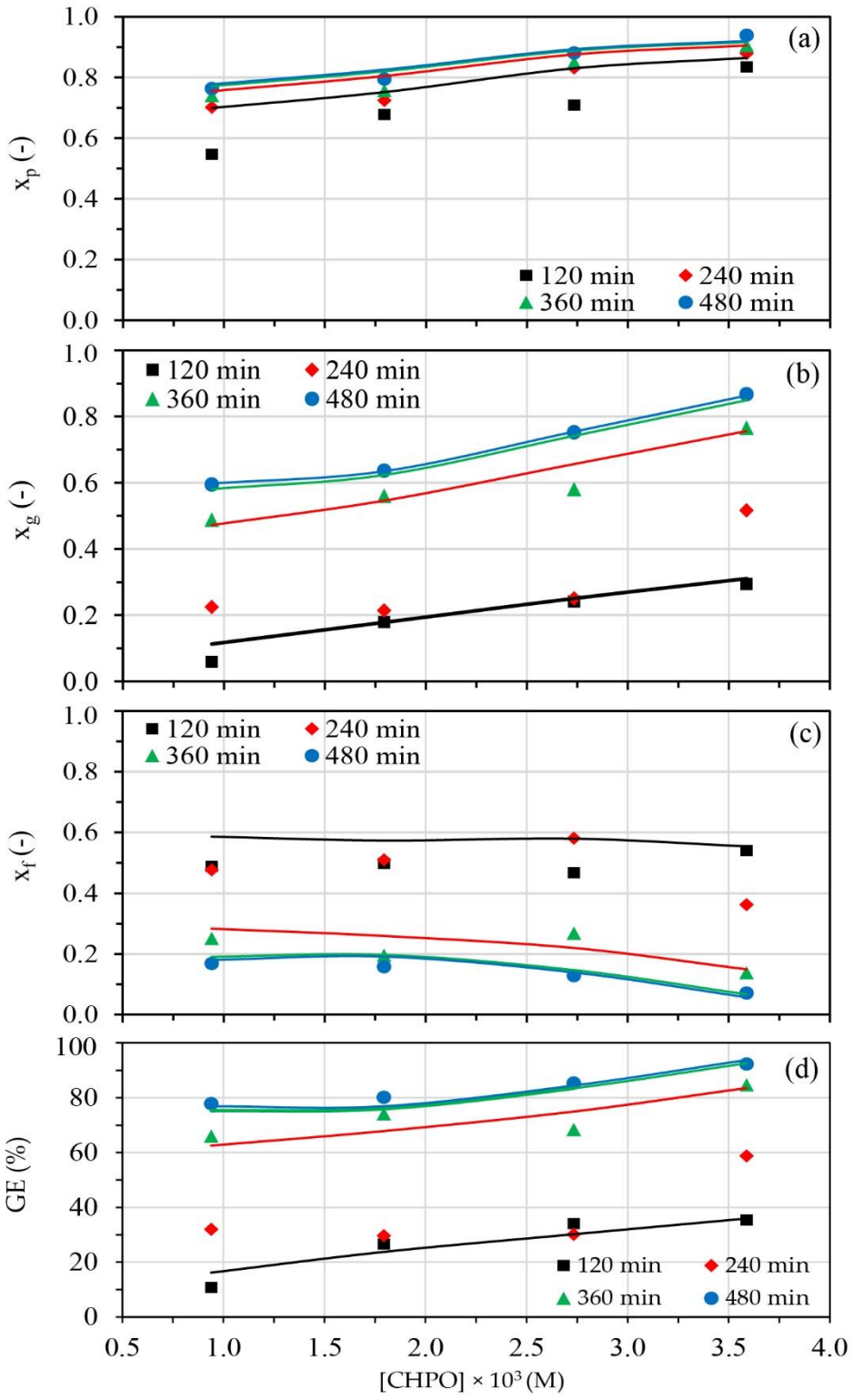

Figure 4.32 Effect of CHPO concentration on (a) x_p, (b) x_g, (c) x_f, and (d) grafting efficiency (symbols) as a function of reaction time with concentration of MMA 1.3719 M and T = 343.15 K. And the line is the kinetic model. .

graft macroradicals. Therefore, it leads to the accumulation of a larger number of radicals on the core and shell phases. This resulted in a higher final x_p.

In the early stage of reaction at $0 < x_p < 0.9$, an increase of initiator concentration resulted in a greater increase of the free MMA content in the graft product, which led to growth increases of the grafting MMA content in the graft product, as shown in Figure 4.32. This indicated that, at higher initiator concentration, free MMA radicals were more greatly terminated with themselves to form free MMA rather than transferred their radicals to LNR chains or terminated with LNR chains to graft. Therefore, a significant increase in the GE when using the higher concentration of initiator was observed at the same time, in the early stage of the reaction.

In the end stage of the reaction, where x_p almost attained a limited value ($x_p \geq 0.9$), the free MMA radicals formed in the early stage were grafted onto LNR backbone chains, leading to a drop of free MMA content in the graft product as shown in Figure 4.32a. An increase of the initiator concentration resulted in a greater consumption of the free MMA content in the graft product (Figure 4.32b), whereas it yielded steeper increases of the grafting MMA content in the graft product and the GE at the same time, as shown in Figure 4.32d. This may be due to the presence of more free MMA radicals in the system caused by an increase in the initiator concentration. Hence, the probability that free MMA radicals attack LNR radicals by forming graft copolymer is enhanced [117, 118].

As discussed above, it can be concluded that GE increases with increasing CHPO concentration, as shown in Figure 4.32d. This is due to the generation of more growing radicals, causing a high probability of a chain transfer reaction of these radicals to the rubber chain to form a graft site. The influence of the initiator on the grafting process is still certain, and some researchers support our findings [121, 122].

The effect of the CHPO concentration on the x_{GR}, x_{FR} and GL has been investigated, as shown in Figure 4.34. The reaction was performed with the concentration of CHPO $9.3961 \times 10^{-4} - 3.5876 \times 10^{-3}$ mol/L and MMA 1.3719 mol/L at 343.15 K for 0 - 480 min. It is revealed that the conversion of grafted rubber and grafted copolymers increased with the increasing concentration of initiator, which

showed a continuous upward trend, while the values of free rubber and free copolymers decreased significantly at the same time. In the part of the GL, it was found that the value of GL increased with the increasing concentration of the initiator at the same time. The value of GL increased from 73.97, 81.56, 96.35, and 96.30 % for reaction time at 480 min, as shown in Figure 4.34d. As discussed above, This can be explained that at higher initiator concentration, free MMA radicals were more greatly terminated with themselves to form free MMA rather than transferred their radicals to LNR chains or terminated with LNR chains to graft.

Figure 4.35 shows the FTIR of LNR and grafted LNR samples performed at various amounts of the initiator at $9.3961 \times 10^{-4} - 3.5876 \times 10^{-3}$ M with keeping amounts of MMA 1.3719 M at 343.15 K for 8 h. The spectra of pure LNR can be attributed to C=C stretching vibration at 1665 cm^{-1} and the = CH out-of-plane bending at 836 cm^{-1}. The formation of the graft copolymer has appeared as a new absorption peak with respect to the LNR. Figure 4.35 shows the spectra of grafted LNR with MMA at various amounts of the initiator. This spectrum exhibited a new absorption peak at 1729 $cm^{-1,}$ which is attributed to the presence of C=O stretching of ester groups of MMA [113, 117, 123]. Therefore, the presence of new absorption peaks confirms the occurrence of the graft copolymer of LNR onto MMA. The variation of a new absorption peak was seen to increase with an increase in the amount of initiator from $9.3961 \times 10^{-4} - 3.5876 \times 10^{-3}$ M. This could be explained by the fact that the radicals transfer to either rubber or monomer, providing macroradicals, which are enhanced with increasing the amount of the initiator, leading to more monomer grafted onto the LNR backbone chain. As a result, the new absorption peak was enhanced clearly.

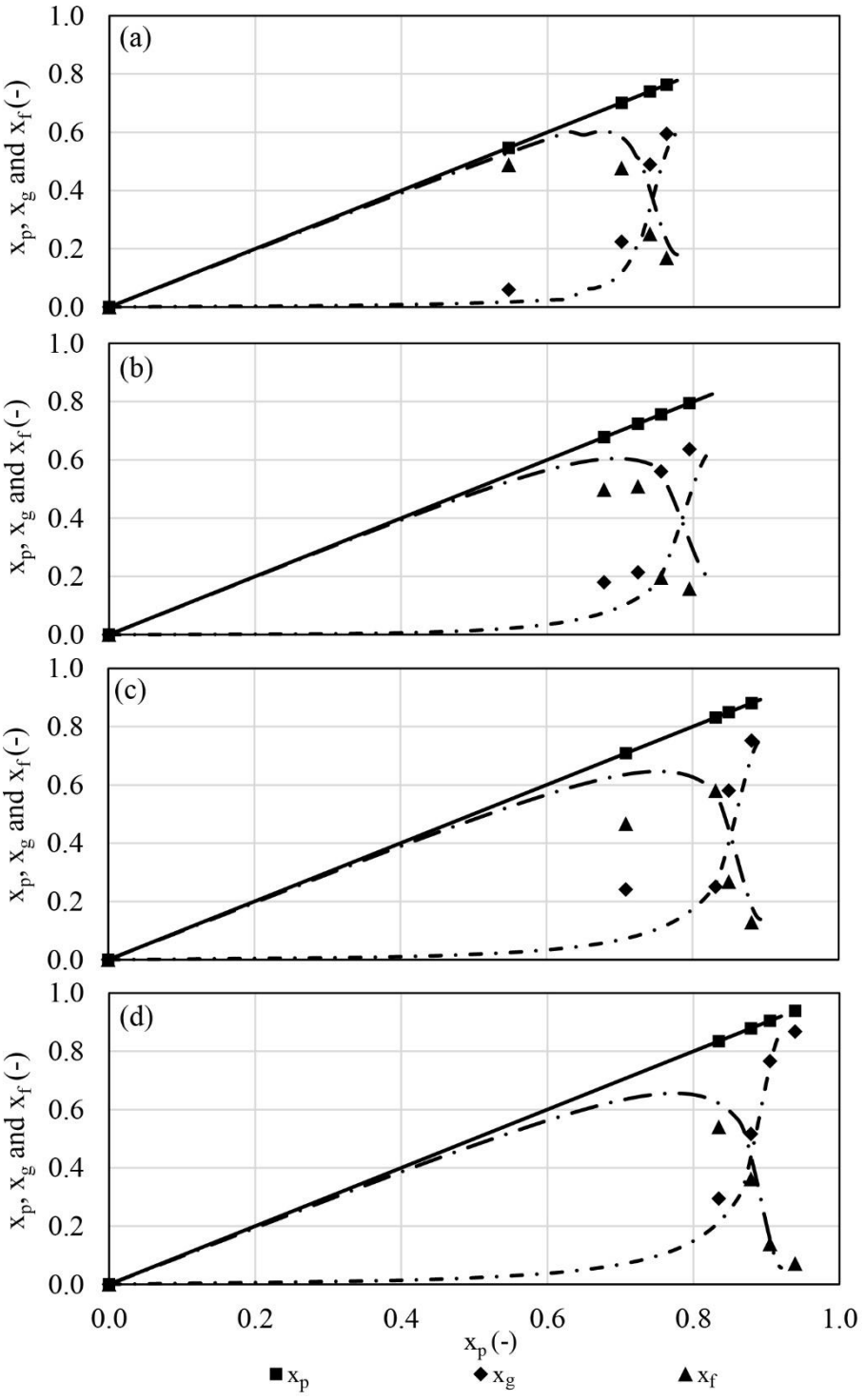

Figure 4.33 Variation of CHPO concentration: (a) CHPO 9.3961 x 10^{-4} M, (b) CHPO 1.7938 x 10^{-3} M, (c) CHPO 2.7334 x 10^{-3} M, and (d) CHPO 3.5876 x 10^{-3} M with conversion of (symbols) with concentration of MMA 1.3719 M and T = 343.15 K. And the line is the kinetic model.

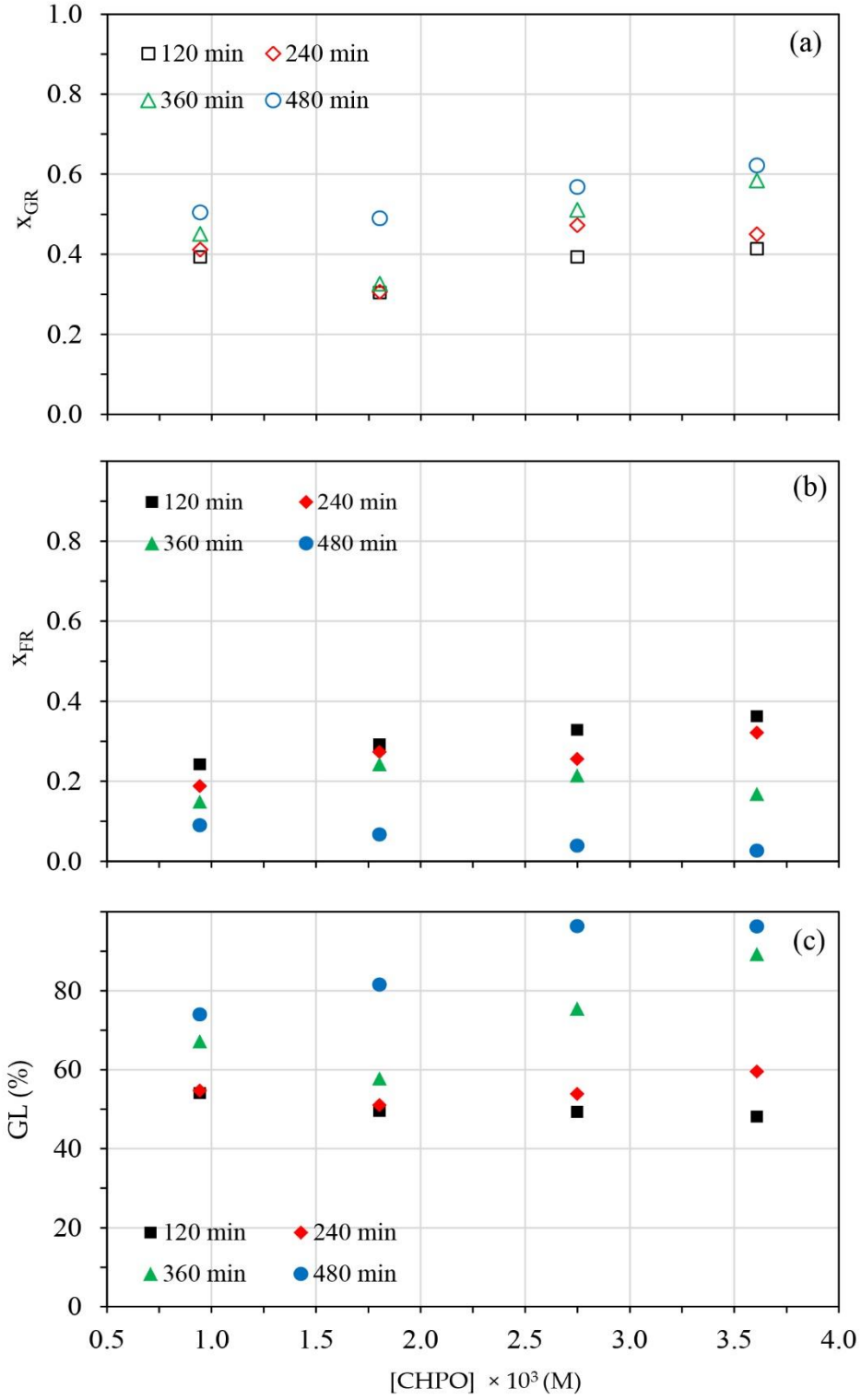

Figure 4.34 Effect of CHPO concentration on (a) graft rubber (open symbols), (b) free rubber (close symbols), and (c) graft level (close symbols) as a function of reaction time with concentration of MMA 1.3719 M and T = 343.15 K.

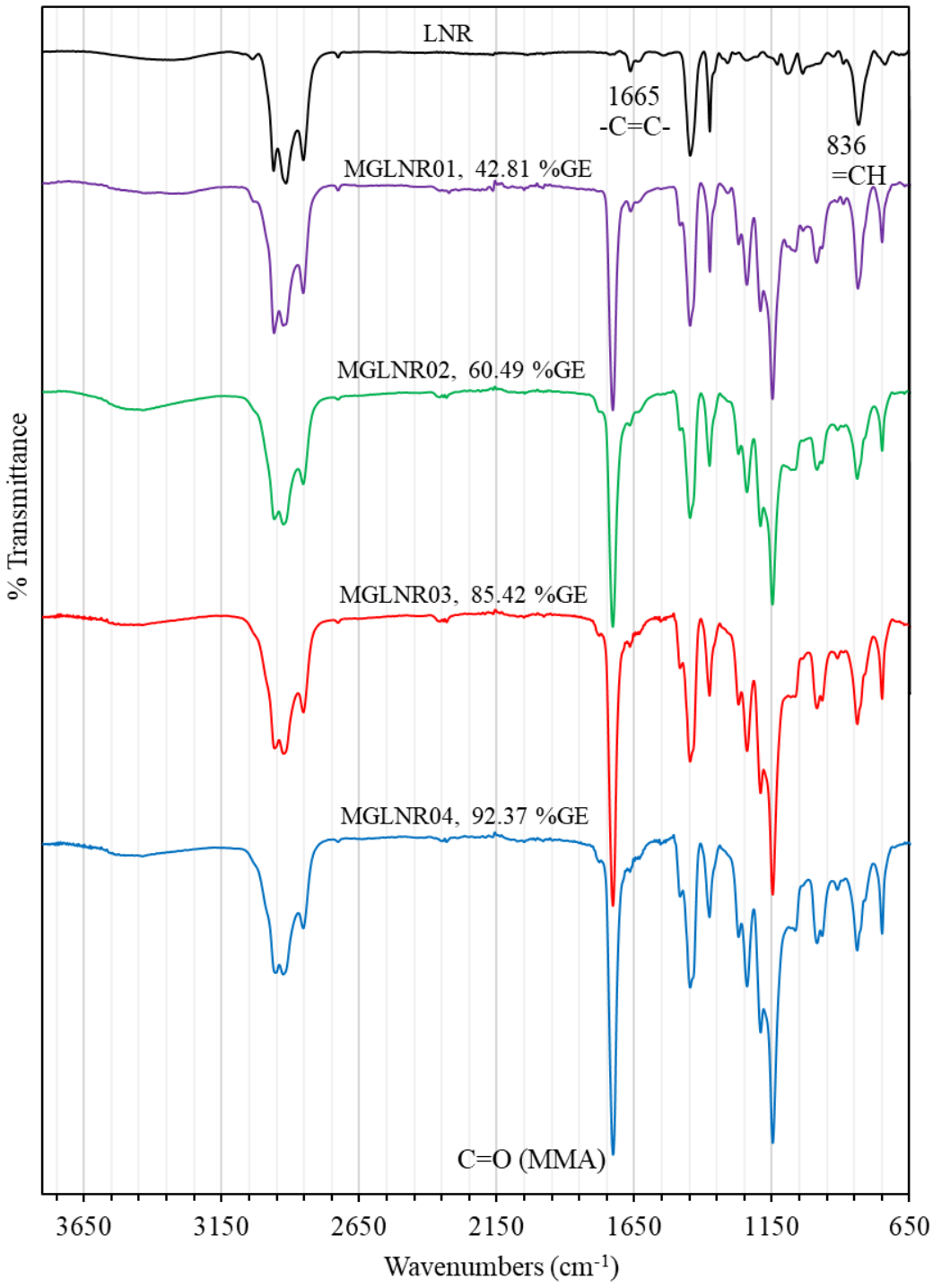

.

Figure 4.35 FTIR spectra (650 – 3800 cm^{-1}) of LNR and MGLNR samples at various CHPO concentrations at 8 h for graft copolymer of MMA onto LNR.

4.2.4 Effect of the MMA concentration

Figure 4.36 shows the influence of MMA concentration on the conversion as the reaction proceeded. The reaction was operated by emulsion polymerization with an MMA concentration of 0.3430 – 1.3719 M and a CHPO concentration at 2.7334 × 10^{-3} M at a temperature of 343.15 K for 0 – 480 min. It is clearly seen that monomer concentration had a few effects on the conversion. An increase in the MMA concentration apparently provided a larger number of total radicals in the core and shell phases at a particular x_p at the same time. In the system, the MMA monomer was induced by cumyloxy radicals ($RO^{\bullet}$), generating MMA radicals. An increase in the MMA concentration increased MMA radicals at the position of reaction inside the particle, promoting the number of MMA radicals formed. Hence, greater numbers of total radicals in both the core and shell phases were observed.

At a particular x_p, an increase in the MMA concentration resulted in a remarkable increase of the free MMA content in the graft product, but it had a weak effect on an increase of the grafting MMA content in the graft product, as shown in Figure 4.37. The larger contents of the free and grafting MMA in graft product at higher MMA concentration were caused by the presence of more MMA monomer at the loci of reaction inside the particle, as mentioned above, thus increasing the formation of graft copolymer and free MMA. The remarkable increase of free MMA content in graft products compared to grafting MMA can be explained by the surface-controlled process of grafting. At higher MMA concentrations, the area of contact between rubber and monomer was low. The probability that either MMA monomer or MMA radicals diffused and grafted onto LNR chains was low [124, 125]. Hence, the LNR chain propagation of MMA radicals is preferred over the LNR chain propagation of graft macroradicals. As a result, the GE was lowered, as shown in Figure 4.36d.

Therefore, it can be summarized that the grafting decreased with increasing monomer concentration. This can be explained by a mechanism involving a surface-controlled grafting process, as described by Merkel et al.[115]. They found similar results for the grafting of MMA onto rubber by Enyiegbulam and Aloka [126].

The effect of the MMA concentration on the x_{GR}, x_{FR}, and GL has been investigated, as shown in Figure 4.38. The reaction was operated out by the

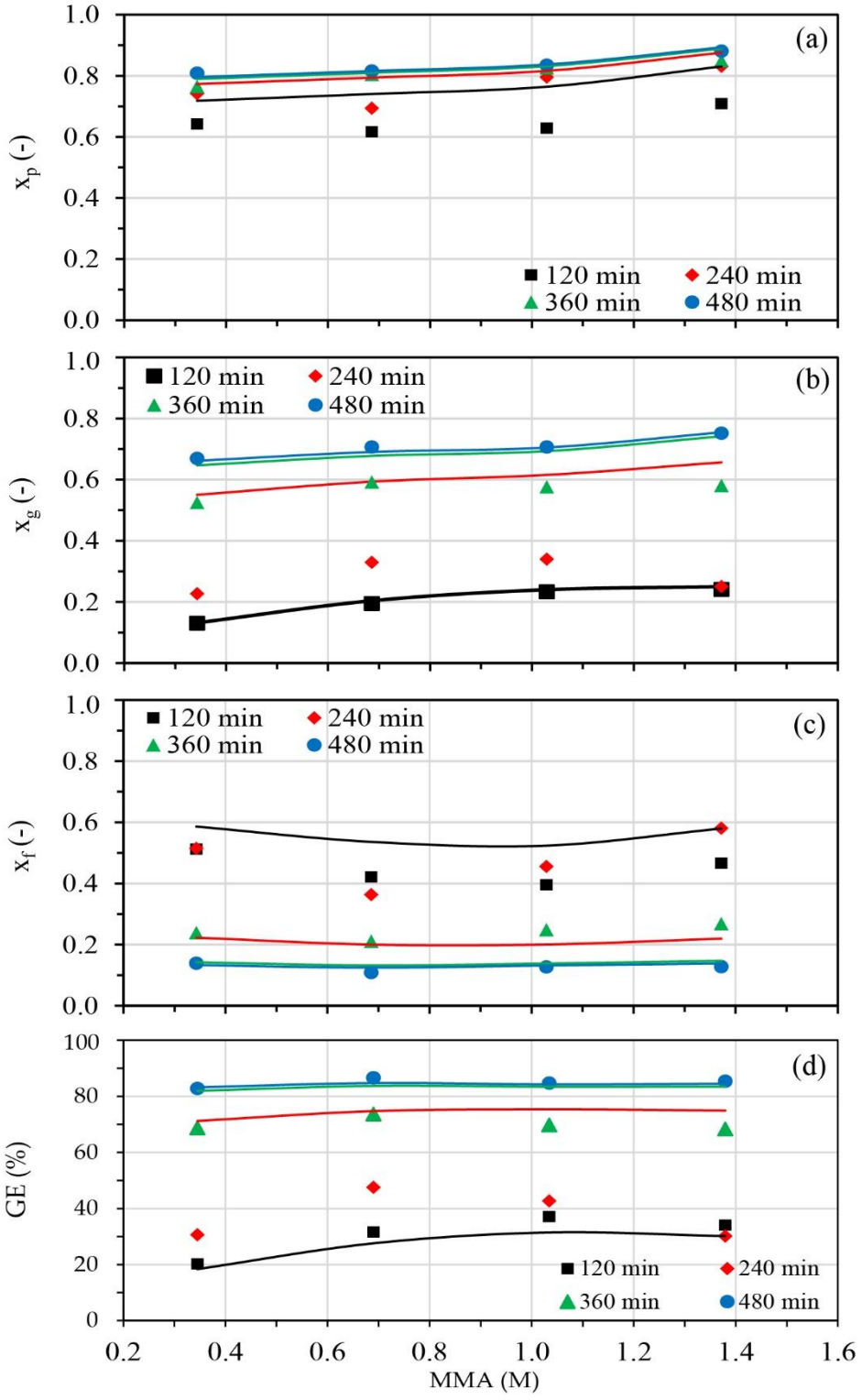

Figure 4.36 Effect of MMA concentration on (a) x_p, (b) x_g, (c) x_f, and (d) grafting efficiency (symbols) as a function of reaction time with concentration of CHPO 2.7334×10^{-3} M and T = 343.15 K. And the line is the kinetic model.

concentration of MMA 0.3430 - 1.3719 M and CHPO 2.7334 × 10^{-3} M at 343.15 K for 0 - 480 min. It is clearly seen that the conversion of grafted rubber and grafted copolymers increased with the increasing MMA concentration, which showed a continuous upward trend, while the values of free rubber and free copolymers decreased significantly at the same time. In the part of the GL, it was found that the value of GL increased with the increasing MMA concentration at the same time. The value of GL increased from 86.77, 86.76, 88.22, and 96.35% for reaction time at 480 min, as shown in Figure 4.38c.

The FTIR spectra of LNR and grafted LNR samples were prepared at various amounts of MMA 0.3430 -1.3719 M by keeping the CPHO 2.7334 × 10^{-3} M at 343.15 K for 8 h, as shown in Figure 4.39. The functional groups of the grafted LNR obtained were characterized by FTIR spectroscopy and compared to the pure LNR. Major absorption peaks were detected at wave numbers 1665 and 836 cm^{-1}, corresponding to the C=C stretching vibration of cis-1, 4-polyisoprene, and the =CH out of plane bending of cis-1, 4-polyisoprene, respectively. Figure 4.39 shows a new absorption peak at wavenumbers 1729 cm^{-1} corresponding to the C=O stretching of the ester groups of MMA. The observation of a new characteristic peak can confirm the occurrence of the formation of the graft copolymer of the MMA monomer grafted onto the LNR chains. However, variations of a new absorption peak at wave numbers of 1729 cm^{-1} for graft copolymers at various amounts of MMA are also observed.

The absorption peak of experiments MGLNR03, which were performed at an amount of MMA at 1.3719 M, is greater when compared to the others, which were performed at an amount of MMA at 0.3430 -1.3719 M. Increasing the amount of MMA raises the concentration in the system, enhancing the amount of MMA grafted onto the LNR backbone chain. The absorption peak is thus higher. A lower %GE for the amount of MMA at 1.3719 M results because of an increase in the amount of MMA, which not only enhances the grafting of the MMA onto LNR backbone chain but also promotes the formation of free homopolymer. Free homopolymer is more produced with respect to graft copolymer on an increasing amount of the MMA, and GE decreases.

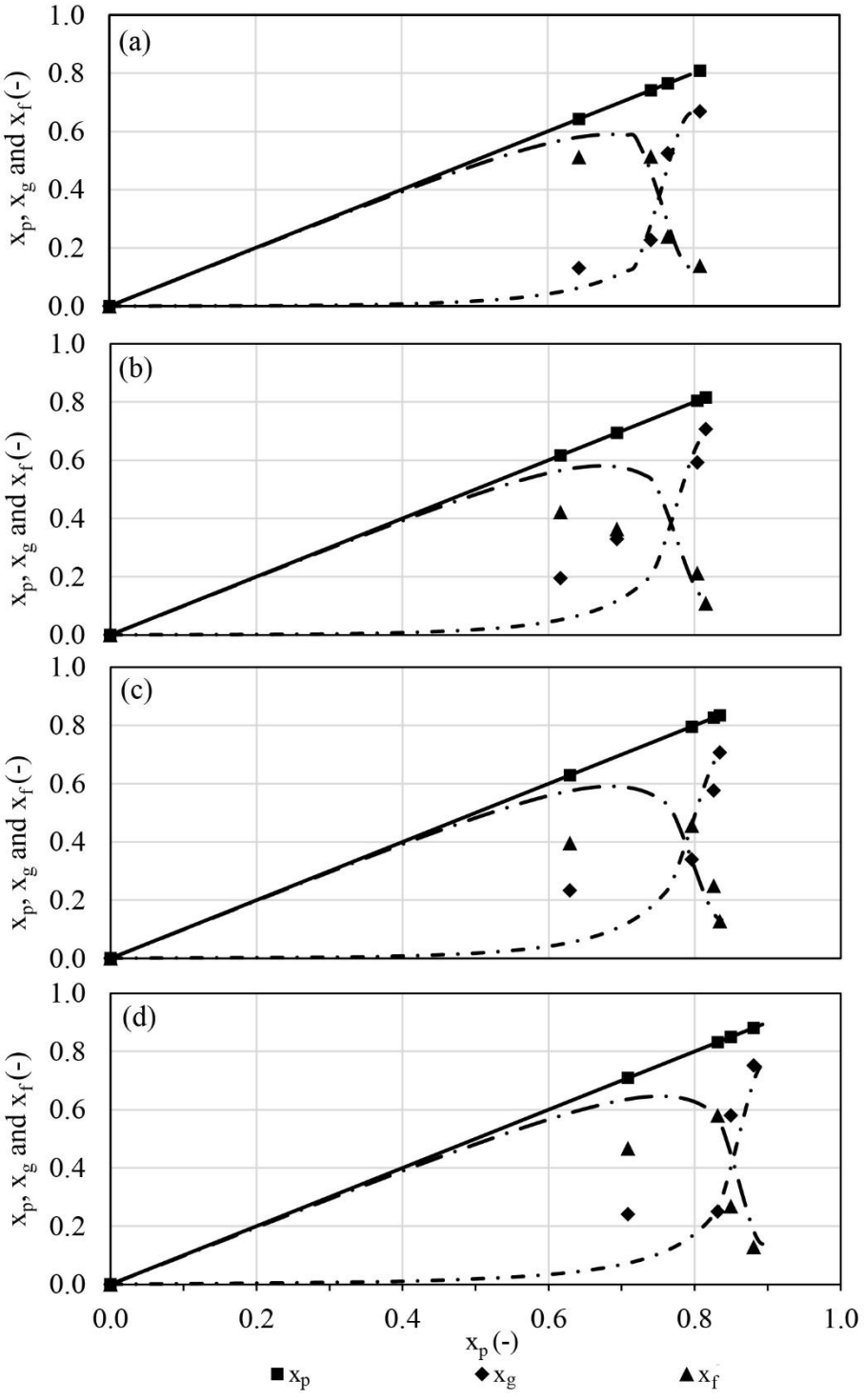

Figure 4.37 Variation of MMA concentration: (a) MMA 0.3430 M, (b) MMA 0.6859 M, (c) MMA 1.0289 M, and (d) MMA 1.3719 M with conversion of (symbols) concentration of CHPO 2.7334×10^{-3} M and T = 343.15 K. And the line is the kinetic model.

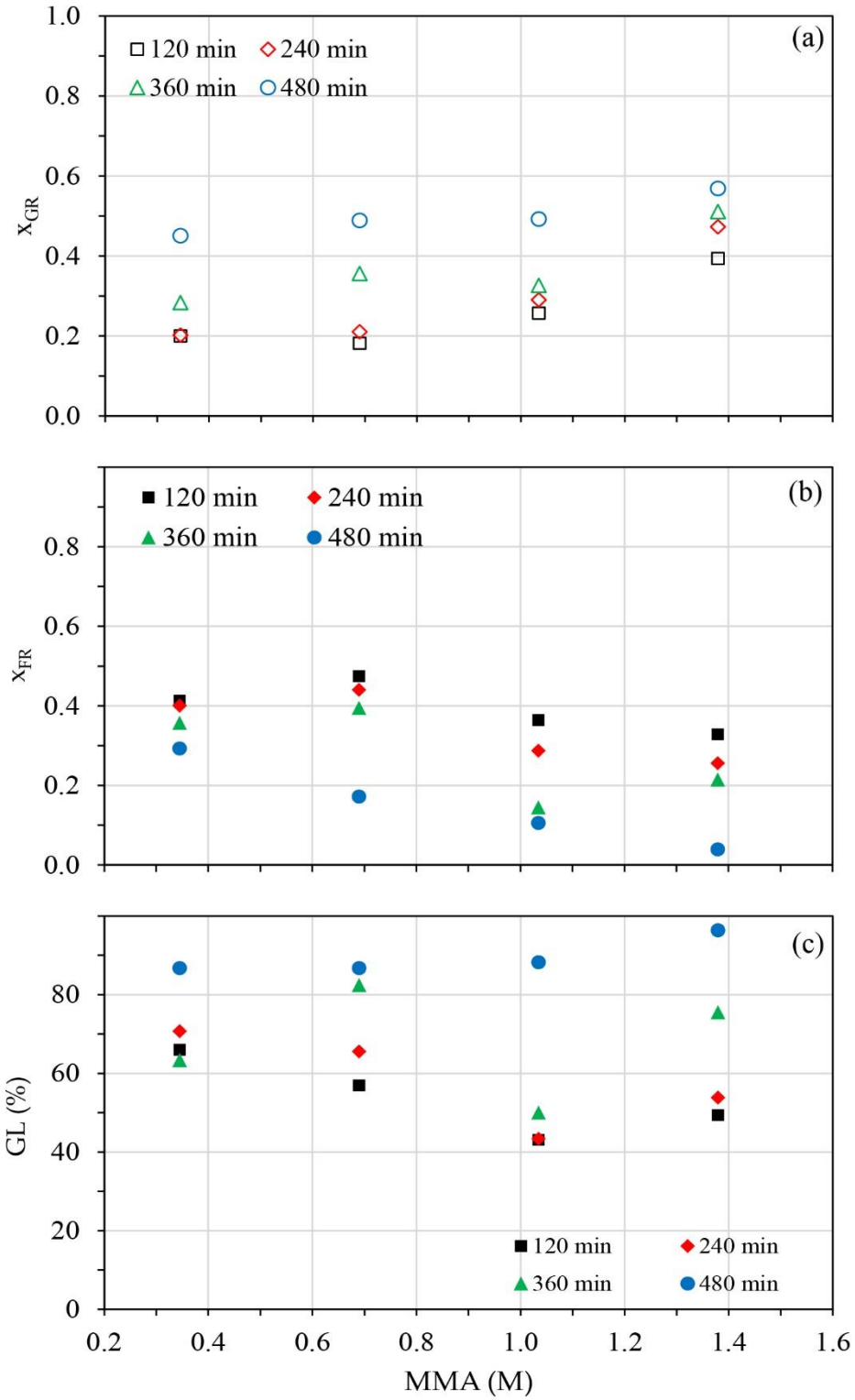

Figure 4.38 Effect of MMA concentration on (a) graft rubber (open symbols), (b) free rubber (close symbols), and (c) graft level (close symbols) as a function of reaction time with concentration of CHPO 2.7334×10^{-3} M and T = 343.15 K.

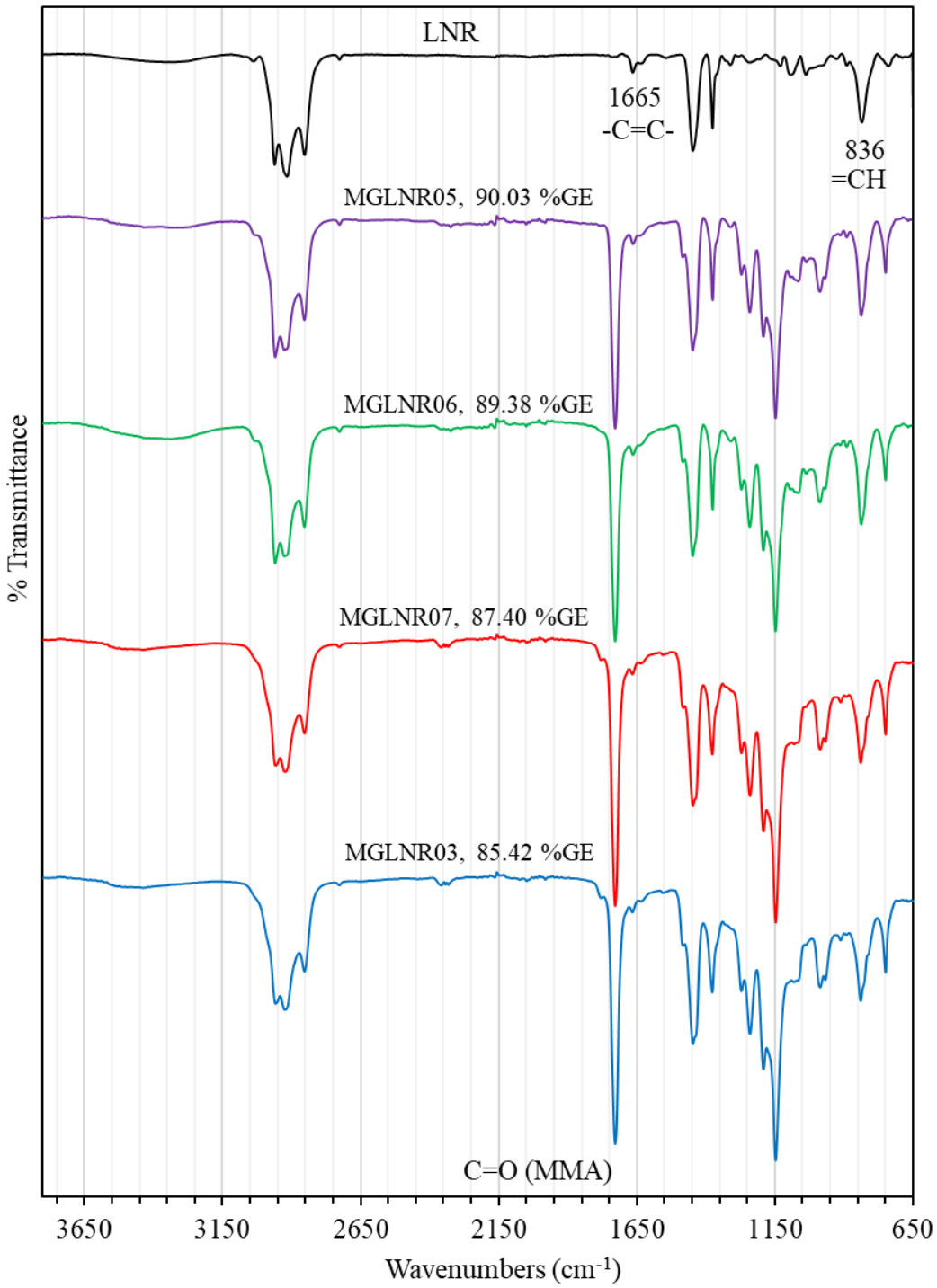

Figure 4.39 FTIR spectra (650 – 3800 cm^{-1}) of LNR and MGLNR samples at various MMA concentration at 8 h for graft copolymer of MMA onto LNR.

4.2.5 Effect reaction temperature

The dependence of the rate on temperature was studied from 328.15 to 343.15 K by keeping the concentrations of CHPO and MMA constant at 2.7334×10^{-3} M and 1.3719 M, respectively. Figure 4.40 shows the influence of temperature on the conversion as the reaction proceeded. It is clearly seen that, at a particular x_p, the larger numbers of total radicals in the core and shell phases were performed polymerization under higher temperatures, as shown in Figure 4.40a. The interaction between CHPO and TEPA is accelerated when the temperature increases, leading to the generation of more cumyloxy radicals. This indicated the number of total radicals both in the core and shell phases. The larger number of total radicals accumulated in the core and shell phases led to a higher final x_p when temperatures were higher at the same time.

The influence of temperature on the conversion is similar to the influence of the initiator but even stronger. In the early stage of the reaction at $0 < x_p < 0.75$, an increase in temperature resulted in a growth of the free MMA content in the system, as shown in Figure 4.41, while it provided a smaller increase of the grafting MMA content in graft product. This indicated that the free MMA radicals were more greatly produced from the graft macroradicals in the early stage of reaction where there is a lot of the monomer. Consequently, a smaller enhancement in GE was observed at higher temperatures, as shown in Figure 4.40d.

In the end stage of the reaction, where x_p almost arrived at a limited value ($x_p \geq 0.75$), a larger consumption of the free MMA content in graft product at higher temperatures was notable. As mentioned above, an increase in temperature promoted the production of cumyloxy radicals, enhancing the formation of free MMA radicals and rubber radicals [75, 127]. This increased the probability that free MMA radicals formed in the early interval attack rubber chains to produce graft copolymer. Hence, more free MMA was consumed to graft onto LNR backbone chains at higher temperatures, leading to steeper increases in the grafting MMA content in the graft product and the higher GE at the end stage of the reaction.

However, it can be further explained that higher temperatures may reduce the viscosity of the system and increase the speed of molecular chain movement to facilitate the grafting reaction. Moreover, a major influence of temperature was the

actual concentration of monomer in the particle, which can be very low at higher temperatures, as reported by Sundberg et al.[128]. On the other hand, this can be described in terms of the rate of polymerization. When the temperature was raised, the rate of monomer grafting into the LNR backbone chain was enhanced, thus resulting in higher GE. Lenka et al.[129] found similar results when studying the graft copolymerization of MMA onto rubber.

The influence of the reaction temperature on the x_{GR}, x_{FR}, and GL has been investigated, as shown in Figure 4.42. The reaction was synthesized with various temperatures at 328.15 – 343.15 K, and the concentration of MMA 1.3719 M and CHPO 2.7334×10^{-3} M for 0 - 480 min. It is clearly seen that the conversion of grafted rubber and grafted copolymers increased with the increasing reaction temperature, which showed a continuous increase trend. In contrast, the values of free rubber and free copolymers decreased significantly at the same time. In the part of the GL, it was found that the value of GL increased with the increasing reaction temperature at the same time. The value of GL increased from 76.70, 87.29, 93.23, and 96.35 % for reaction time at 480 min, as shown in Figure 4.42c. At the moment, this indicates an increase in temperature, which resulted in a growth of the free MMA content in the system.

FTIR spectra of LNR and grafted LNR samples were performed at various temperatures with keeping amounts of CHPO 2.7334×10^{-3} M and MMA 1.3719 M for 8 h. The spectra of the grafted PMMA onto LNR chain appeared to be a new absorption peak at 1729 cm^{-1}. The variations of the new absorption peak depend on the amount of monomer grafted onto the LNR chain. Therefore, it is generally known that polymerization reaction under higher temperatures accelerates the interaction between CHPO and TEPA, providing a larger number of cumyloxy radicals. An increasing amount of cumyloxy radicals promotes an increase in the rate of copolymerization [75], causing a greater GE. This results in an increase in the new absorption peak. When the temperature increases, an increasing amount of cumyloxy radicals promotes an increase in the rate of copolymerization [40], causing a greater GE, which also results in an increase in the new absorption peak, as shown in Figure 4.43.

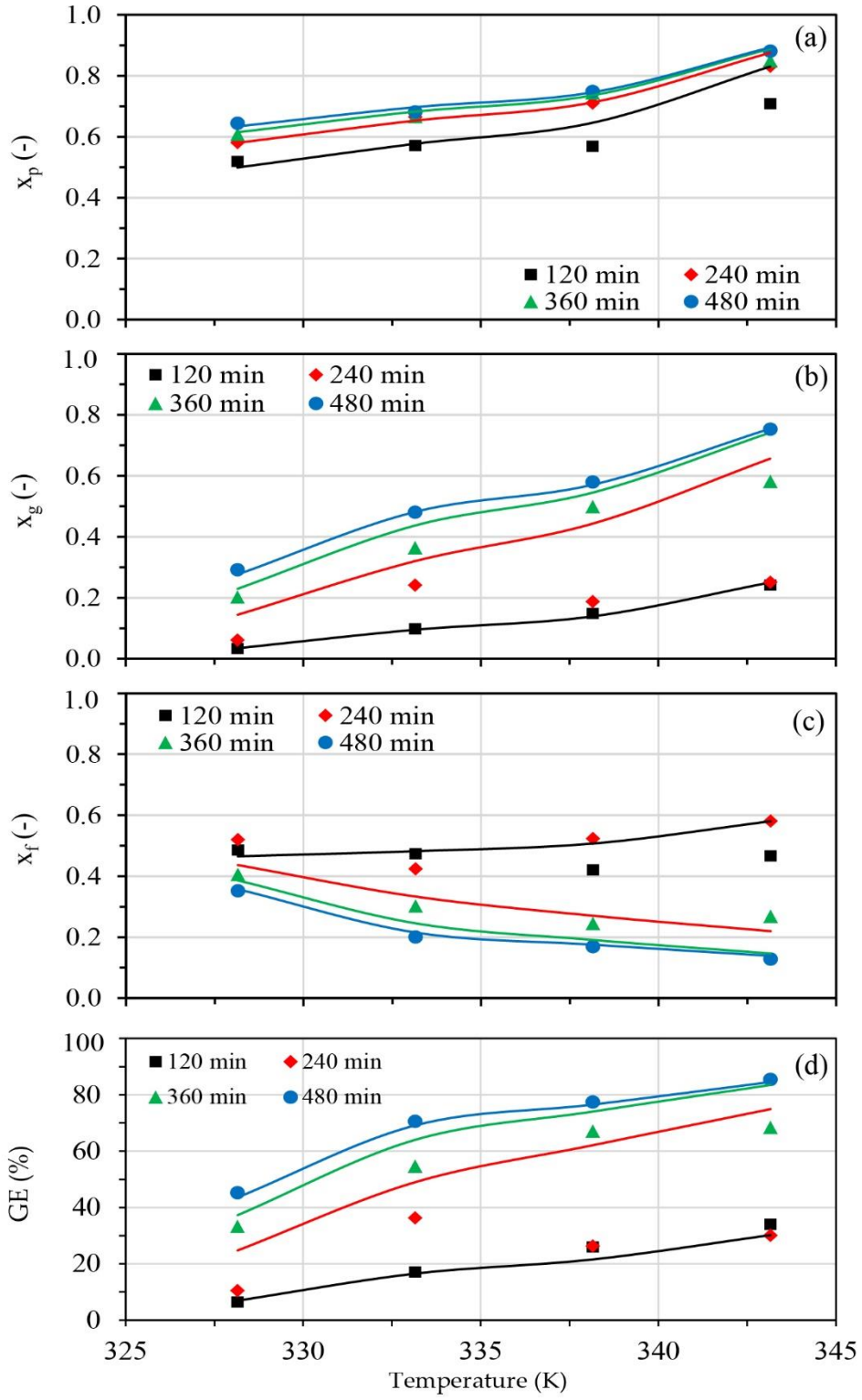

Figure 4.40 Effect of reaction temperature on (a) x_p, (b) x_g, (c) x_f, and (d) grafting efficiency (symbols) as a function of reaction time with concentration of CHPO 2.7334×10^{-3} M and MMA 1.3719 M. And the line is the kinetic model.

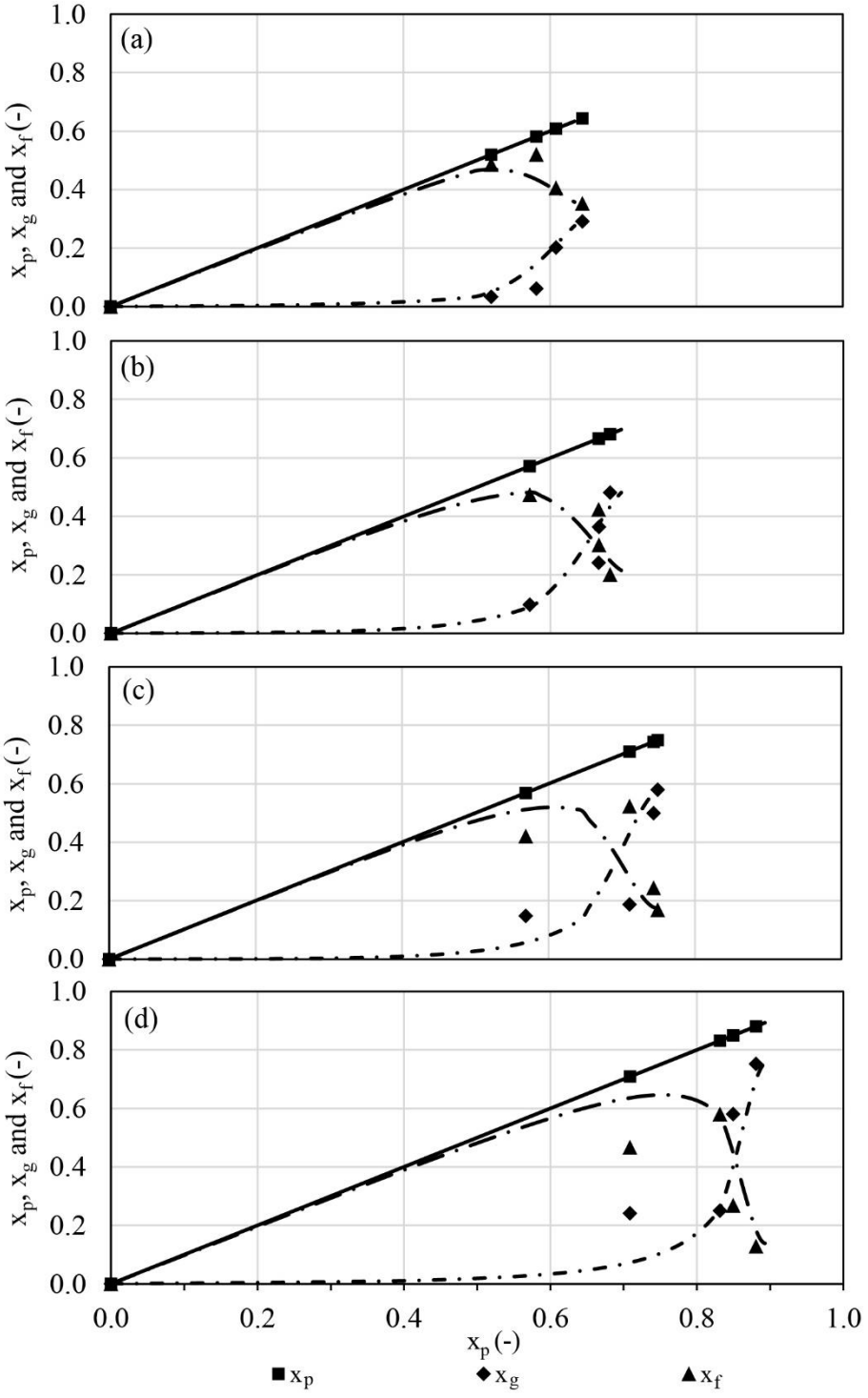

Figure 4.41 Variation of reaction temperature: (a) T = 328.15 K, (b) T = 333.15 K, (c) T = 338.15 K, and (d) T = 343.15 K with conversion of (symbols) concentration of CHPO 2.7334 × 10^{-3} M and MMA 1.3719 M. And the line is the kinetic model.

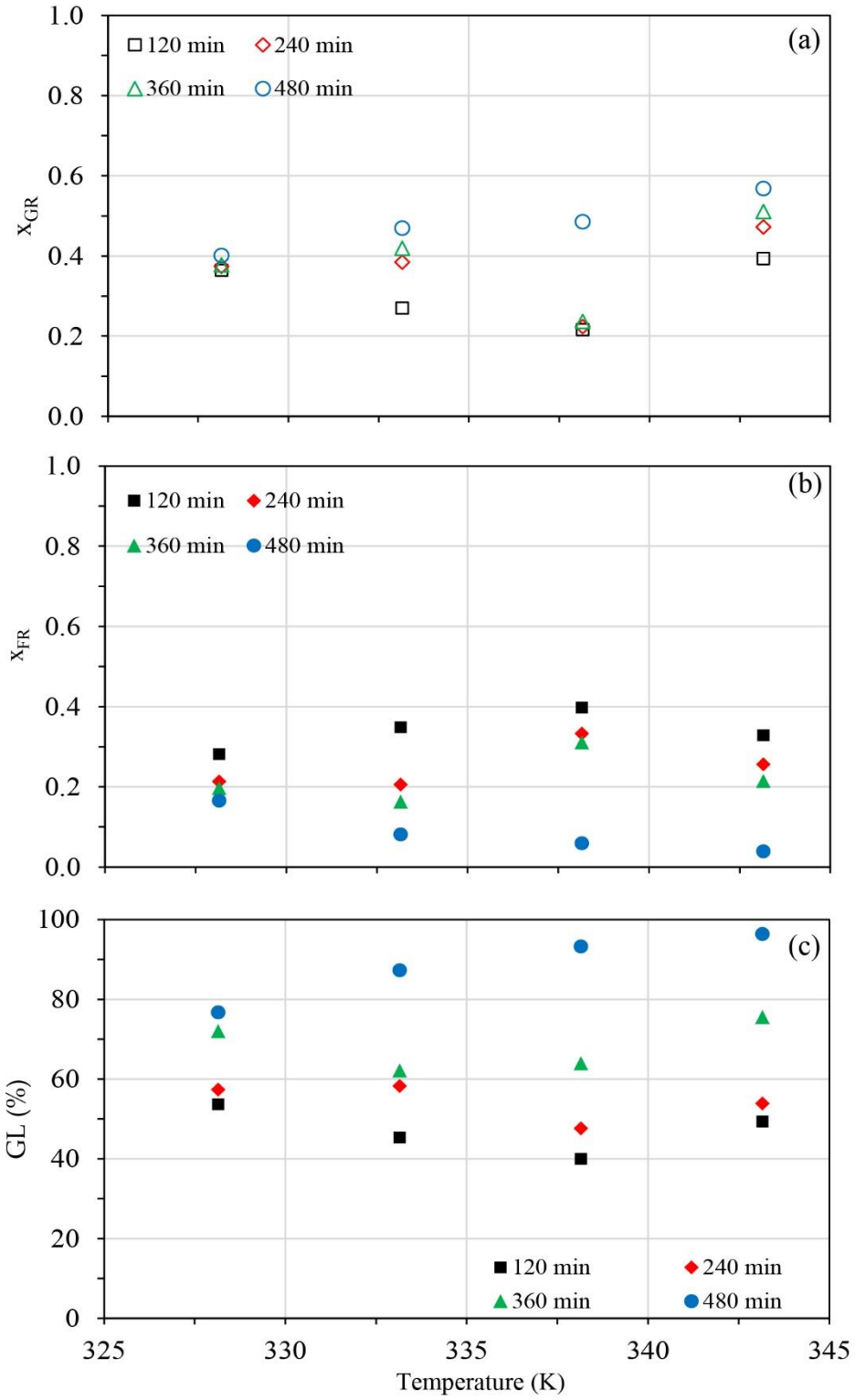

Figure 4.42 Effect of reaction temperature on (a) graft rubber (open symbols), (b) free rubber (close symbols), and (c) graft level (close symbols) as a function of reaction time with concentration of CHPO 2.7334×10^{-3} M and MMA 1.3719 M. .

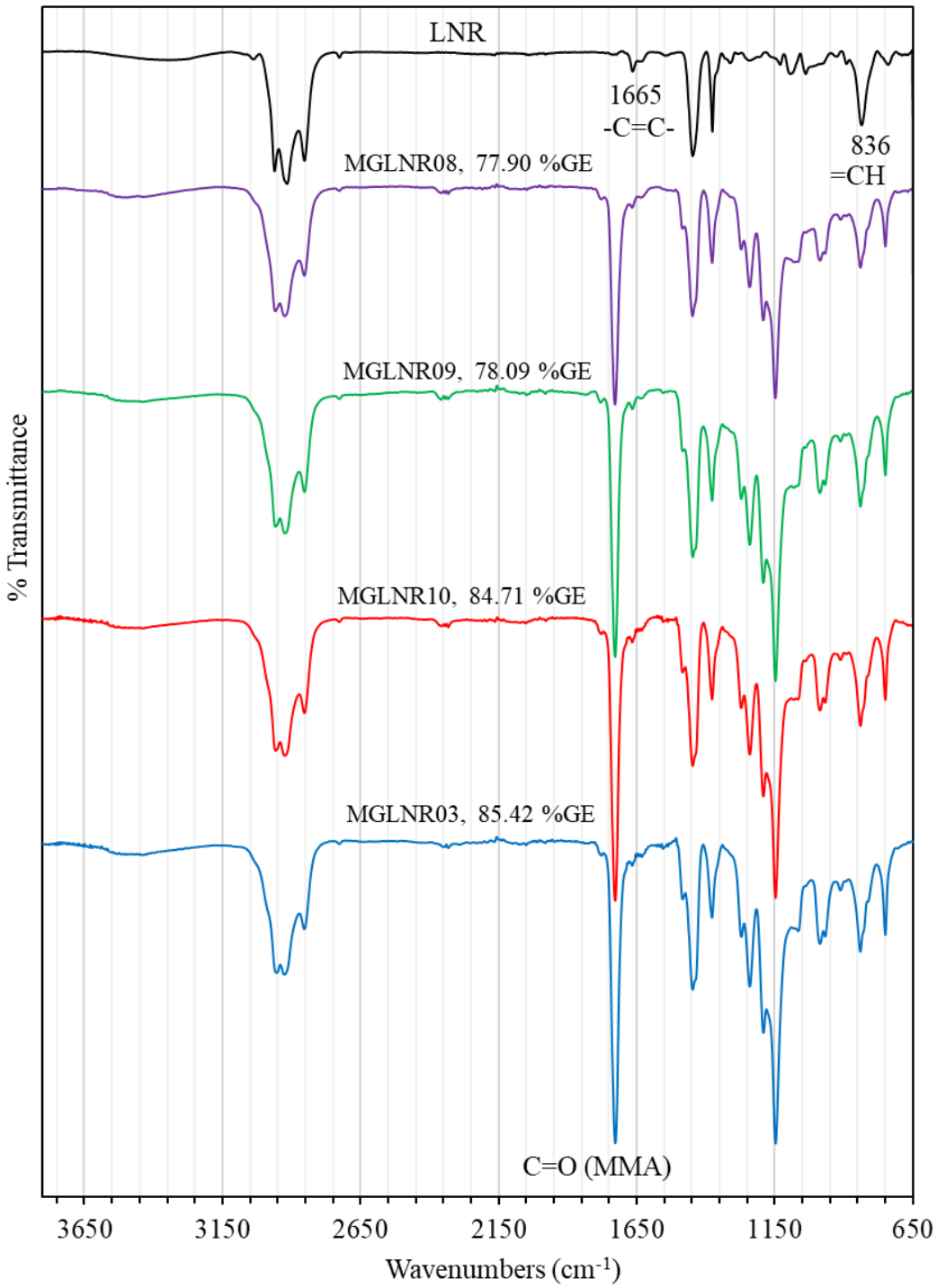

Figure 4.43 FTIR spectra (650 – 3800 cm^{-1}) of LNR and MGLNR samples at various reaction temperatures at 8 for graft copolymer of MMA onto LNR.

4.2.6 Grafting kinetics

The reaction of graft copolymerization of the monomer onto the LNR chain. The rapid polymerization during the early stage of polymerization might be explained by the rapid decomposition of the CHPO/TEPA initiator into the reaction, and the CHPO is reduced by the TEPA generating cumyloxy radicals ($RO^{\bullet}$). The cumyloxy radicals can not only initiate LNR chains to produce polyisoprene radicals, which interact with monomer to become graft macroradicals during the polymerization, but also induce monomer to form free homopolymeric radicals, which can further interact with polyisoprene radicals to yield graft copolymer. The homopolymeric radicals and graft macroradicals can transfer to monomer and to rubber, yielding homopolymer and graft copolymer. Moreover, some of the free homopolymeric radicals can terminate by combination to produce free homopolymer. Refer to Figures 4.32, 4.36, 4.40. The polymerization rate is presented as a function of conversion, the observed conversion-time curves for x_p, x_g, and x_f. During the early stages of the reaction (0 - 240 minutes), the x_f - t curve shows a similar trend as x_p - t; conversion increases greatly with time. Since x_p is the summation of x_g and x_f, it indicates that most of the monomer polymerizes to produce free homopolymeric radicals during the early stages of the reaction. After 240 minutes, where x_p starts to level off, x_g continuously increases with time, but x_f decreases. This phenomenon implies that the free homopolymeric radicals produced in the early stage favorably form a chemical bond with the LNR backbone, producing graft copolymer.

According to the conversion-time profiles, x_p and x_g are nonlinear functions of time (t), and both of them can be fitted well into the simple power function [130, 131]. Therefore, the relation of conversion and time can be written as:

$$x = K\, t^{n} \tag{4.8}$$

Equation (4.8) can be differentiated with t and multiplied with M_0, which gives:

$$M_0 \frac{dx}{dt} = k\, t^{n-1} \tag{4.9}$$

Where k and n are constants, M_0 is the initial monomer concentration (M), and t is time in unit min. Based on the relationship of $Rate_{product} = - Rate_{reactant} = -(-M_0 dx/dt)$,

which represents an abbreviation with the R_p and R_g (Figure 4.44), the rate equation can be rewritten in the forms.

$$R_p = k_p\, t^{n_p-1} \quad \text{; for the rate of monomer conversion} \tag{4.10}$$

$$R_g = k_g\, t^{n_g-1} \quad \text{; for the rate of grafting of monomer conversion} \tag{4.11}$$

where subscript p and g represent overall copolymerization and grafting reactions, respectively. As previously discussed, the reaction parameters studied include initiator concentration, monomer concentration, and reaction temperature, which have a great influence on the graft copolymerization process. These variables have been proposed to relate to the rate as a power function [131-136]. Therefore, Equations (4.10) and (4.11) can be rewritten as:

$$R_p = k_p\, [CHPO]^a [MMA]^b\, t^{n_p-1} \tag{4.12}$$

$$R_g = k_g\, [CHPO]^c [MMA]^d\, t^{n_g-1} \tag{4.13}$$

where [CHPO] and [MMA] are the initial concentration of initiator (mol/L) and monomer (mol/L), respectively. The power function equation can be rewritten in the linear form: $\ln R = \ln k + (n-1)\cdot \ln t$. The exponents n (both subscript p and g) can be determined by using a natural logarithm plot of R_p and R_g versus reaction time and the linear regression technique, and the n value can be calculated from the slope (n-1) of that line, as shown in Figure 3.45. Moreover, the exponents represent the concentration of the reactants a, b, c, and d, which are referred to as partial orders of the reaction. Following the Arrhenius relation, $k = A\cdot\exp(-E_a/RT)$ where A, E_a, R, and T represent the pre-exponential factor, activation energy, universal gas constant, and temperature, respectively, Equations (4.12) and (4.13) can thus be reformulated as follows:

$$R_p = A_p e^{-Ea_p/RT}\, [CHPO]^a [MMA]^b\, t^{n_p-1} \tag{4.14}$$

$$R_g = A_g e^{-Ea_g/RT}\, [CHPO]^c [MMA]^d\, t^{n_g-1} \tag{4.15}$$

In general, the rate equation, which is a power function of the process variables, is independent of reaction time. Their reaction orders (a and b) and Arrhenius parameters can be evaluated by using a natural logarithm plot of R_p/t^{n_p-1} and

R_g/t^{n_g-1} versus reactant concentration and the linear regression technique, as shown in Figures 3.46 and 3.47. The rate equation proposed is a nonlinear function of reaction time. Hence, Equations (4.14) and (4.15) can be rearranged as follows:

$$\frac{R_p}{t^{n_p-1}} = A_p e^{-Ea_p/RT} [CHPO]^a [MMA]^b \quad (4.16)$$

$$\frac{R_g}{t^{n_g-1}} = A_g e^{-Ea_g/RT} [CHPO]^c [MMA]^d \quad (4.17)$$

Therefore, the rate/t^{n-1} shown in Equations (4.16) and (4.17) is constant at any reaction time. The ln-ln plots of the rat/t^{n-1} with respect to various process factors for the graft copolymerization systems are presented in Figures 4.46 - 4.47. Only the variable of interest was varied, while the other variables were kept constant. At any magnitude of the variable of interest, there are sixteen points of data representing the values of ln rate/t^{n-1} at any time studied. The variance of the observed value of ln rate/t^{n-1} at any magnitude of the variable of interest. The reaction orders and Arrhenius parameters can be obtained from the slope of the ln-ln plot. The value of reaction orders is Equation (4.18) and (4.19). As a result, the rate equations for the grafting of MMA into LNR can be summarized as follows:

$$R_p\ (mol/L \cdot min) = 9.75 \times 10^2 \cdot e^{-19,677.97/RT} [CHPO]^{0.19} [MMA]^{0.88}\ t^{-0.83} \quad (4.18)$$

$$R_g\ (mol/L \cdot min) = 1.45 \times 10^{11} \cdot e^{-75087.26/RT} [CHPO]^{0.55} [MMA]^{0.62}\ t^{0.13} \quad (4.19)$$

Based on Figures 4.46c and 4.47c, a plot of ln k versus 1/T provided a straight line, and the E_a value can be calculated from the slope ($-E_a/R$) of that line, the value of A also provided from intercept with the y-axis, as demonstrated in Figure 3.46c and 3.47c.

The influence of reaction time on R_p and R_g for grafting MMA onto LNR is shown in Figure 4.44. It is evident from these figures that the values of R_p decrease with an increase in reaction time. This effect can be explained by the fact that the relative increase in the total yield is very much when compared to that of reaction time, and the value of R_p is almost constant when the reaction time for the reaction is raised. This may also be due to the depletion of concentration radicals of the initiator with the increase in reaction time. On the other hand, the value of R_g continues to

increase as the reaction time. This trend can indicate that the radicals of monomer were greatly grafted onto the LNR chain, leading to an increase in the R_g value but resulting in a decrease in the free homopolymer. It was clearly seen that the reaction orders with respect to CHPO concentration and MMA concentration deviate from 1, indicating a nonlinear relationship for both R_p and R_g. However, the negative power of reaction time indicates that the rate is inversely proportional to reaction time. Hence, an increase in reaction time retards the R_p. On the other hand, the positive power of reaction time reveals that the rate is directly varied with reaction time, causing the R_g to increase continually.

The reaction orders of CHPO concentration for the R_p and R_g are 0.19 and 0.55 (Figure 4.46a and 4.47a) for graft copolymerization systems, respectively, while the reaction orders of MMA concentration are 0.88 and 0.62 (Figure 4.46b and 4.47b). It was found that R_p has a considerably lower activation energy than that of R_g. This phenomenon can be explained by the fact that R_p is the formation rate of the monomer conversion consisting of the grafting of monomer conversion and free homopolymer conversion, while R_g is only for the formation rate of the grafting of monomer conversion. Hence, the activation energy for the monomer reacting with the growing polymer chains is lower than that for attaching to rubber. Furthermore, the observed activation energy is quite low with respect to those reported for graft copolymerization induced by a thermal initiator. The relatively lower activation energy of the reaction is a unique feature of the polymerization in the presence of the redox initiator. Many researchers have studied the activation energy of grafting. The activation energy for the redox initiator process is lower by 1.5 - 3 times than that of the thermal process, reported by Wang [137]. Odian [75] was reported to have lower activation energy, allowing the polymerization to take place at a moderate temperature of 0 - 50°C. A similar phenomenon was also observed when MMA was grafted onto cellulose fiber using ascorbic acid and hydrogen peroxide as redox initiators [134]. It was found that the activation energy for the overall polymerization and the graft copolymerization are

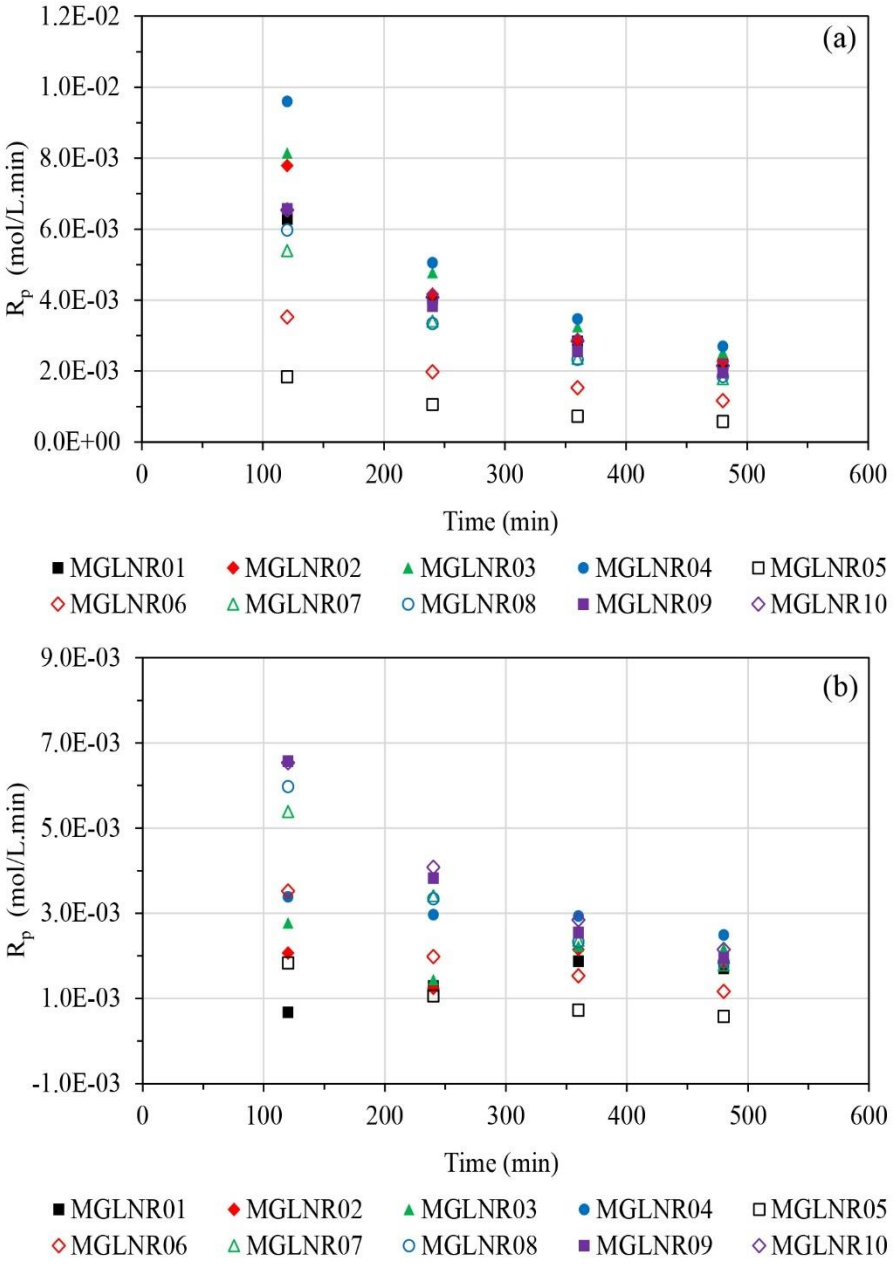

Figure 4.44 A plot of (a) R_p and (b) R_g versus reaction time for MMA-g-LNR graft copolymerization with the condition for the concentration of [CHPO] = *9*.3961 $\times 10^{-4}$ - 3.5876 $\times 10^{-3}$ M, and [MMA] = 0.3430 – 1.3719 M at T = 328.15 – 343.15 K for 480 min.

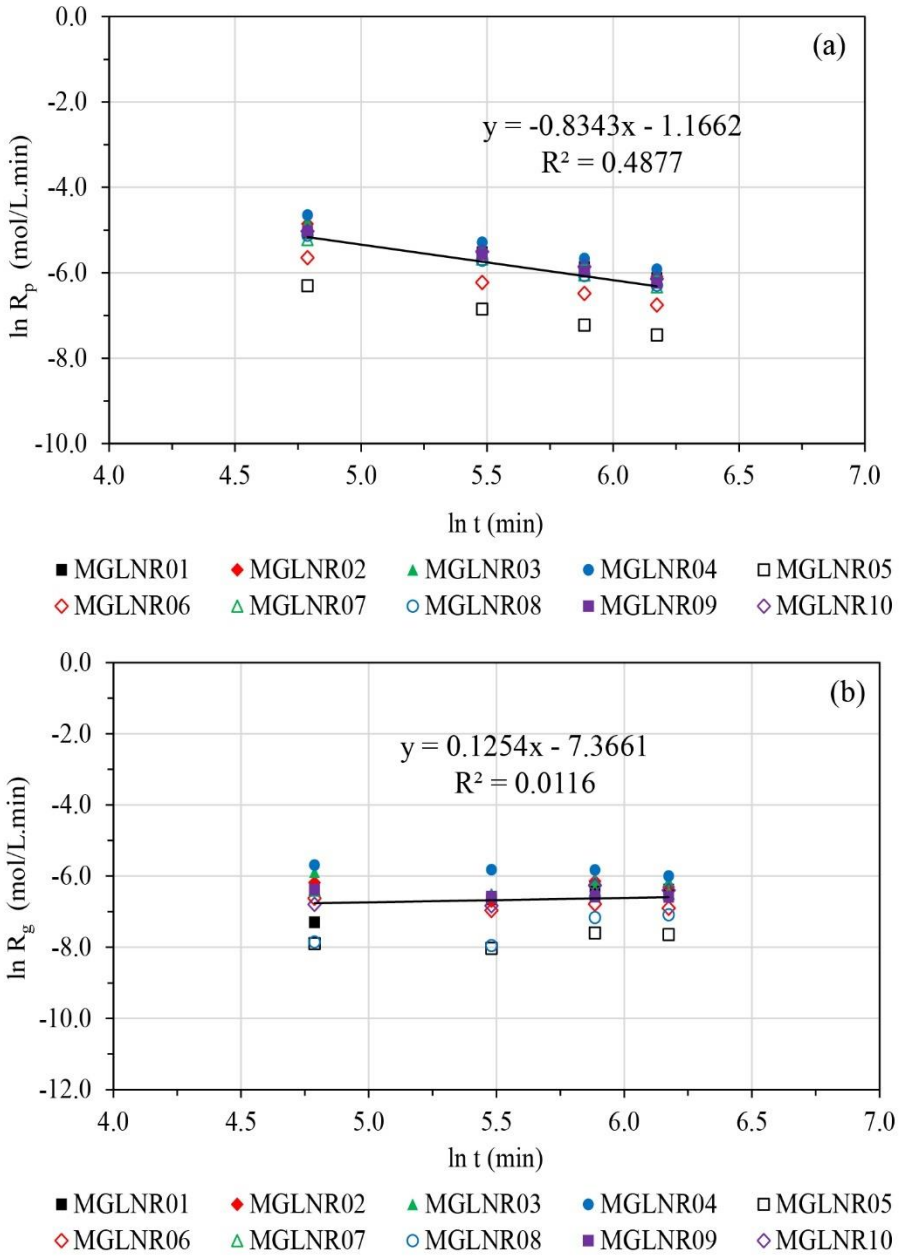

Figure 4.45 A natural logarithm plot of (a) R_p and (b) R_g versus reaction time for MMA-g-LNR graft copolymerization with the condition for the concentration of [CHPO] = 9.3961 $\times 10^{-4}$ - 3.5876 $\times 10^{-3}$ M, and [MMA] = 0.3430 – 1.3719 M at T = 328.15 – 343.15 K for 480 min.

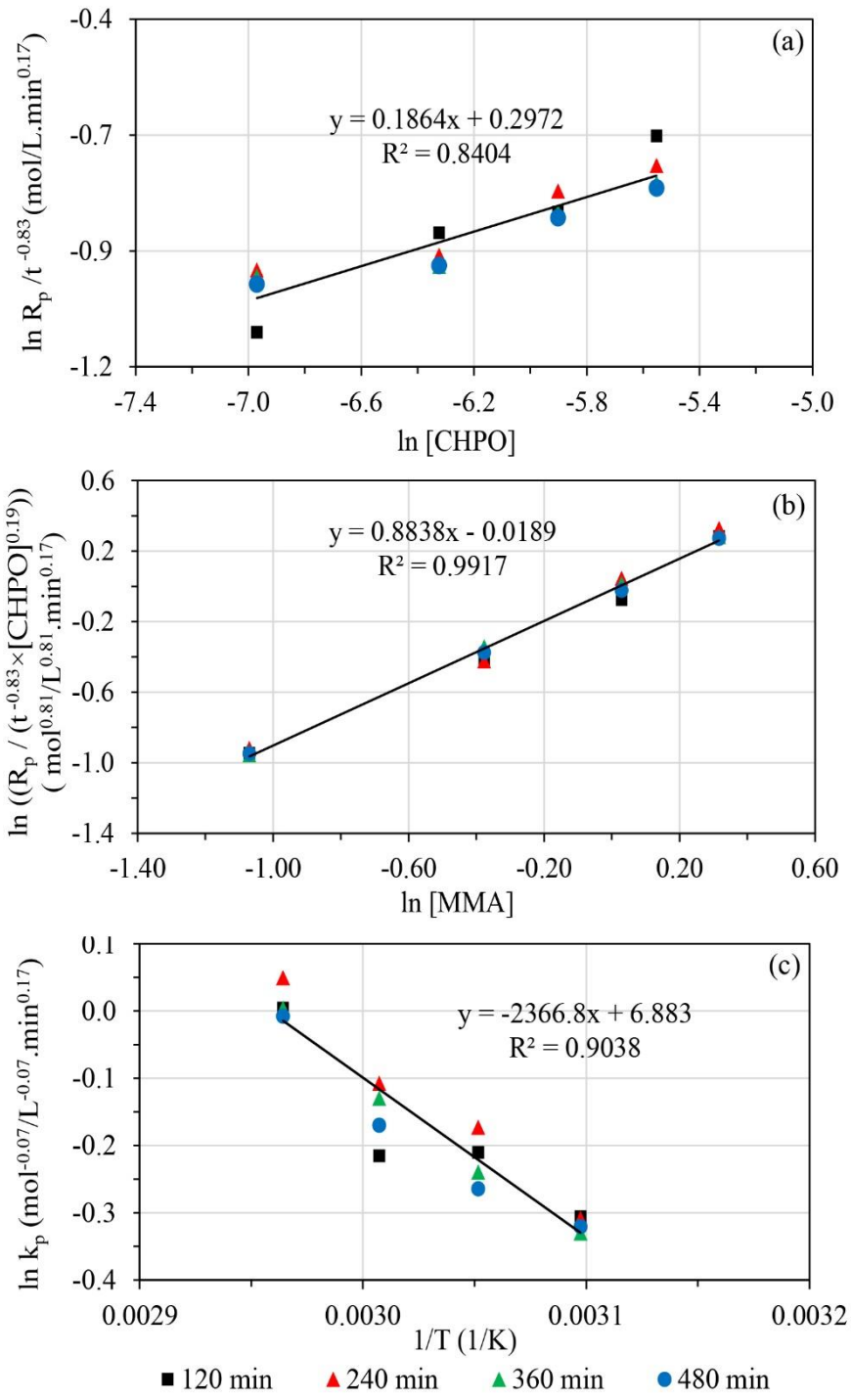

Figure 4.46 a plot of ln rate/t^{n-1} versus CHPO concentration, (b) a plot of ln rate/t^{n-1} versus MMA concentration, and (c) a plot of ln k_p versus 1/T at reaction time for monomer conversion with the condition for the concentration of [CHPO] = 9.3961 $\times 10^{-4}$ - 3.5876 $\times 10^{-3}$ M, and [MMA] = 0.3430 – 1.3719 M at T = 328.15 – 343.15 K for 480 min.

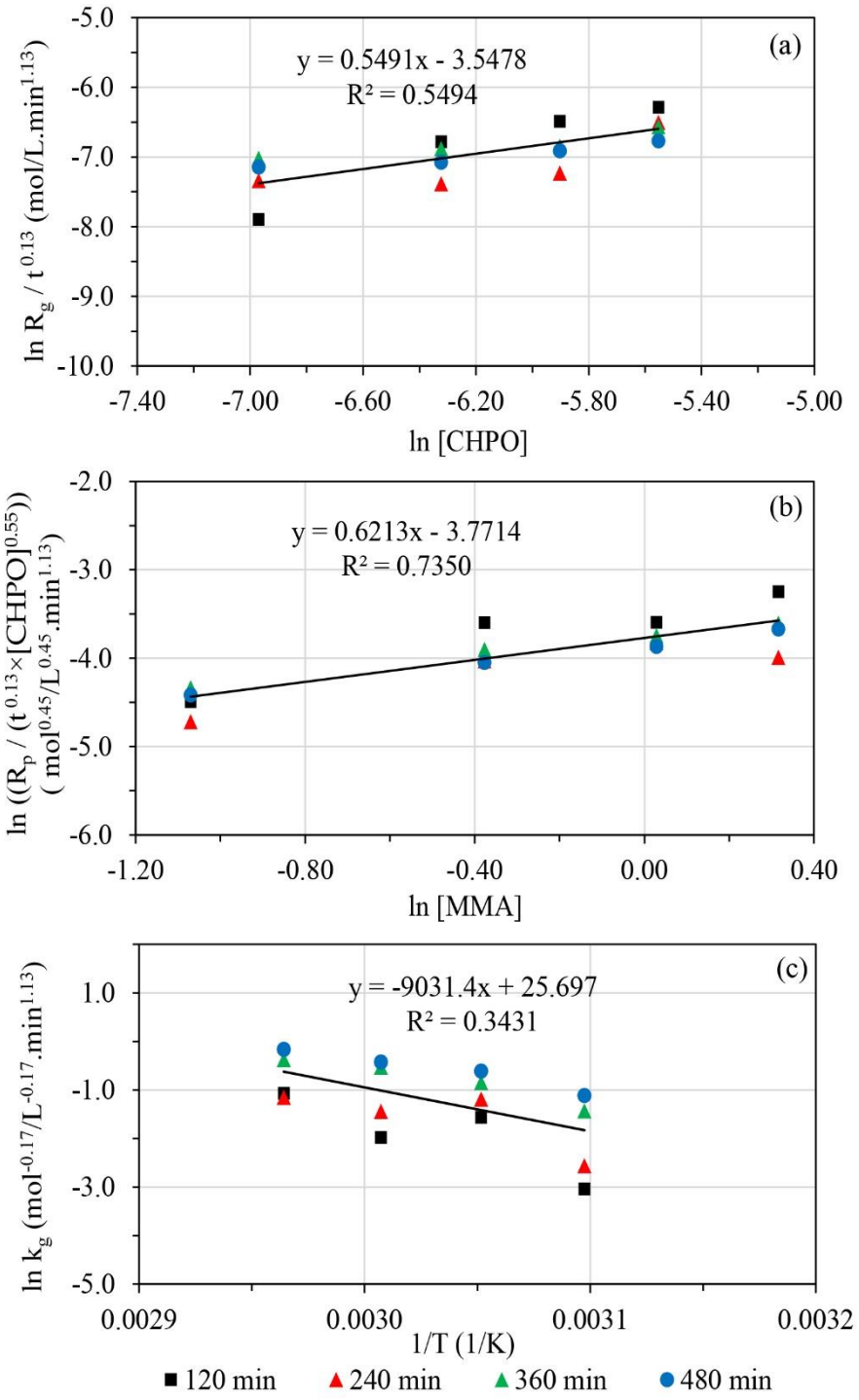

Figure 4.47 (a) a plot of ln rate/t^{n-1} versus CHPO concentration, (b) a plot of ln rate/t^{n-1} versus MMA concentration, and (c) a plot of ln k_g versus 1/T at reaction time for grafting of monomer conversion with the condition for the concentration of [CHPO] = 9.3961 $\times 10^{-4}$ - 3.5876 $\times 10^{-3}$ M, and [MMA] = 0.3430 – 1.3719 M at T = 328.15 – 343.15 K for 480 min.

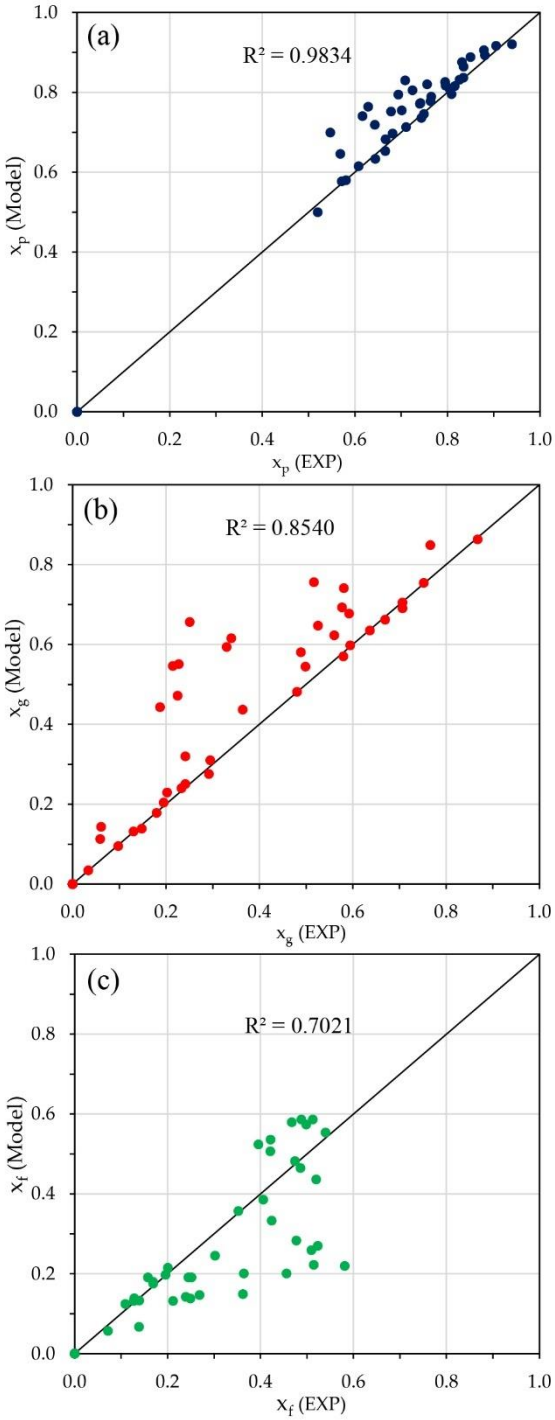

Figure 4.48 Correlation between the Model values obtained and experimental data with of (a) x_p, (b) x_g and (c) x_f with the condition for the concentration of [CHPO] = 9.3961×10^{-4} - 3.5876×10^{-3} M, and [MMA] = 0.3430 – 1.3719 M at T = 328.15 – 343.15 K for 480 min.

19.68 kJ/mol and 75.09 kJ/mol, respectively. Figure 4.48 illustrates a strong correlation between the predicted values and the experimental values for the graft copolymer of MMA onto LNR, showing a high degree of linearity with an R^2 value of 0.9834 (for x_p), 0.8540 (for x_g), and 0.7021 (for x_f). This indicates that the predicted values closely match the experimental data, demonstrating good performance and a high correlation.

4.3 Application of MMA-g-LNR

The resulting graft product of MMA-g-LNR can be used as a compatibilizer to improve the miscibility of PLA and PP, as represented in Scheme 4.3. MMA-g-LNR shows highly polar functional groups that facilitate reactivity. The terminal carboxyl groups of PLA can react with the ester group of MMA-g-LNR, as depicted in Scheme 4.3a. Additionally, the interaction between the hydroxyl and carbonyl groups of PLA and the ester group of MMA in MMA-g-LNR is illustrated in Scheme 4.3a. Meanwhile, the isoprene segment of MMA-g-LNR and PP are linked via non-polar physical interactions, as shown in Scheme 4.3b [112].

4.3.1 Tensile strength

Figure 4.49a-c illustrates the tensile properties of pure PLA and PP and PLA/PP (70:30 wt%) blends with varying amounts of MMA-g-LNR. It is generally recognized that the stress-strain curves significantly depend on the blend compositions, as shown in Figure 4.49a. Figure 4.49b displays the tensile strength of pure PLA and PP and the PLA/PP blend with the MMA-g-LNR compatibilizer. Pure PLA and PP exhibited tensile strengths of 55.31 MPa and 31.61 MPa, respectively. The tensile strength of pure PLA was notably higher than that of pure PP due to the toughness of PP. The lower tensile strength observed in the polymer blends compared to pure PLA and PP can be attributed to the incompatibility between polar PLA and non-polar PP, which prevents effective stress transfer through the interface of the blended components. For the PLA/PP (70:30 wt%) blends with MMA-g-LNR as a compatibilizer, the tensile strength increased with higher MMA-g-LNR content. The addition of MMA-g-LNR to the PLA/PP blends enhanced the miscibility of the MMA component as a shell in

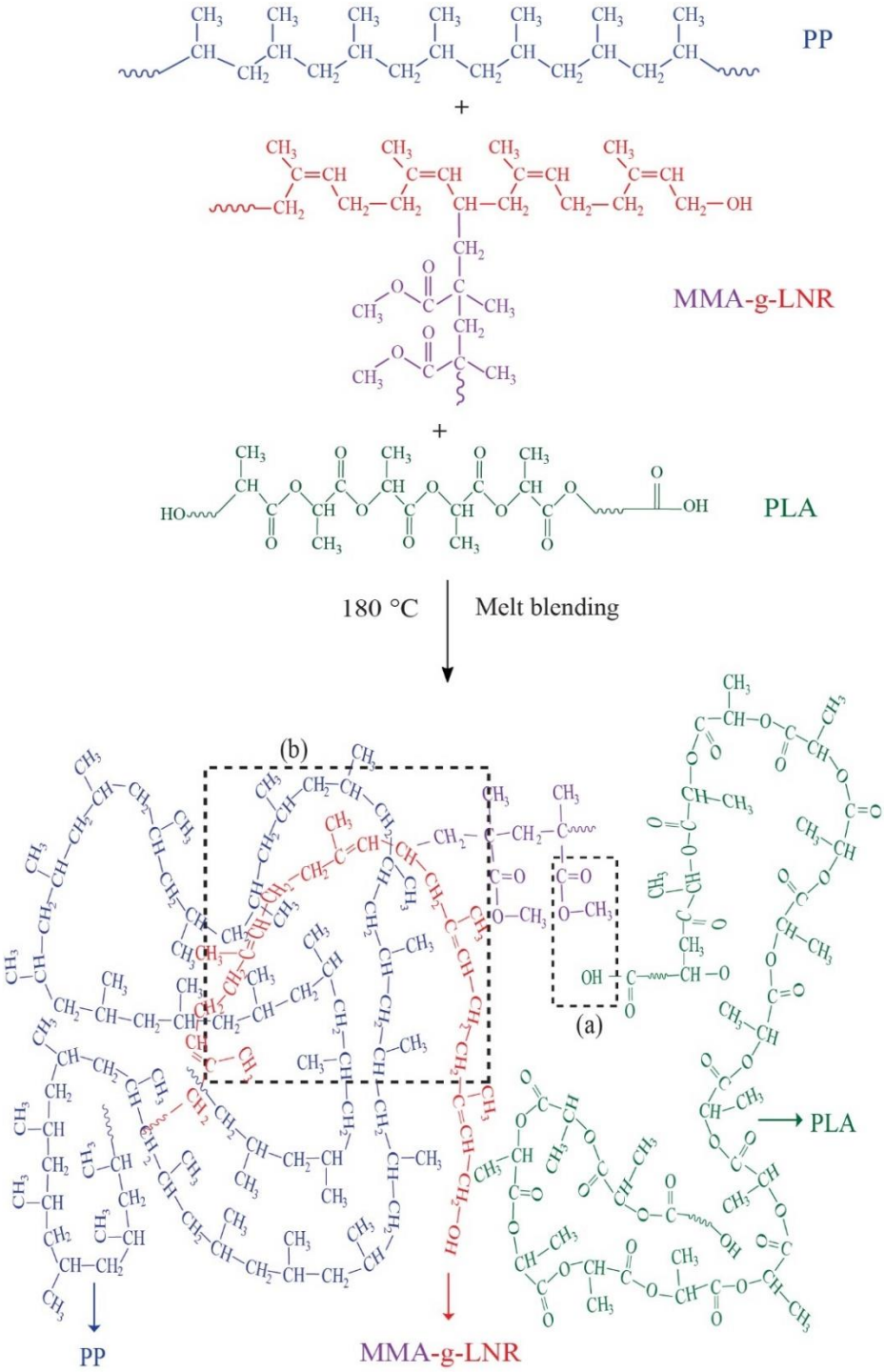

Scheme 4.3 Possible mechanism of PLA/PP blends in the presence of MMA-g-LNR [112].

the PLA phase and improved yield strength, thanks to the elastomeric properties of the LNR component acting as a core in the MMA-g-LNR particle.Pangrahi et al. [138] proposed that thermoplastic elastomers (TPEs) based on polar epichlorohydrin rubber (ECR) and non-polar isotactic polypropylene (i-PP) using the ethylene-acrylic ester-maleic anhydride terpolymer (E-AE-MA-TP) acting as the compatibilizer. They reported that the i-PP/ECR composite, with a 40/60 weight ratio and 5% compatibilizer, demonstrated excellent mechanical properties. The excellent properties of TPEs based on ECR and i-PP using the E-AE-MA-TP as a compatibilizer were characterized by chemical interactions between ethyl acrylate portions of the E-AE-MA-TP compatibilizer and the saturated ester of the maleic anhydride portions and the C-O groups of ECR and physical interactions between the i-PP chains and the ethylene part of the E-AEMA-TP compatibilizer. In addition, Bijarimi et al. [139] reported the preparation of PLA by melt blending with LLDPE and LNR as compatibilizers. The PLA/LLDPE blend showed poor mechanical properties due to the incompatibility between PLA and LLDPE. To address this, LNR was introduced as a third-phase polymer to reduce the phase boundary between PLA and LLDPE, enhancing their compatibility. Consequently, LNR facilitated physical interfacial interactions between PLA and LLDPE.

Figure 4.49c shows that pure PLA had a lower elongation at break compared to pure PP, which is attributed to the brittleness of PLA. Incorporating PP into the PLA matrix improved the elongation at break of the blend, suggesting that the blend transitioned from being brittle to more ductile with the addition of PP. Blends containing MMA-g-LNR exhibited an increase in elongation at break compared to those without MMA-g-LNR. Furthermore, the elongation at break gradually increased as the amount of MMA-g-LNR was increased. Thus, adding MMA-g-LNR to the blend system enhanced both the tensile strength and elongation at break of the blends.

4.3.2 Izod impact test

Figure 4.49d illustrates the impact strength of pure PLA and PP and a PLA/PP (70:30 wt%) blend with and without the MMA-g-LNR compatibilizer. Pure PLA and

PP exhibit impact strengths of 2.75 kJ/m^2 and 3.64 kJ/m^2, respectively, indicating that pure PLA is more brittle than pure PP. For the PLA/PP (70:30 wt%) blend without MMA-g-LNR, the impact strength slightly decreased to 3.09 kJ/m^2. Due to the polarity difference between pure PLA and PP, the polymer blend undergoes phase separation. However, the impact strength of the polymer blends gradually increased from 3.14 kJ/ m^2 to 3.57 kJ/m^2 as the MMA-g-LNR content was increased from 2.5 to 10.0 phr. This suggests that MMA-g-LNR acts as an impact modifier in the PLA/PP blends, owing to the elastomeric properties of the LNR core in the MMA-g-LNR particles. A similar observation was reported by Bijarmi et al. [42], who found that PLA toughness was improved through direct melt blending with PP and the LNR compatibilizer, leading to enhanced elongation at break, flexural properties, and impact strength.

4.3.3 Water absorption

Figure 4.49e summarizes the water absorption percentages of pure PLA and PP and a PLA/PP (70:30 wt%) blend, both with and without the MMA-g-LNR compatibilizer. It is evident that pure PLA has a significantly higher water absorption rate than pure PP. This is because pure PLA is a hydrophilic material with polar molecules that include hydroxyl groups capable of forming intermolecular hydrogen bonds with water molecules, leading to high water absorption in pure PLA. The figure also shows that the PLA/PP (70:30 wt%) blend without MMA-g-LNR compatibilizer absorbs more water than both pure PP and pure PLA. Typically, when pure PLA and PP are combined, they form interfacial regions with numerous micropores due to their immiscible two-phase morphology. These micropores facilitate water absorption. However, adding the compatibilizer to the PLA/PP blends results in a more uniform dispersion of PP within the PLA matrix, reducing the size and number of micropores and thereby preventing water from penetrating the polymer chains. Consequently, the water absorption percentage decreases as the MMA-g-LNR content increases. The presence of MMA-g-LNR enhances the miscibility of the PLA/PP composite and reduces the size and number of micropores, leading to a more homogenized and refined matrix [90, 140].

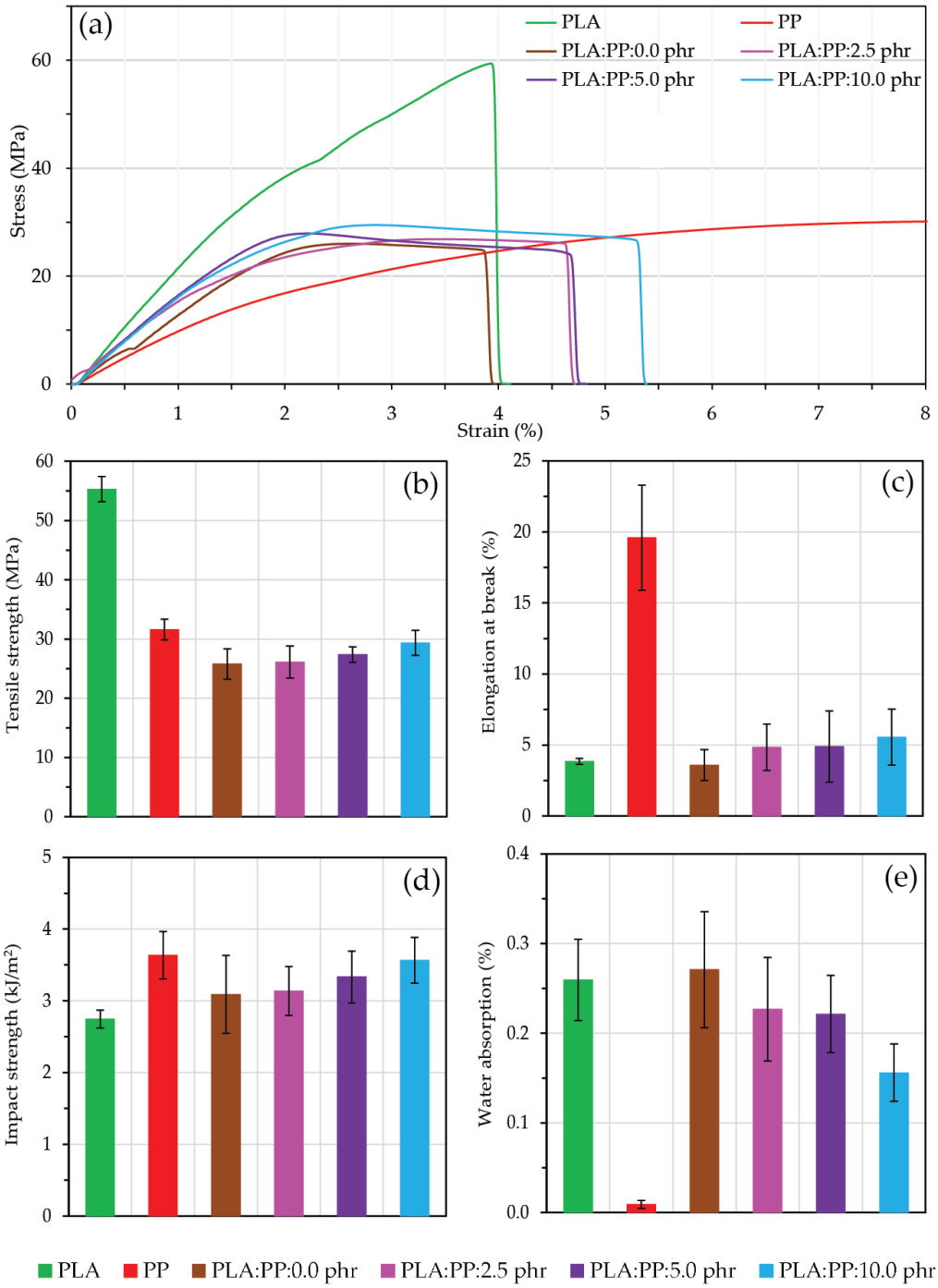

Figure 4.49 The effect of PLA, PP, and PLA/PP blends without and with MMA-g-LNR content on physical properties: (a) stress-strain curves, (b) tensile strength, (c) elongation at break, (d) impact strength, and (e) water absorption. The error bars indicate the stand

4.3.4 Morphology

The morphology of pure PLA and PP, and PLA/PP (70:30 wt%) blends with varying MMA-g-LNR contents was examined using SEM on the tensile-fractured surfaces, as depicted in Figure 4.50. PLA exhibited a brittle fracture, as shown in Figure 4.50a, while PP demonstrated a ductile fracture with whitening deformation scattered across the entire surface (Figure 4.50b). Generally, combining pure PP and PLA leads to immiscibility due to their differing polarities, resulting in phase separation. Small PP spheres were uniformly dispersed in the PLA matrix, highlighting the incompatible morphology of the two-polymer blend. Figure 4.50c shows numerous voids where PP was extracted from the PLA matrix, with PP particles separating from the PLA. The addition of MMA-g-LNR to the blend reduced the interfacial tension between PLA and PP and improved miscibility. The compatibilizer, consisting of an LNR core and a PMMA shell, facilitated the compatibility of the PLA/PP system [42], with LNR enhancing PLA/PP integration and PMMA being well-compatible with the PLA phase [141], leading to improved compatibility. The inclusion of MMA-g-LNR in the PLA/PP blends resulted in smaller dispersed PP particle sizes compared to the blend without MMA-g-LNR. As shown in Figure 4.50d-f, the PP droplet size noticeably decreased with increasing MMA-g-LNR content. Particularly, the PLA/PP blend with 10 phr MMA-g-LNR exhibited very small PP particles and an almost homogeneous morphology, as illustrated in Figure 4.50f.

4.3.5 FTIR spectroscopy

The functional groups of pure PLA and PP, and PLA/PP blends with and without MMA-g-LNR as a compatibilizer were examined using FT-IR analysis, as illustrated in Figure 4.51. For PLA, absorption peaks were observed at 1746 cm^{-1} for C=O stretching, 1178 cm^{-1} for symmetric C-O-C stretching, and 1084 cm^{-1} for asymmetric CH_3 stretching [142], as shown in Figure 4.51a . For PP, absorption peaks appeared at 2918-2835 cm^{-1} for C-H stretching, 1457 cm^{-1} for - CH_3 bending, and 1375 cm^{-1} for C-H bending, as depicted in Figure 4.51b. The MMA-g-LNR compatibilizer exhibited an absorption peak at 1729 cm^{-1}, corresponding to the ester

linkage, as shown in Figure 4.51c. However, in the PLA/PP (70:30 %wt) blends with and without 5.0 phr of MMA-g-LNR, the absorption peaks of PLA and PP were present in the polymer blends at 2918-2835, 1746, 1457, 1375, 1178, and 1084 cm^{-1}, as illustrated in Figures 4.51d-e.

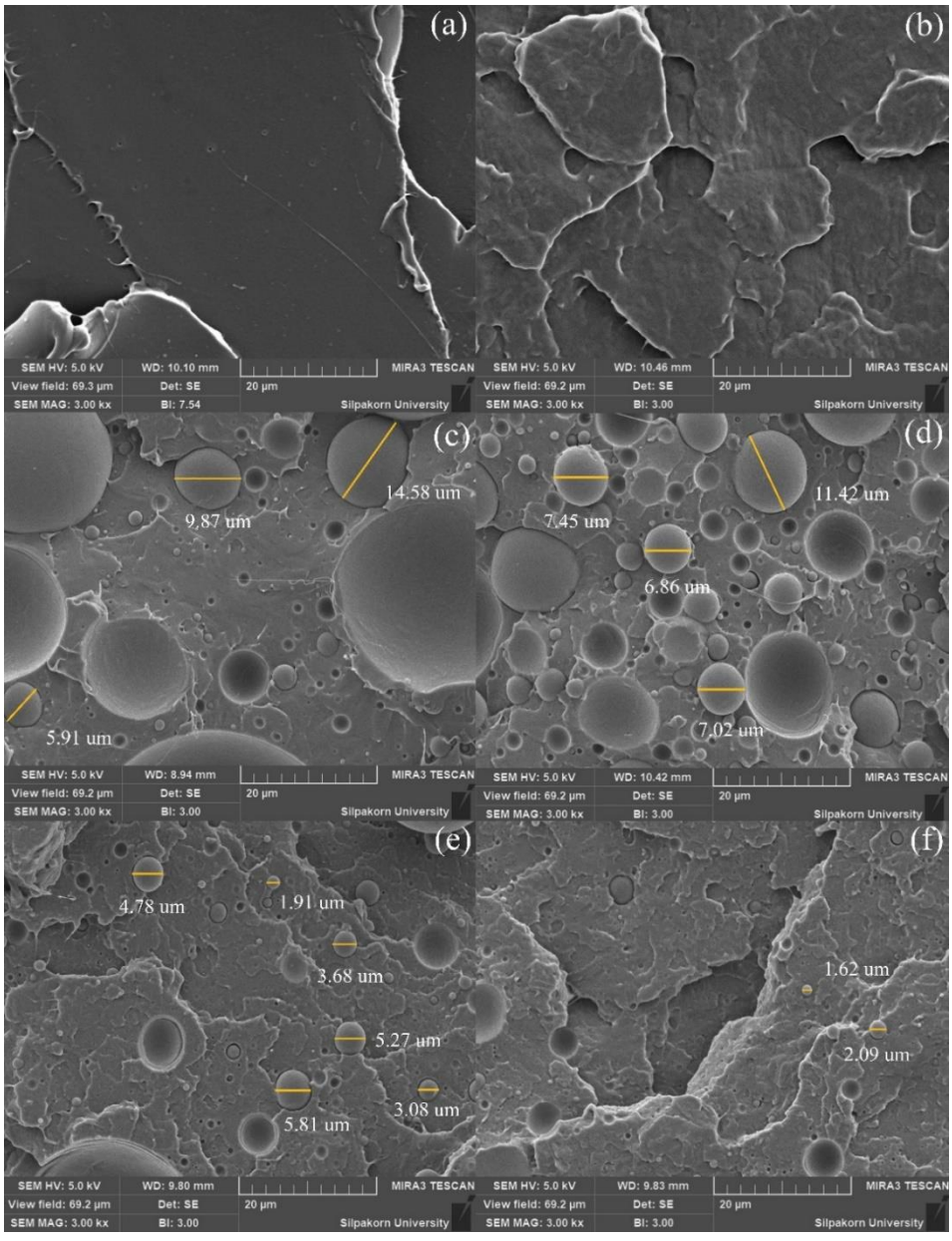

Figure 4.50 SEM micrograph of PLA, PP, and PLA/PP/ blend without and with MMA-g-LNR as a compatibilizer. (a) PLA, (b) PP, (c) PLA/PP/0.0, (d) PLA/PP/2.5, (e) PLA/PP/5.0, and (f) PLA/PP/10.0. The yellow lines indicate the diameter.

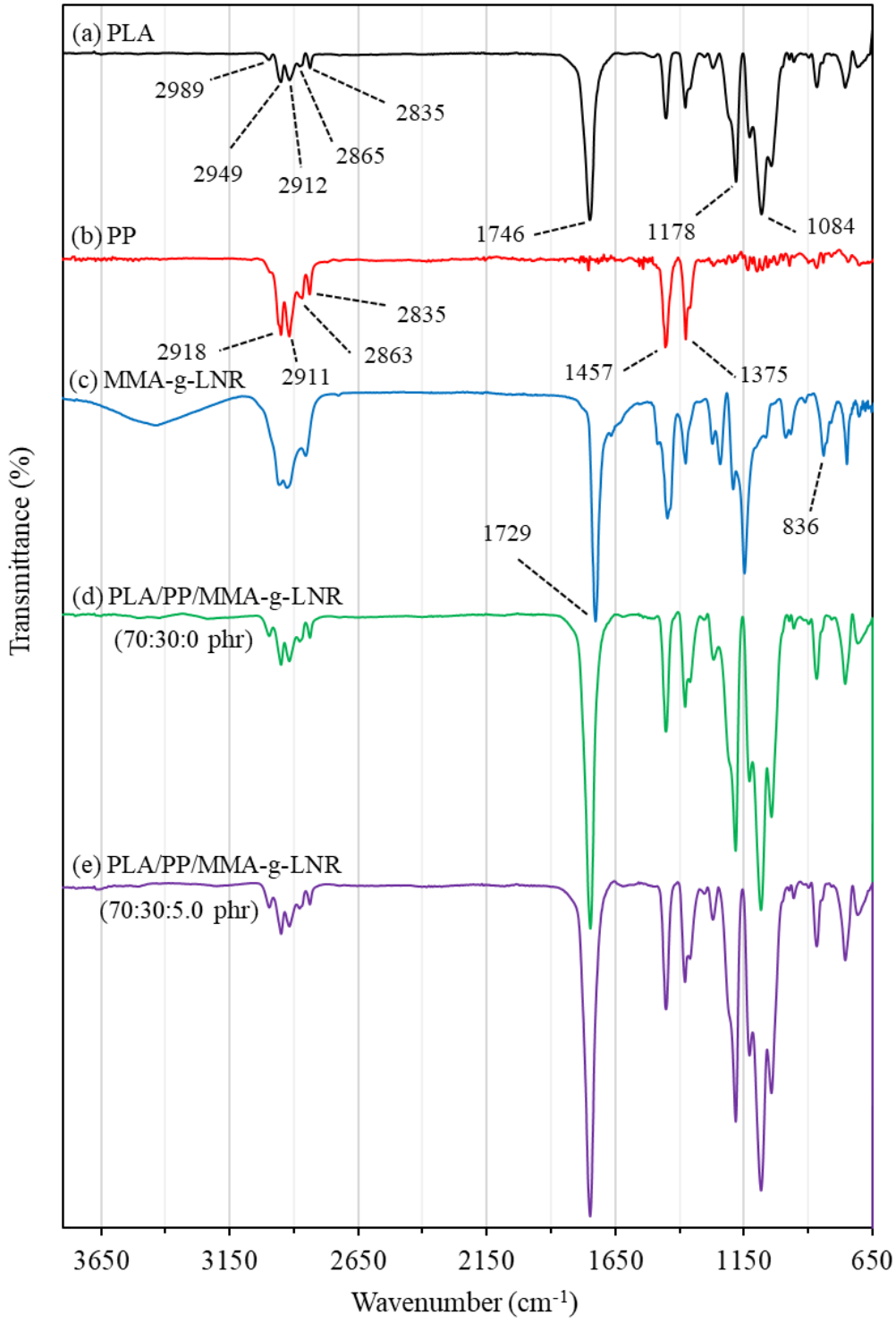

Figure 4.51 FTIR spectra of (a) PLA, (b) PP, (c) MMA-g-LNR, and PLA/PP blends with MMA-g-LNR of (d) 0 phr, and (e) 5.0 phr.

4.3.6 Thermal analysis

4.3.6.1 Thermal stability

Following ASTM E 1877 B9 [143], which provides the necessary mathematical procedures used to determine activation energy and lifetime, TGA analysis was performed, followed by thermal stability evaluation. Decomposition kinetics and lifetime of PLA, PP, and PLA/PP blends. The samples were carried out by heating rates of 10, 20, 30, and 40 °C/min in the range of 50 and 800 °C in an air atmosphere. TG curves and DTG for pure polymers and polymer blends with a PLA/PP ratio of 70:30 wt.% and MMA-g-LNR with contents of 0.0, 2.5, 5.0, and 10.0 phr as compatibilizers used in the present study, As shown in Figures 4.52 - 4.53, for the four heating rates used. Both pure polymers show one-step degradation. As shown in Fig. 4.52a-b, unlike conventional PLA and PP, a two-step degradation process in the immiscible polymer blend is clearly visible in the PLA/PP blend, as shown in Figure 4.52c-f. DTG curves, Two decay peaks were identified. This is even more noteworthy, as shown in Figure 4.53c-f. The first peak is related to the PLA decomposition of the mixture, while the second peak appears at a higher temperature. Relative to the degradation of PP [73]. The decomposition temperature shifted to a higher temperature with an increasing heating rate. The TG data showed the thermal decomposition temperature of the neat polymer and po blends. Polymers of PLA/PP ratio 70:30 wt % using MMA-g-LNR contents of 0.0, 2.5, 5.0, and 10.0 phr as compatibilizers are summarized in Table 4.2. The initial temperature (T_i) and the final temperature (T_f) are obtained by the bitangent method, and T_m is the temperature at which the rate of weight loss is maximum. This can be obtained from the DTG peaks at different heating rates. All ingredients under investigation showed exothermic effects consistent with a thermal decomposition process. Compared with neat PP, the thermal decomposition curve of neat PLA shifts towards low temperature. This indicates that PLA is less thermally stable than PP. The introduction of PP significantly changed the temperature trend of degradation.

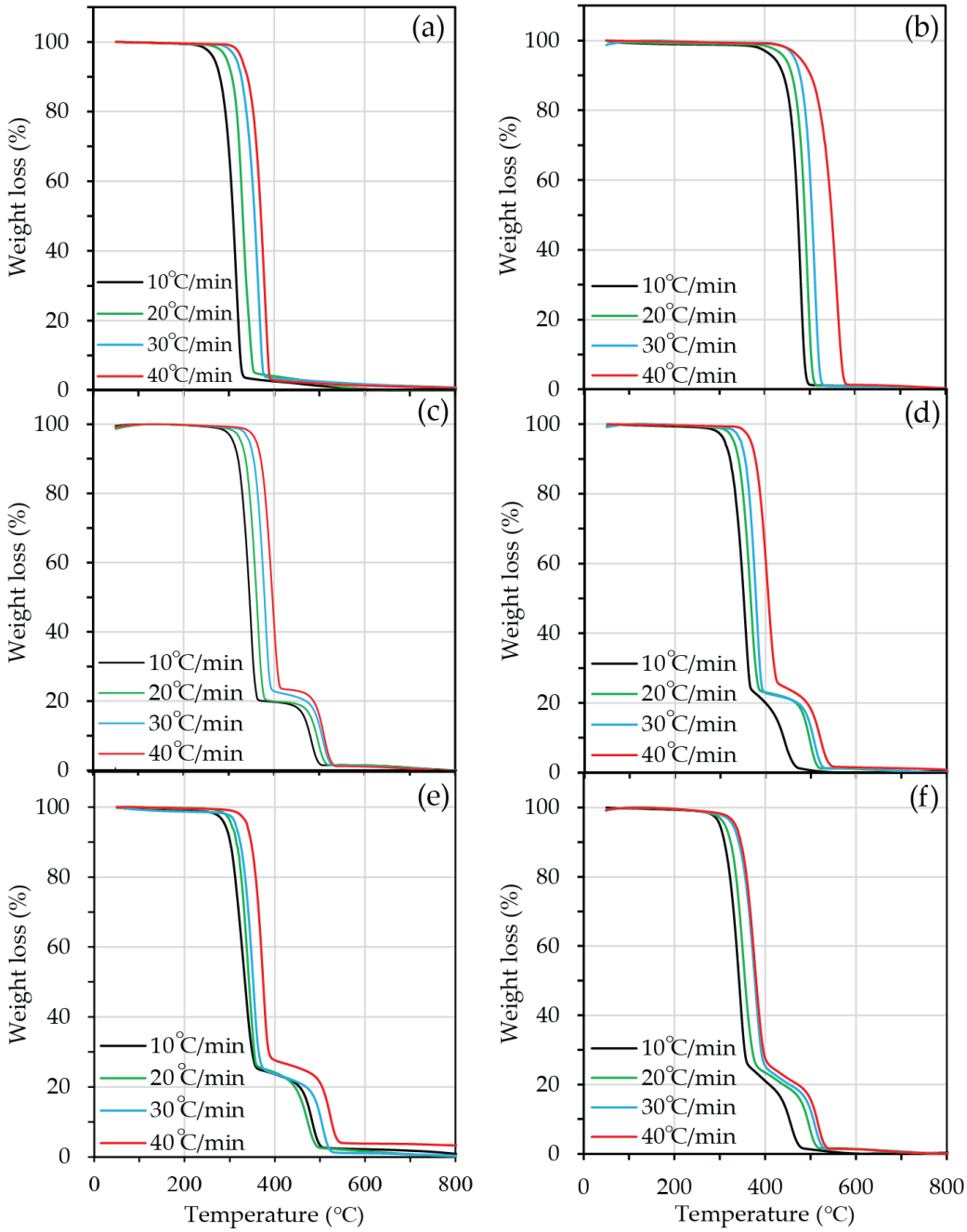

Figure 4.52 Experimental TG curves at different heating rates of (a) PLA, (b) PP, and PLA/PP blends with MMA-g-LNR of (c) 0.0, (d) 2.5, (e) 5.0, and (f) 10.0 phr.

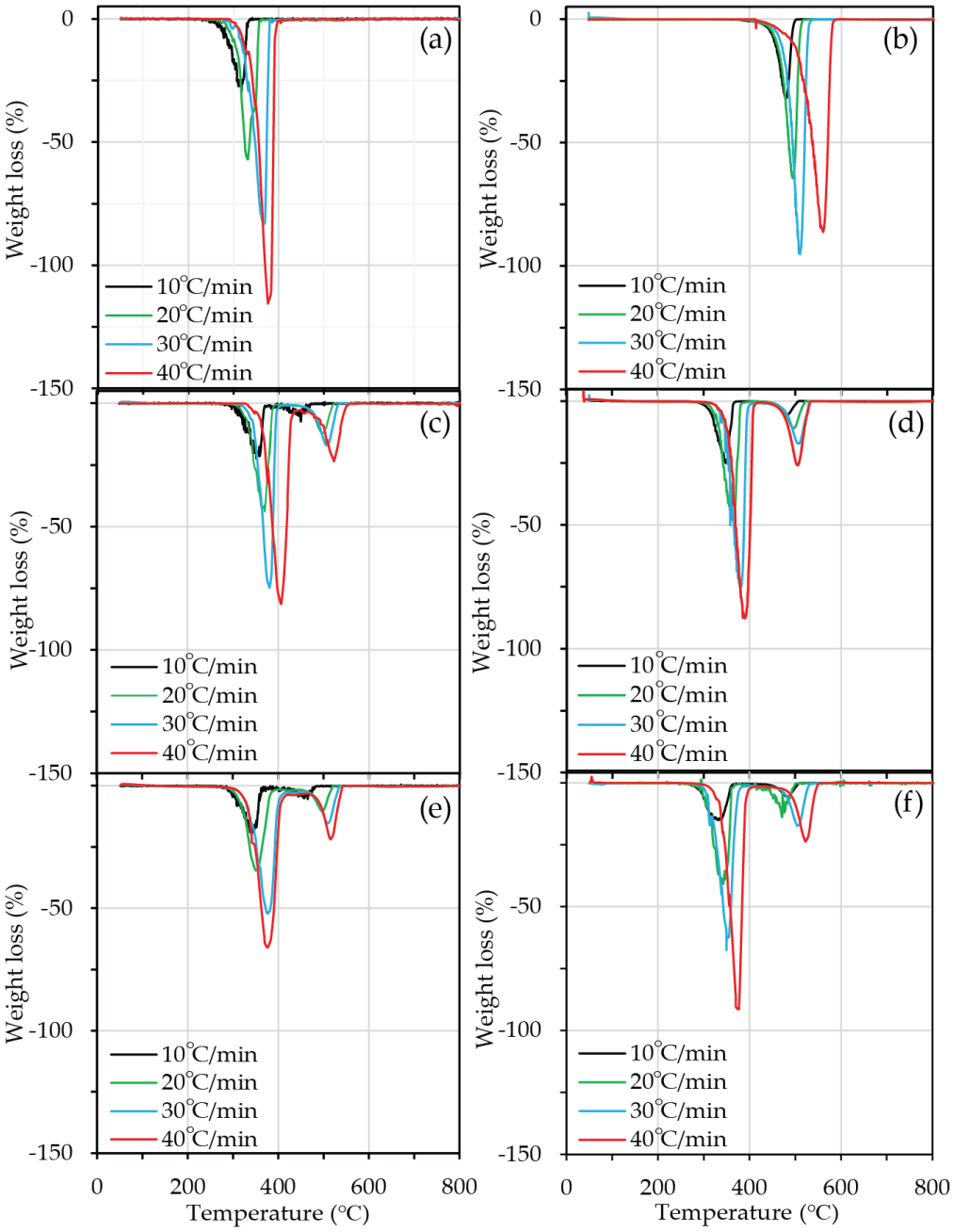

Figure 4.53 Experimental DTG curves at different heating rates of (a) PLA, (b) PP, and PLA/PP blends with MMA-g-LNR of (c) 0.0, (d) 2.5, (e) 5.0, and (f) 10.0 phr.

Table 4.2 T_i, T_{m1}, T_{m2}, and T_f value of PLA, PP, and PLA/PP without and with compatibilizer.

Sample	T_i (°C)	T_{m1} (°C)	T_{m2} (°C)	T_f (°C)
β = 10 °C/min				
PLA	295	314	-	335
PP	445	482	-	495
PLA/PP/0.0 phr	340	357	498	490
PLA/PP/2.5 phr	336	351	492	479
PLA/PP/5.0 phr	325	345	462	476
PLA/PP/10.0 phr	305	320	445	575
β = 20 °C/min				
PLA	315	329	-	350
PP	380	497	-	520
PLA/PP/0.0 phr	350	370	506	518
PLA/PP/2.5 phr	345	367	503	515
PLA/PP/5.0 phr	335	356	489	510
PLA/PP/10.0 phr	320	346	475	495
β = 30 °C/min				
PLA	340	364	-	380
PP	490	508	-	530
PLA/PP/0.0 phr	370	380	514	528
PLA/PP/2.5 phr	365	378	512	526
PLA/PP/5.0 phr	350	375	504	524
PLA/PP/10.0 phr	335	350	502	520
β = 40 °C/min				
PLA	360	376	-	390
PP	530	562	-	570
PLA/PP/0.0 phr	385	405	523	536
PLA/PP/2.5 phr	380	394	522	535
PLA/PP/5.0 phr	360	375	520	530
PLA/PP/10.0 phr	350	374	513	529

Mixing PLA and PP increased the thermal stability of the mixture. Or makes it more temperature resistant compared to pure PLA. However, the addition of compatibilizers reduces the thermal stability of the mixture by increasing interfacial adhesion and interactions between the polymer phases.

4.3.6.2 Thermal kinetics

The kinetic parameters for thermal degradation can be derived from the data obtained through TGA analysis. Typically, these parameters are assessed using a model-free kinetic approach. The reaction rate (dα/dt) for thermal degradation can be calculated as follows:

$$\frac{d\alpha}{dt} = k(T) \cdot f(\alpha) \tag{4.20}$$

where k(T) represents the reaction rate constant, α denotes the conversion degree during the degradation reaction, f(α) signifies the reaction model, and T stands for the absolute temperature (K). The Arrhenius equation is employed to describe the rate constant depends on temperature.

$$k(T) = A \cdot \exp(-\frac{E_a}{RT}) \tag{4.21}$$

where A represents the pre-exponential factor, E_a denotes the activation energy, and R is the gas constant (8.314 J/mol · K). For non-isothermal TGA, α can be determined as the ratio of the actual weight loss at time (t) to the total weight loss corresponding to the degradation process.

$$\alpha = \frac{w_0 - w_t}{w_0 - w_f} \tag{4.22}$$

where w_0, w_t, and w_f are the actual weight of the sample at the initial weight, weight at time (t), and final weight of a sample, respectively. By combining Equations (4.20) and (4.21), the following Equation (4.23) can be obtained:

$$\frac{d\alpha}{dt} = A \cdot \exp(-\frac{E_a}{RT}) \cdot f(\alpha) \tag{4.23}$$

For non-isothermal conditions, in which the samples are at a heating rate (β = dT/dt):

$$\frac{d\alpha}{dt} = \frac{d\alpha}{dT} \times \frac{dT}{dt} = \beta \frac{d\alpha}{dT} \quad (4.24)$$

The rate of degradation ($d\alpha/dt$) equal to $\beta(d\alpha/dT)$ is arranged and modified as follows:

$$\frac{d\alpha}{dT} = \frac{A}{\beta} \cdot \exp\left(-\frac{E_a}{RT}\right) \cdot f(\alpha) \quad (4.25)$$

Following this rearrangement, Equation (4.25) is the fundamental form of kinetic analytical methods, which is used to evaluate the kinetic parameters for the thermal degradation data.

One of the most popular methods is the Kissinger-Akahira-Sunose (KAS) method [144-148], which is known as the isoconversional model-free kinetic approach that uses multiple heating rates. The KAS method is commonly employed to determine the E_a through the following procedure:

$$\ln\frac{\beta}{T^2} = \text{constant} - \frac{E_a}{RT} \quad (4.26)$$

The same α exists at different heating rates. Hence, the E_a can be derived from the slope of a linear plot of $\ln(\beta/T^2)$ against $1000/T$ at the α constant.

The kinetic analysis of the non-isothermal data was obtained using the KAS method. It is well known that the E_a can be used to predict the lifetime of materials. Using the E_a obtained for a conversion degree of 0.05, the material lifetime (t_T) was calculated by analyzing the lifetime of rubber at various operating temperatures (T_T). This conversion degree value might cause a substantial drop in the mechanical properties of a material. The proposed thermal lifetime calculation employed Equation (4.27):

$$\log(t_T) = \frac{E_a}{2.303RT_T} + \log\left(\frac{E_a}{R\beta}\right) - a \quad (4.27)$$

where t_T is the estimated thermal time to failure for a constant degree of conversion; T_T is the operating temperature; E_a is the activation energy for 0.05 conversion

degree; and *a* is a tabulated value that is determined using E_a/RT_c, calculated from the numerical integration table given in reference [149]. T_c is the temperature for a heating rate of 20 °C/min at $\alpha = 0.05$.

The E_a values for pure polymers and polymer blends were determined using the KAS method with TGA data obtained at various heating rates. Figure 4.54 illustrates $\ln(\beta/T^2)$ plotted against 1000/T for different conversion levels ranging from 0.025 to 0.5, demonstrating linear fits that confirm the model's validity. The slope of these lines was used to calculate the E_a value for the degradation process. As depicted in Figure 4.55, E_a initially increases up to a conversion level of 0.2, followed by a more gradual rise. The calculated values within the conversion range of 0.025 to 0.2, at intervals of 0.025, are considered reliable. Results outside this range serve as reference only [150]. Ea indicates the rate of reaction. For instance, at $\alpha = 0.05$, the Ea values for PLA and PP are 108.5 and 156.4 kJ/mol, respectively.

As a result, PP exhibited higher thermal stability due to its higher E_a value for degradation compared to PLA. The introduction of PP into the PLA matrix increased the E_a value ($\alpha = 0.05$) to 144.9 kJ/mol. Conversely, the E_a values ($\alpha = 0.05$) for PLA/PP/MMA-g-LNR blends at ratios of 70:30 with MMA-g-LNR contents of 2.5 phr, 5.0 phr, and 10.0 phr were 134.3, 125.5, and 109.8 kJ/mol, respectively. The addition of PP to PLA raised the E_a value due to their inherent incompatibility. However, incorporating compatibilizers enhances polymer compatibility and reduces activation energy, consequently lowering the thermal stability of the blend.

4.3.7 Lifetime Estimation

Figure 4.56 illustrates the predicted thermal lifetime of PLA, PP, and PLA/PP blends with and without MMA-g-LNR under various failure temperatures. The estimated lifetime is determined based on a 0.05 conversion level at a heating rate of 20 °C/min during thermogravimetric analysis. Lifetime values for PLA, PP, and PLA/PP blends across temperatures ranging from 25 to 150 °C were calculated using Equation (4.27) and are depicted in Figure 4.56. Regardless of the methodology used for estimation, it is evident that the lifespan of all materials is temperature-dependent

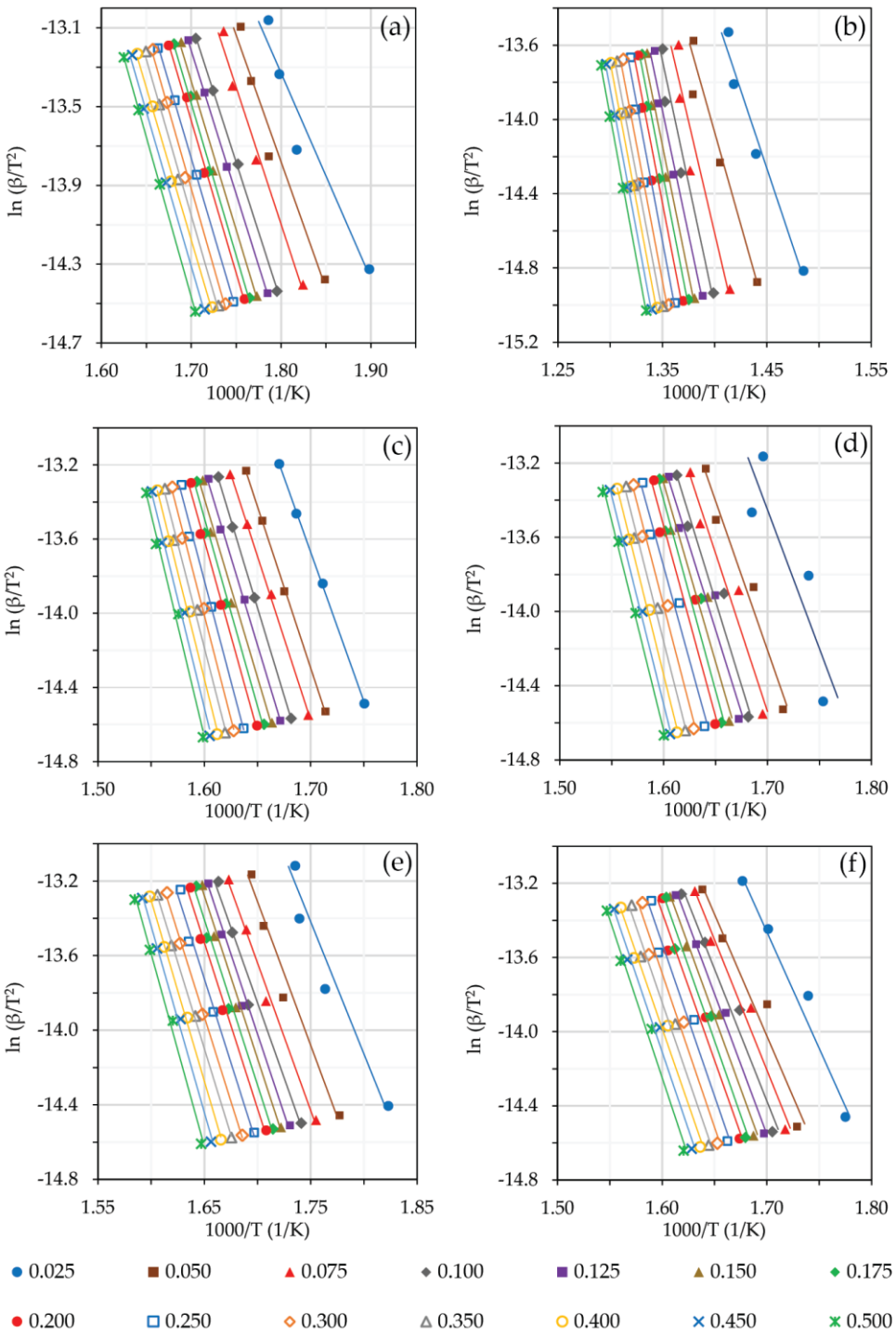

Figure 4.54 The plots of ln (β/T^2) versus 1000/T at different degrees of conversion of (a) PLA, (b) PP, and PLA/PP blends with MMA-g-LNR of (c) 0.0, (d) 2.5, (e) 5.0, and (f) 10.0 phr based on the KAS method.

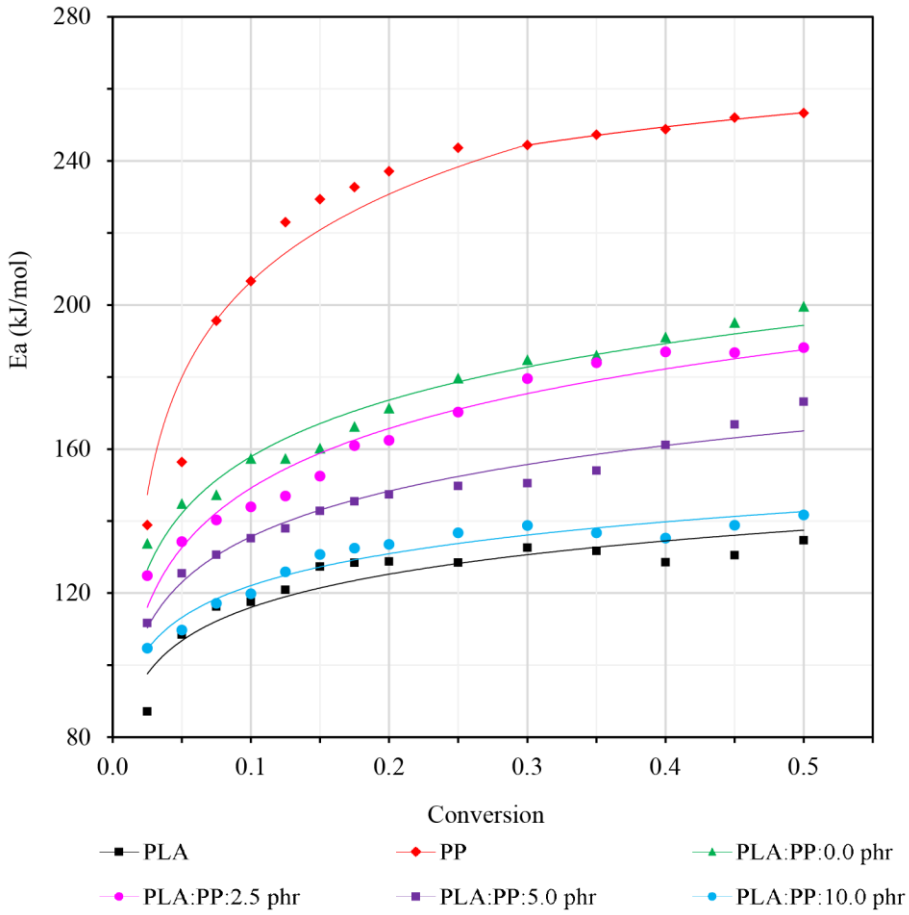

Figure 4.55 The activation energy of PLA, PP, and PLA/PP blends without and with a compatibilizer as a function of the conversion.

and increases exponentially as temperature rises. The estimation of service life was determined using a conversion degree failure of 0.05 at a heating rate of 20 °C/min of PLA, PP, and PLA/PP mixed with MMA-g-LNR of 0.0, 2.5, 5.0 and 10.0 phr are equal to 2.95×10^3, 3.37×10^{10}, 3.54×10^7, 2.30×10^6, 2.99×10^5, and 6.23×10^3 at 25 °C and 1.00×10^2, 2.56×10^8, 3.85×10^5, 3.48×10^4, 5.95×10^3 and 2.03×10^2 years at 50 °C, respectively. An increase in temperature tends to reduce the durability of the material. Therefore, temperature affects the entire service life of the material.

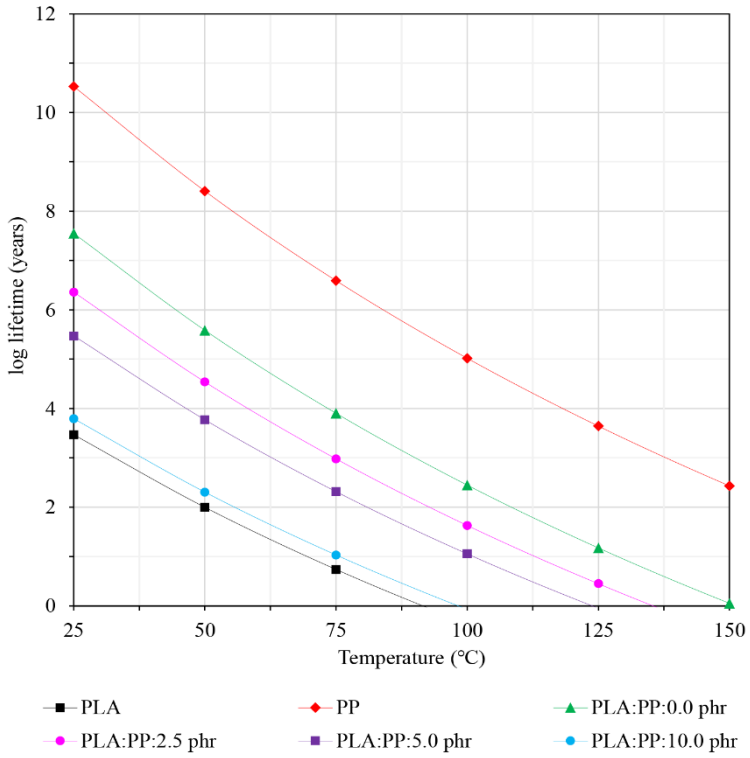

Figure 4.56 Lifetime estimation for PLA, PP, and PLA/PP blend without and with compatibilizer as obtained for different operating temperatures (TT) at α = 0.05 and 20 °C/min.

Because the service life depends on E_a, PP has a longer service life than PLA and PLA/PP blends. The PLA/PP mixture without MMA-g-LNR has a longer service life than the PLA and PLA/PP blend. It lasted longer than PLA/PP blended with MMA-g-LNR content. This study shows how the E_a affects the thermal efficiency of PLA/PP/MMA-g-LNR blends. As a result, the lifespan is greatly shortened.

CHAPTER 5

CONCLUSIONS

In the first section of the work, liquid natural rubber (LNR) was successfully prepared from natural rubber (NR) latex via oxidation degradation using $NaNO_2$, H_2O_2, and HCOOH as reagents. NR latex has a high molecular weight that was degraded to LNR with a shorter chain. This study resulted in the Mark-Houwink-Sakurada (MHS) Equation with the value of the constants *a* and K being 1.3071×10^{-3} and 0.6382, respectively, which can be used to calculate the $\overline{M}_n$ of other samples. The $\overline{M}_n$ of LNR obtained depended on H_2O_2, HCOOH, $NaNO_2$, and reaction temperature and reaction time. The value of $\overline{M}_n$ values exhibited an abrupt initial decrease and began to decrease slightly with increasing reaction time. It can be concluded that the higher H_2O_2 concentration and HCOOH resulted in faster rates of degradation reaction, and a higher $NaNO_2$ concentration, resulting in a decrease in the $\overline{M}_n$. A higher decomposition temperature accelerates the breakage of the NR chains. The results showed that the lowest of the $\overline{M}_n$ for the LNR sample was 10,825 g/mol, derived from the starting the $\overline{M}_n$ of 630,439 g/mol. From FTIR analysis, the degradation mechanisms of LNR samples were prepared in acidic and alkaline conditions and found to have hydroxyl and carbonyl end-groups, respectively. The morphology of NR latex particles showed spherical and large pear-shaped particles. The LNR latex particles clearly revealed smaller spherical-shaped particles with respect to the NR particles until the LNR latex particles were almost uniform after the degradation reaction. Consequently, the reduction of average molecular weights was used to generate a kinetic model for the degradation reaction, $(\overline{M}_0/\overline{M}_{n(t)}) - (\overline{M}_0/\overline{M}_{n(0)}) = [(1.04\times10^9\ M^{-1.72}t^{-1}\times Exp(78.66\ kJ\cdot mol^{-1})][H_2O_2]^{1.58}\ [HCOOH]^{0.79}[NaNO_2]^{-0.65}\times t$.

In the second section of the work, the graft emulsion copolymerization with MMA onto LNR backbone chain is carried out by using CHPO/TEPA as redox initiators. This study affects the process variables such as reaction time, initiator content, monomer content, and reaction temperature on the grafting reaction, followed by the study of the kinetic analysis of the graft copolymers. The kinetics of the graft copolymerization process were investigated over the temperature range of 40 - 70°C

to describe the effect of relevant process factors on the overall copolymerization and grafting rates, as well as on grafting efficiency. The current work also established the rate equations for the overall copolymerization and grafting reactions in the form of power functions with the process factors. Observations by FTIR, SEM, and TEM confirm the formation of the graft copolymer in which MMA form a fully closed shell layer on the surface of the LNR core particles, providing core/shell composites. It can be concluded that low monomer concentration results in the highest %GE for grafting copolymers of MMA onto LNR. The study on the kinetic rate of PMMA/LNR graft copolymerization gives the relationship of R_p (mol/L.min) = 9.75×10^2 $(mol^{-0.07}/L^{-0.07}\cdot min^{0.17})\cdot exp[-19.68\ (kJ/mol)/RT][CHPO]^{0.19}[MMA]^{0.88}t^{-0.83}$ and R_g (mol/L.min) = 1.45×10^{11} $(mol^{-0.17}/L^{-0.17}\cdot min^{1.13})\cdot exp[-75.09\ (kJ/mol)/RT][CHPO]^{0.55}[MMA]^{0.62}t^{0.13}$. An increase in the concentrations and reaction temperature of CHPO and monomer enhances both R_p and R_g, whereas an increase in time retards these rates. For the effect of monomer on R_p and R_g, the monomer grafted has clearly influenced the reaction order. However, it affects the activation energy of the reaction. For PMMA/LNR graft copolymerization, as mentioned above, the activation energy for reactions of copolymerization (Ea_p = 19.68 kJ/mol) and reactions of grafting (Ea_g = 75.09 kJ/mol).

In the last section of the work, the resulting graft product of MMA-g-LNR affects the mechanical properties, morphology, thermal stability, and a lifetime of polymer blends based on pure PLA and PP and PLA/PP blend with and without MMA-g-LNR as compatibilizers with a content of 0.0 - 10.0 phr, all polymer ingredients including pure polymer and compatibilizer were carried out by using internal mixing and compression molding. The morphology of the pure PLA and PP and PLA/PP blend exhibited phase separation, showing the dispersion of droplet size of PP evenly in the form of small balls in the PLA matrix. With the addition of MMA-g-LNR compatibilizer in the PLA/PP blend, the PP droplet sizes in the PLA matrix were dramatically reduced, leading to the morphology being an almost homogenized and refined polymer blend. MMA-g-LNR is used as a compatibilizer to improve the compatibility of the PLA and PP. This study showed that the tensile strength of the pure PLA and PP is equal to 55.31 and 31.61 MPa, while elongation at a break is 3.85 and 19.60%, respectively. Nevertheless, the value of tensile strength and elongation at

the break of the PLA/PP blend was lower than that of pure polymer. However, gradually increasing from 25.78 to 29.35 MPa and from 3.59 to 5.56%, respectively, when the presence of the MMA-g-LNR content increased by 0.0, 2.5, 5.0, and 10.0 phr, both tensile strength and elongation at a break marginally increased from 25.78 to 29.35 MPa and from 3.59 to 5.56%, respectively. The value of the impact strength of 2.75 kJ/m^2 of pure PLA indicates a brittle polymer, while pure PP revealed an impact strength of 3.64 kJ/m^2, denoting toughness with respect to pure PLA and polymer blend. In the PLA/PP blend system, it was found that the impact strength gradually enhanced from 3.09 to 3.57 kJ/m^2, with the increase of the MMA-g-LNR content from 0.0 to 10.0 phr. Totally the presence of the MMA-g-LNR content increased, resulting in an increase in the value of the tensile strength, elongation at break, and impact strength of the polymer blends. In contrast, the value of water absorption decreased. Thermal degradation kinetics of the pure PLA and PP and PLA/PP blends were carried out at a temperature range of 50 - 800 °C with different heating rates of 10, 20, 30, and 40 °C/min. The pure PP and PLA/PP blends were more stable or resistant to temperature than pure PLA since pure PP is very stable, resulting in the polymer blended with pure PP becoming more stable as well. However, the addition of MMA-g-LNR content reduces the thermal stability of the polymer blend because it enhances interfacial adhesion and interaction of PLA and PP phases. The results above indicate that the addition of pure PP into the PLA matrix leads to an increase in the E_a. However, the addition of compatibilizer content increased the compatibility of two polymers and also decreased the E_a, leading to a decrease in the thermal stability of blends. Hence, the E_a obtained can be used to estimate the lifetime of the polymers. It was found that pure PP was more durable than pure PLA and the polymer blend. Followed by the PLA/PP blend with MMA-g-LNR content had a shorter lifetime with an increase of MMA-g-LNR content of 0.0 - 10.0 phr. The thermal stability of materials influences the utilization and processing of polymer materials. Therefore, knowledge of the thermal lifetime under specific end-points and operating temperature criteria is required.

REFERENCES

1. Morton, M., P. Salatiello, and H. Landfield, *Absolute propagation rates in emulsion polymerization. II. Butadiene in hydroperoxide-polyamine systems.* Journal of Polymer Science, 1952. **8**(2): p. 215-224.
2. Morton, M., S. Kaizerman, and M.W. Altier, *Swelling of latex particles.* Journal of Colloid Science, 1954. **9**(4): p. 300-312.
3. Kroschwitz, J., *Concise Encyclopedia of Polymer Science and Technology*. 1990, John Wiley and Sons, New York.
4. Azhar, N.H.A., et al., *Studies on hydrogenation of liquid natural rubber using diimide.* International Journal of Polymer Science, 2015. **2015**(1): p. 243038.
5. Abdullah, I. *Liquid natural rubber: preparation and application*. in *Progress in Pacific Polymer Science 3: Proceedings of the Third Pacific Polymer Conference Gold Coast, Queensland, December 13–17, 1993*. 1994. Springer.
6. Sillapasuwan, A., et al., *The preparation of hydroxyl-terminated deproteinized natural rubber latex by photochemical reaction utilizing nanometric TiO2 depositing on quartz substrate as a photocatalyst.* Polymers, 2022. **14**(14): p. 2877.
7. Ibrahim, S., et al., *Preparation and characterization of low-molecular-weight natural rubber latex via photodegradation catalyzed by nano TiO2.* Polymers, 2018. **10**(11): p. 1216.
8. Dahlan, H., M. Khairul Zaman, and A. Ibrahim, *Liquid natural rubber (LNR) as a compatibilizer in NR/LLDPE blends.* Journal of applied polymer science, 2000. **78**(10): p. 1776-1782.
9. Abdullah, I., S. Ahmad, and C.S. Sulaiman, *Blending of natural rubber with linear low-density polyethylene.* Journal of applied polymer science, 1995. **58**(7): p. 1125-1133.
10. Ibrahim, A. and M. Dahlan, *Thermoplastic natural rubber blends.* Progress in Polymer Science, 1998. **23**(4): p. 665-706.
11. Panwiriyarat, W., et al., *Effect of the diisocyanate structure and the molecular weight of diols on bio-based polyurethanes.* Journal of Applied Polymer Science, 2013. **130**(1): p. 453-462.
12. Panwiriyarat, W., et al., *Preparation and properties of bio-based polyurethane containing polycaprolactone and natural rubber.* Journal of Polymers and the Environment, 2013. **21**: p. 807-815.
13. Saetung, A., et al., *Preparation and physico-mechanical, thermal and acoustic properties of flexible polyurethane foams based on hydroxytelechelic natural rubber.* Journal of Applied Polymer Science, 2010. **117**(2): p. 828-837.
14. Dileep, U. and S.A. Avirah, *Studies on carboxy-terminated liquid natural rubber in NBR.* Journal of applied polymer science, 2002. **84**(2): p. 261-267.
15. Nor, H.M. and J.R. Ebdon, *Ozonolysis of natural rubber in chloroform solutionPart 1. A study by GPC and FTIR spectroscopy.* Polymer, 2000. **41**(7): p. 2359-2365.
16. Isa, S.Z., et al., *The influence of temperature and reaction time in the degradation of natural rubber latex.* Malays. J. Anal. Sci, 2007. **11**: p. 42-47.
17. Bac, N.V., L. Terlemezyan, and M. Mihailov, *Epoxidation of natural rubber in latex in the presence of a reducing agent.* Journal of applied polymer science, 1993. **50**(5): p. 845-849.

18. Ibrahim, S., R. Daik, and I. Abdullah, *Functionalization of liquid natural rubber via oxidative degradation of natural rubber.* Polymers, 2014. **6**(12): p. 2928-2941.
19. Thuong, N.T., N.D. Manh, and N.N. Tue, *Characterization of liquid deproteinized natural rubber prepared via oxidative degradation.* Vietnam Journal of Chemistry, 2020. **58**(6): p. 826-831.
20. Fadhillah, I., A. Wiranata, and I. Zahrina. *Molecular Weight of Liquid Natural Rubber (LNR) Product from the Chemical Depolymerization Process of High Molecular Weight Narutal Rubber Latex*. in *Journal of Physics: Conference Series*. 2020. IOP Publishing.
21. Phetphaisit, C.W. and P. Phinyocheep, *Kinetics and parameters affecting degradation of purified natural rubber.* Journal of applied polymer science, 2003. **90**(13): p. 3546-3555.
22. Neoh, S., A. Azura, and A.S. Hashim, *Comparison of the different vulcanization techniques of styrene modified natural rubber (SNR) as an impact modifier of natural rubber-based high impact polystyrene (NRHIPS).* Polymer-Plastics Technology and Engineering, 2011. **50**(2): p. 121-126.
23. Rezaifard, A., et al., *Toughening epoxy resins with poly (methyl methacrylate)-grafter-natural rubber, and its use in adhesive formulations.* International Journal of Adhesion and Adhesives, 1994. **14**(2): p. 153-159.
24. Oliveira, P.C., et al., *Poly (dimethylaminoethyl methacrylate) grafted natural rubber from seeded emulsion polymerization.* Polymer, 2005. **46**(4): p. 1105-1111.
25. George, B., S. Maiti, and I. Varma, *Graft copolymerization of methyl methacrylate on to natural rubber: effect of polymerization conditions on particle morphology.* Journal of Elastomers & Plastics, 2006. **38**(4): p. 319-331.
26. Rouilly, A., L. Rigal, and R.G. Gilbert, *Synthesis and properties of composites of starch and chemically modified natural rubber.* Polymer, 2004. **45**(23): p. 7813-7820.
27. Hinchiranan, N., et al., *2, 2, 2-Trifluoroethyl methacrylate-graft-natural rubber: Synthesis and application as compatibilizer in natural rubber/fluoroelastomer blends.* Materials Chemistry and Physics, 2013. **139**(2-3): p. 689-698.
28. Man, S.H.C., A.S. Hashim, and H.M. Akil, *Properties of styrene-methyl methacrylate grafted DPNR latex at different monomer concentrations.* Journal of applied polymer science, 2008. **109**(1): p. 9-15.
29. Bevilacqua, E., *Grafting in natural rubber.* Journal of Polymer Science, 1957. **24**(106): p. 292-296.
30. Onyeagoro, G., *Preparation and characterization of natural rubber latex grafted with ethylacrylate (EA)-methylmethacrylate (MMA) monomers mixture.* Academic Research International, 2012. **3**(1): p. 387.
31. Asaletha, R., et al., *Melt rheology and morphology of physically compatibilized natural rubber–polystyrene blends by the addition of natural rubber-g-polystyrene.* Journal of applied polymer science, 1998. **69**(13): p. 2673-2690.

32. Nikolic, V., S. Velickovic, and A. Popovic, *Influence of amine activators and reaction parameters on grafting reaction between polystyrene and starch.* Journal of Polymer Research, 2014. **21**: p. 1-10.
33. Wang, H., M. Wang, and X. Ge, *Graft copolymers of polyurethane with various vinyl monomers via radiation-induced miniemulsion polymerization: Influential factors to grafting efficiency and particle morphology.* Radiation Physics and Chemistry, 2009. **78**(2): p. 112-118.
34. Kalkornsurapranee, E., et al., *From a laboratory to a pilot scale production of natural rubber grafted with PMMA.* Journal of applied polymer science, 2009. **114**(1): p. 587-597.
35. Budianto, E., W. Priyono, and Y. Yulizar, *The Kinetics and Mechanism of the Core-shell Styrene-butyl Acrylate Polymerisation.* 2010.
36. Shaffei, K., A. Moustafa, and W. Mohamed, *Grafting emulsion polymerization of glycidyl methacrylate onto leather by chemical initiation systems.* Journal of applied polymer science, 2008. **109**(6): p. 3923-3931.
37. Rohani, R., et al., *Effect of reaction conditions on electron induced graft copolymerization of styrene onto poly (ethylene-co-tetrafluoroethylene) films: Kinetics study.* Chemical Engineering Journal, 2007. **132**(1-3): p. 27-35.
38. Anbarasan, R., et al., *Redox initiated graft copolymerization of 4-vinyl pyridine onto wool fiber.* International Journal of Polymeric Materials, 2004. **53**(10): p. 901-913.
39. Zhou, Z., H. Huang, and N. Liu, *Kinetics and mechanism of grafting of oleic acid onto acrylonitrile-butadiene-styrene terpolymer.* European polymer journal, 2001. **37**(10): p. 1967-1974.
40. Arayapranee, W. and G. Rempel, *Factorial experimental design for grafting of vinyl monomers onto natural rubber latex.* Journal of applied polymer science, 2004. **93**(1): p. 455-463.
41. Yoo, T.W., et al., *Effects of compatibilizers on the mechanical properties and interfacial tension of polypropylene and poly (lactic acid) blends.* Macromolecular Research, 2010. **18**: p. 583-588.
42. Bijarimi, M., S. Ahmad, and R. Rasid. *Mechanical, thermal and morphological properties of PLA/PP melt blends*. in *International Conference on Agriculture, Chemical and Environmental Sciences (ICACES 2012)*. 2012.
43. Choudhary, P., et al., *Poly (L-lactide)/polypropylene blends: evaluation of mechanical, thermal, and morphological characteristics.* J. Appl. Polym. Sci. , 2011. **121**(6): p. 3223-3237.
44. Ebadi-Dehaghani, H., et al., *Experimental and theoretical analyses of mechanical properties of PP/PLA/clay nanocomposites.* Composites Part B: Engineering, 2015. **69**: p. 133-144.
45. Pivsa-Art, S., et al., *Effect of compatibilizer on PLA/PP blend for injection molding.* Energy Procedia, 2016. **89**: p. 353-360.
46. Lee, H.S. and J.D. Kim, *Effect of a hybrid compatibilizer on the mechanical properties and interfacial tension of a ternary blend with polypropylene, poly (lactic acid), and a toughening modifier.* Polym. Compos., 2012. **33**(7): p. 1154-1161.

47. Bijarimi, M., S. Ahmad, and R. Rasid. *Mechanical, thermal and morphological properties of PLA/PP melt blends*. in *International Conference on Agriculture, Chemical and Environmental Sciences*. 2012.
48. Zeng, Z., et al., *Relationship of intrinsic viscosity to molecular weight for poly (1, 4-butylene adipate).* Polymer testing, 2010. **29**(1): p. 66-71.
49. Chen, L., W. Xue, and Z. Zeng, *Synthesis and Intrinsic Viscosity-molecular Weight Relationship of Poly (ethylene adipate).* Synthesis, 2017. **20**(1): p. 1-9.
50. Kasaai, M.R., J. Arul, and G. Charlet, *Intrinsic viscosity–molecular weight relationship for chitosan.* Journal of Polymer Science Part B: Polymer Physics, 2000. **38**(19): p. 2591-2598.
51. Kasaai, M.R., *Intrinsic viscosity–molecular weight relationship and hydrodynamic volume for pullulan.* Journal of applied polymer science, 2006. **100**(6): p. 4325-4332.
52. Manaresi, P., et al., *A general intrinsic viscosity-molecular weights relationship for polydisperse polymers.* European polymer journal, 1988. **24**(6): p. 575-578.
53. Blackley, D.C., *High polymer latices: their science and technology*. (No Title), 1966.
54. Birley, A., *Natural rubber science and technology Edited by AD Roberts, Oxford University Press, 1988. pp. xvii+ 1136, price£ 75.00. ISBN 0-19-855225-4*. 1989, Wiley Online Library.
55. Paul, D.R., *Polymer Blends Volume 1*. Vol. 1. 2012: Elsevier.
56. Palosuo, T., et al., *Measurement of natural rubber latex allergen levels in medical gloves by allergen-specific IgE-ELISA inhibition, RAST inhibition, and skin prick test.* Allergy, 1998. **53**(1): p. 59-67.
57. Blackley, D.C., *Polymer latices: science and technology volume 3: applications of latices*. 2012: Springer Science & Business Media.
58. Hourston, D. and J. Romaine, *Modification of natural rubber latex—I. Natural rubber-polystyrene composite latices synthesized using an amine-activated hydroperoxide.* European polymer journal, 1989. **25**(7-8): p. 695-700.
59. Kadir, A.A.S., *Advances in natural rubber production.* Rubber chemistry and technology, 1994. **67**(3): p. 537-548.
60. Nor, H.M. and J.R. Ebdon, *Telechelic liquid natural rubber: A review.* Progress in polymer science, 1998. **23**(2): p. 143-177.
61. Baharulrazi, N., H. Mohd Nor, and W.K. Wan Ali, *Hydroxyl terminated natural rubber (HTNR) as a binder in solid rocket propellant.* Applied Mechanics and Materials, 2015. **695**: p. 174-178.
62. Saetung, A., et al., *Synthesis, characteristic, and properties of waterborne polyurethane based on natural rubber.* Journal of Applied Polymer Science, 2012. **124**(4): p. 2742-2752.
63. Kwanming, K., P. Klinpituksa, and W.-a. Waehamad, *Ultraviolet curing of acrylated liquid natural rubber for surface coating application.* Songklanakarin Journal of Science & Technology, 2009. **31**(1).
64. Lenka, S., et al., *Grafting of vinyl monomers onto natural rubber. I. Graft copolymerization of methyl methacrylate onto natural rubber using quinquevalent vanadium ion as the initiator.* Journal of applied polymer science, 1985. **30**(1): p. 429-433.

65. Huy, H.T., et al., *Depolymerization of natural rubber latex using phenylhydrazine-FeCl2 system.* Journal of Macromolecular Science, Part A: Pure and Applied Chemistry, 1996. **33**(12): p. 1923-1930.
66. Klinklai, W., et al., *Depolymerization and ionic conductivity of enzymatically deproteinized natural rubber having epoxy group.* European Polymer Journal, 2003. **39**(8): p. 1707-1712.
67. Phinyocheep, P., et al., *Chemical degradation of epoxidized natural rubber using periodic acid: Preparation of epoxidized liquid natural rubber.* Journal of applied polymer science, 2005. **95**(1): p. p. 6-15.
68. Anbar, M. and H. Taube, *Interaction of nitrous acid with hydrogen peroxide and with water.* Journal of the American Chemical Society, 1954. **76**(24): p. 6243-6247.
69. Crow, J.P., et al., *On the pH-dependent yield of hydroxyl radical products from peroxynitrite.* Free Radical Biology and Medicine, 1994. **16**(3): p. 331-338.
70. Halfpenny, E. and P. Robinson, *168. Pernitrous acid. The reaction between hydrogen peroxide and nitrous acid, and the properties of an intermediate product.* Journal of the Chemical Society (Resumed), 1952: p. 928-938.
71. Dahlan, H., M.K. Zaman, and A. Ibrahim, *Liquid natural rubber (LNR) as a compatibiliser in NR/LLDPE blends—II: the effects of electron-beam (EB) irradiation.* Radiation Physics and Chemistry, 2002. **64**(5-6): p. 429-436.
72. Kargarzadeh, H., et al., *Functionalized liquid natural rubber and liquid epoxidized natural rubber: A promising green toughening agent for polyester.* Journal of applied polymer science, 2015. **132**(3).
73. Mathew, V.S., et al., *Epoxy resin/liquid natural rubber system: secondary phase separation and its impact on mechanical properties.* Journal of materials science, 2010. **45**: p. 1769-1781.
74. Shamsuri, A.A., et al., *Nylon-6/liquid natural rubber blends prepared via emulsion dispersion.* Journal of polymer research, 2009. **16**: p. 381-387.
75. Odian, G., *Principles of polymerization*. 2004: John Wiley & Sons.
76. Kohjiya, S. and Y. Ikeda, *Chemistry, manufacture and applications of natural rubber*. 2021: Woodhead Publishing.
77. Anil, K.B. and L. Howard, *Handbook of elastomers*. 2001, Marcel Dekker, New York, NY.
78. Barnard, D., *Ozonolytic degradation of interpolymers of natural rubber with methyl methacrylate and styrene.* Journal of Polymer Science, 1956. **22**(101): p. 213-216.
79. Brant, D.A., *Polymer-polymer miscibility (Olabisi, O.; Robeson, LM; Shaw, MT)*. 1981, ACS Publications.
80. Xavier, P., P. Rao, and S. Bose, *Nanoparticle induced miscibility in LCST polymer blends: critically assessing the enthalpic and entropic effects.* Physical Chemistry Chemical Physics, 2016. **18**(1): p. 47-64.
81. Harrats, C., S. Thomas, and G. Groeninckx, *Micro-and nanostructured multiphase polymer blend systems: phase morphology and interfaces*. 2005: CRC press.

82. Armentano, I., et al., *Multifunctional nanostructured PLA materials for packaging and tissue engineering.* Progress in Polymer Science, 2013. **38**(10-11): p. 1720-1747.
83. Davey, J.E. and M.J.R. Loadman, *A chemical demonstration of the randomness of epoxidation of natural rubber.* British Polymer Journal, 1984. **16**(3): p. 134-138.
84. Hamzah, R., et al., *A structural study of epoxidized natural rubber (ENR-50) and its cyclic dithiocarbonate derivative using NMR spectroscopy techniques.* Molecules, 2012. **17**(9): p. 10974-10993.
85. Wang, L., et al., *Nanocomposite Polymer Electrolyte Doped with Nanosized Li0. 1Ca0. 9TiO3 for Lithium Polymer Batteries.* Electrochemical and Solid-State Letters, 2009. **13**(1): p. A7.
86. Roy, S., S. Bhattacharjee, and B. Gupta, *Hydrogenation of epoxidized natural rubber.* Journal of applied polymer science, 1993. **49**(3): p. 375-380.
87. Carter, W.C., R.L. Scott, and M. Magat, *The Viscosity-Molecular Weight Relation for Natural Rubber.* Rubber Chemistry and Technology, 1947. **20**(1): p. 78-83.
88. Yoksan, R., *Epoxidized natural rubber for adhesive applications.* Agriculture and Natural Resources, 2008. **42**(5): p. 325-332.
89. Wisetkhamsai, K., W. Patthaveekongka, and W. Arayapranee, *Study on Degradation of Natural Rubber Latex Using Hydrogen Peroxide and Sodium Nitrite in the Presence of Formic Acid.* Polymers, 2023. **15**(4): p. 1031.
90. Mustafa, S.N., *Effect of kaolin on the mechanical properties of polypropylene/polyethylene composite material.* Diyala Journal of Engineering Sciences, 2012. **5**(2): p. 162-178.
91. Wisetkhamsai, K., W. Patthaveekongka, and W. Arayapranee, *Intrinsic Viscosity-Molecular Weight Relationship for Liquid Natural Rubber.*
92. Pasch, H. and B. Trathnigg, *HPLC of Polymers*. 1999: Springer Science & Business Media. 14.
93. Ibrahim, S., N. Othman, and H. Ismail, *Degradation of natural rubber latex.* Natural rubber: properties, behavior and applications, 2016: p. 105-136.
94. Ibrahim, S. and A. Mustafa, *Effect of reagents concentration and ratio on degradation of natural rubber latex in acidic medium.* Malaysian Journal of Analytical Sciences, 2014. **18**(2): p. 405-414.
95. Ibrahim, S., N. Othman, and N.H. Yusof, *Preparation, characterization and properties of liquid natural rubber with low non-rubber content via photodegradation.* Polymer Bulletin, 2021. **78**(2): p. 559-575.
96. Abdullah, I., *Liquid Natural Rubber: Preparation and Application*, in *Progress in Pacific Polymer Science 3*, K.P. Ghiggino, Editor. 1994, Springer Berlin Heidelberg: Berlin, Heidelberg. p. 351-365.
97. Panwiriyarat, W., et al. *Synthesis and Characterization of Block Copolymer from Natural Rubber, Toluene-2, 4-Diisocyanate and Poly (ξ-aprolactone) Diol-Based Polyurethane*. 2011. Trans Tech Publ.
98. Phinyocheep, P., *Chemical modification of natural rubber (NR) for improved performance.* Chemistry, manufacture and applications of natural rubber, 2014: p. 68-118.

99. Halfpenny, E. and P. Robinson, *Pernitrous acid. The reaction between hydrogen peroxide and nitrous acid, and the properties of an intermediate product.* Journal of the Chemical Society (Resumed), 1952: p. 928-938.
100. Marussi, G. and D. Vione, *Secondary formation of aromatic nitroderivatives of environmental concern: Photonitration processes triggered by the photolysis of nitrate and nitrite ions in aqueous solution.* Molecules, 2021. **26**(9): p. 2550.
101. Elliot, A.J. and A.S. Simsons, *Reactions of NO2 and nitrite ion with organic radicals.* Canadian journal of Chemistry, 1984. **62**(9): p. 1831-1834.
102. Yousif, E. and R. Haddad, *Photodegradation and photostabilization of polymers, especially polystyrene.* SpringerPlus, 2013. **2**: p. 1-32.
103. Mielewski, D., D. Bauer, and J. Gerlock, *The role of hydroperoxides in the photo-oxidation of crosslinked polymer coatings.* Polymer degradation and stability, 1991. **33**(1): p. 93-104.
104. Kissinger, H.E., *Variation of peak temperature with heating rate in differential thermal analysis.* Journal of research of the National Bureau of Standards, 1956. **57**(4): p. 217-221.
105. Ibrahim, S., et al. *Preliminary Study on Photochemical Degradation of Natural Rubber Latex.* in *Macromolecular Symposia*. 2017. Wiley Online Library.
106. Liao, L.-S., et al., *CURING KINETICS AND PROPERTIES OF NATURAL RUBBER COAGULATED USING MICROWAVE RADIATION.* Rubber Chemistry and Technology, 2014. **87**(1): p. 43-52.
107. Wang, Z., et al., *Rheological behavior of raw natural rubber coagulated by microorganisms.* Polímeros, 2014. **24**: p. 143-148.
108. Elias, H.-G., *An introduction to polymer science*. 1997. 166.
109. Tasakorn, P. and W. Amatyakul, *Photochemical reduction of molecular weight and number of double bonds in natural rubber film.* Korean Journal of Chemical Engineering, 2008. **25**: p. 1532-1538.
110. Mohapatra, S. and G.B. Nando, *Cardanol: a green substitute for aromatic oil as a plasticizer in natural rubber.* Rsc Advances, 2014. **4**(30): p. 15406-15418.
111. Di Somma, I., et al., *Thermal decomposition of cumene hydroperoxide: chemical and kinetic characterization.* AIChE journal, 2008. **54**(6): p. 1579-1584.
112. Wisetkhamsai, K., W. Patthaveekongka, and W. Arayapranee, *Effect of LNR-g-MMA on the Mechanical Properties and Lifetime Estimation of PLA/PP Blends.* Polymers, 2023. **15**(7): p. 1712.
113. Kochthongrasamee, T., P. Prasassarakich, and S. Kiatkamjornwong, *Effects of redox initiator on graft copolymerization of methyl methacrylate onto natural rubber.* Journal of Applied Polymer Science, 2006. **101**(4): p. 2587-2601.
114. Vanderhoff, J., J. Park, and M.S. El-Aasser, *Preparation of Particles for Microvoid Coatings by Seeded Emulsion Polymerization: Soft Hydrophilic Polymer Core—Hard Hydrophobic Polymer Shell*. 1992, ACS Publications.
115. Merkel, M., et al., *Process parameters and their effect on grafting reactions in core/shell latexes.* Journal of Polymer Science Part A: Polymer Chemistry, 1987. **25**(7): p. 1755-1767.

116. Carter, W.C., R.L. Scott, and M. Magat, *The Viscosity-Molecular Weight Relation for Natural Rubber1*. Journal of the American Chemical Society, 1946. **68**(8): p. 1480-1483.
117. Arayapranee, W. and G.L. Rempel, *Preparation of a natural rubber core/polymer shell in a nanomatrix by graft copolymerization.* Journal of applied polymer science, 2008. **110**(4): p. 2475-2482.
118. Arayapranee, W., P. Prasassarakich, and G. Rempel, *Synthesis of graft copolymers from natural rubber using cumene hydroperoxide redox initiator.* Journal of Applied Polymer Science, 2002. **83**(14): p. 2993-3001.
119. Arayapranee, W., P. Prasassarakich, and G. Rempel, *Process variables and their effects on grafting reactions of styrene and methyl methacrylate onto natural rubber.* Journal of applied polymer science, 2003. **89**(1): p. 63-74.
120. Lee, J.S. and F.C. Chang, *Effect of the core-shell impact modifier shell thickness on toughening PVC.* Polymer Engineering & Science, 2004. **44**(10): p. 1885-1889.
121. Wang, C., et al., *Effect of reaction conditions on grafting ratio and properties of starch nanocrystals-g-polystyrene.* Journal of applied polymer science, 2014. **131**(15).
122. Khullar, R., et al., *Grafting of acrylonitrile onto cellulosic material derived from bamboo (Dendrocalamus strictus).* Express Polym. Lett, 2008. **2**(1): p. 12-18.
123. Kongparakul, S., P. Prasassarakich, and G.L. Rempel, *Catalytic hydrogenation of methyl methacrylate-g-natural rubber (MMA-g-NR) in the presence of OsHCl (CO)(O2)(PCy3) 2.* Applied Catalysis A: General, 2008. **344**(1-2): p. 88-97.
124. Singh, V., et al., *Peroxydisulfate initiated synthesis of potato starch-graft-poly (acrylonitrile) under microwave irradiation.* Express Polymer Letters, 2007. **1**(1): p. 51-58.
125. Liu, Y., et al., *Graft copolymerization of butyl acrylate onto casein initiated by potassium diperiodatonickelate (IV) in alkaline medium.* European polymer journal, 2002. **38**(8): p. 1619-1625.
126. Enyiegbulam, M. and I. Aloka, *Graft characteristics and solution properties of natural rubber-g-methyl methacrylate copolymer in MEK/toluene.* Journal of applied polymer science, 1992. **44**(10): p. 1841-1845.
127. Chanda, M., *Introduction to polymer science and chemistry: a problem-solving approach*. 2006: CRC press.
128. Sundberg, D.C., J. Arndt, and M.-Y. Tang, *Grafting of styrene onto polybutadiene latices in batch and semi-continuous reactors.* Journal of Dispersion Science and Technology, 1984. **5**(3-4): p. 433-445.
129. Lenka, S., P.L. Nayak, and A.P. Das, *Graft copolymerization onto rubber. VII. Graft copolymerization of methyl methacrylate onto rubber using potassium peroxydisulfate catalyzed by silver ion.* Journal of applied polymer science, 1985. **30**(7): p. 2753-2759.
130. Wahba, M.M., A.M. Aziz, and A.M. Zaghloul, *Evaluation of Kinetic Approach in Describing Potassium Bioavailability.* Am. J. Heterocycl. Chem, 2017. **3**: p. 78.

131. Schwaab, M. and J.C. Pinto, *Optimum reparameterization of power function models.* Chemical engineering science, 2008. **63**(18): p. 4631-4635.
132. Tong, G.-S., et al., *Modelling of the kinetics of the supercritical CO2 assisted grafting of maleic anhydride onto isotactic polypropylene in the solid state.* Chemical engineering science, 2007. **62**(18-20): p. 5290-5294.
133. TAGHI, Z.M. and A. Mehrdad, *Kinetic study of graft polymerization of acrylic acid and ethyl methacrylate onto starch by ceric ammonium nitrate.* 2006.
134. Singha, A., A. Guleria, and R.K. Rana, *Ascorbic acid/H2O2-initiated graft copolymerization of methyl methacrylate onto Abelmoschus esculentus fiber: A kinetic approach.* International Journal of Polymer Analysis and Characterization, 2013. **18**(1): p. 1-14.
135. Taghizadeh, M. and S. Ghaffari, *Kinetics and Mechanism Studying of Graft Copolymerization of Acrylic Monomers on PVC.* Iran. Int. J. Sci, 2003. **4**: p. 23-36.
136. Chmela, Š., et al., *Synthesis and homopolymerization kinetics of 7-(methacroyloxy)-2-oxo-heptylphosphonic acid and its copolymerization with methyl methacrylate.* Designed monomers and polymers, 2019.
137. Wang, S., *Redox-initiated adiabatic emulsion polymerization*. 2013: Lehigh University.
138. Panigrahi, H., P.R. Sreenath, and D.K. Kotnees, *Unique compatibilized thermoplastic elastomer with high strength and remarkable ductility: effect of multiple point interactions within a rubber-plastic blend.* ACS omega, 2020. **5**(22): p. 12789-12808.
139. Bijarimi, M., S. Ahmad, and A.M. Alam, *Toughening effect of liquid natural rubber on the morphology and thermo-mechanical properties of the poly (lactic acid) ternary blend.* Polymer Bulletin, 2017. **74**: p. 3301-3317.
140. Dan-Mallam, Y., M.Z. Abdullah, and P.S.M. Yosuff, *Impact strength, microstructure, and water absorption properties of kenaf/polyethylene terephthalate (PET) fiber-reinforced polyoxymethylene (POM) hybrid composites.* Journal of Materials Research, 2013. **28**(16): p. 2142-2146.
141. Li, Z., et al., *Grafting modification of the reactive core-shell particles to enhance the toughening ability of polylactide.* Materials, 2017. **10**(8): p. 957.
142. Bijarimi, M., S. Ahmad, and R. Rasid, *Mechanical, thermal and morphological properties of poly (lactic acid)/epoxidized natural rubber blends.* J. Elastomers Plast., 2014. **46**(4): p. 338-354.
143. International, A., *Standard Practice for Calculating Thermal Endurance of Materials from Thermogravimetric Decomposition Data*, in *ASTM International*. 2005, PA: West Conshohocken.
144. Arshad, M.A., et al., *Kinetics of the thermal decomposition mechanisms of conducting and non-conducting epoxy/Al composites.* Journal of Materials and Environmental Science, 2014. **5**(5): p. 1342-1354.
145. Mohanraj, G., et al., *Kinetics of thermal degradation and thermo-oxidative degradation of conductive styrene-butadiene rubber-carbon black composites.* Journal of materials science, 2006. **41**: p. 4777-4789.
146. Das, P. and P. Tiwari, *Thermal degradation kinetics of plastics and model selection.* Thermochimica Acta, 2017. **654**: p. 191-202.

147. Singh, A., T.C. Sharma, and P. Kishore, *Thermal degradation kinetics and reaction models of 1, 3, 5-triamino-2, 4, 6-trinitrobenzene-based plastic-bonded explosives containing fluoropolymer matrices.* Journal of Thermal Analysis and Calorimetry, 2017. **129**: p. 1403-1414.
148. Bashpa, P., et al., *Thermal degradation kinetics and solvent transport behavior of natural rubber composites filled with polyurethane rich shoe sole waste from footwear industry.* Journal of Thermal Analysis and Calorimetry, 2023. **148**(20): p. 10871-10883.
149. Toop, D.J., *Theory of life testing and use of thermogravimetric analysis to predict the thermal life of wire enamels.* IEEE transactions on Electrical Insulation, 1971(1): p. 2-14.
150. Chen, Y. and Q. Wang, *Thermal oxidative degradation kinetics of flame-retarded polypropylene with intumescent flame-retardant master batches in situ prepared in twin-screw extruder.* Polym. Degrad. Stab. , 2007. **92**(2): p. 280-291.

REFERENCES

มหาวิทยาลัยศิลปากร

VITA

NAME	Kraiwut Wisetkhamsai
DATE OF BIRTH	07 Jan 1993
PLACE OF BIRTH	Nam Som District, Udon Thani
INSTITUTIONS ATTENDED	Department of Chemical Engineering, Faculty of Engineering and Industrial Technology, Silpakorn University, Muang, Nakorn Pathom 73000, Thailand.
HOME ADDRESS	190 Village No. 5, Samakkhi Subdistrict, Nam Som District, Udon Thani Province, 41210
PUBLICATION	1. Wisetkhamsai, K., Patthaveekongka, W., & Arayapranee, W. (2023). Study on Degradation of Natural Rubber Latex Using Hydrogen Peroxide and Sodium Nitrite in the Presence of Formic Acid. Polymers, 15(4), 1031. 2. Wisetkhamsai, K., Patthaveekongka, W., & Arayapranee, W. (2023). Effect of LNR-g-MMA on the Mechanical Properties and Lifetime Estimation of PLA/PP Blends. Polymers, 15(7), 1712.